



Calhoun: The NPS Institutional Archive DSpace Repository

Theses and Dissertations

Thesis and Dissertation Collection

2014-06

Low-cost direct detect spaceborne LIDAR

DeMello, John E.

Monterey, California: Naval Postgraduate School

<http://hdl.handle.net/10945/42606>

Downloaded from NPS Archive: Calhoun



Calhoun is a project of the Dudley Knox Library at NPS, furthering the precepts and goals of open government and government transparency. All information contained herein has been approved for release by the NPS Public Affairs Officer.

Dudley Knox Library / Naval Postgraduate School
411 Dyer Road / 1 University Circle
Monterey, California USA 93943

<http://www.nps.edu/library>



NAVAL POSTGRADUATE SCHOOL

MONTEREY, CALIFORNIA

THESIS

LOW-COST DIRECT DETECT SPACEBORNE LIDAR

by

John E. DeMello

June 2014

Thesis Advisor:
Second Reader:

Richard Olsen
Susan Durham

Approved for public release; distribution is unlimited

THIS PAGE INTENTIONALLY LEFT BLANK

REPORT DOCUMENTATION PAGE
Form Approved OMB No. 0704-0188

Public reporting burden for this collection of information is estimated to average 1 hour per response, including the time for reviewing instruction, searching existing data sources, gathering and maintaining the data needed, and completing and reviewing the collection of information. Send comments regarding this burden estimate or any other aspect of this collection of information, including suggestions for reducing this burden, to Washington Headquarters Services, Directorate for Information Operations and Reports, 1215 Jefferson Davis Highway, Suite 1204, Arlington, VA 22202-4302, and to the Office of Management and Budget, Paperwork Reduction Project (0704-0188) Washington, DC 20503.

1. AGENCY USE ONLY (Leave blank)	2. REPORT DATE June 2014	3. REPORT TYPE AND DATES COVERED Master's Thesis
4. TITLE AND SUBTITLE LOW-COST DIRECT DETECT SPACEBORNE LIDAR		5. FUNDING NUMBERS
6. AUTHOR(S) John E. DeMello		
7. PERFORMING ORGANIZATION NAME(S) AND ADDRESS(ES) Naval Postgraduate School Monterey, CA 93943-5000		8. PERFORMING ORGANIZATION REPORT NUMBER
9. SPONSORING /MONITORING AGENCY NAME(S) AND ADDRESS(ES) N/A		10. SPONSORING/MONITORING AGENCY REPORT NUMBER
11. SUPPLEMENTARY NOTES The views expressed in this thesis are those of the author and do not reflect the official policy or position of the Department of Defense or the U.S. Government. IRB Protocol number ____ N/A ____.		
12a. DISTRIBUTION / AVAILABILITY STATEMENT Approved for public release; distribution is unlimited		12b. DISTRIBUTION CODE

13. ABSTRACT (maximum 200 words)

LIDAR has widely been used to create very accurate 3-D models for use in a wide range of commercial, governmental and nonprofit applications. This thesis identifies how recent advancements in Nd:YAG fiber lasers and InGaAs GmAPDs could be applied to space-borne missions, enabling low-cost solutions that fulfill NASA's ICESat-2 and United States Geological Survey (USGS) objectives. An analysis of launch vehicles, standard spacecraft buses and payload technologies identified three potential low-cost solutions: one hosted aboard Iridium and two onboard a BCP2000 commercial bus. These systems were evaluated using NASA's mass-based and aperture-based cost models to provide a rough estimate of cost versus NASA's CALIPSO, ICESat-1 and ICESat-2 missions.

Preliminary analysis shows a potential for these new technologies to outperform any previous space-based LIDAR mission. At \$55M, the Iridium-hosted solution is 1/16th the cost of ICESat-2 at roughly one-third its capability. Two other solutions were estimated at \$216.6M and \$370.586M and provided over 3X and 10X the estimated capability of ICESat-2, respectively. Both systems are anticipated to fulfill NASA's ice sheet and vegetation objectives while delivering a return on investment of roughly \$1B per year based on USGS's analysis of advanced 3-D data for the United States.

14. SUBJECT TERMS LIDAR, 3-D, NASA, Elevation data, Laser Altimeter, LADAR, CALIPSO, ICESat, GmAPD, Fiber lasers, USGS		15. NUMBER OF PAGES 129	
16. PRICE CODE			
17. SECURITY CLASSIFICATION OF REPORT Unclassified	18. SECURITY CLASSIFICATION OF THIS PAGE Unclassified	19. SECURITY CLASSIFICATION OF ABSTRACT Unclassified	20. LIMITATION OF ABSTRACT UU

THIS PAGE INTENTIONALLY LEFT BLANK

Approved for public release; distribution is unlimited

LOW-COST DIRECT DETECT SPACEBORNE LIDAR

John E. DeMello
Captain, United States Air Force
B.S., Worcester Polytechnic Institute, 2006

Submitted in partial fulfillment of the
requirements for the degree of

MASTER OF SCIENCE IN SPACE SYSTEMS OPERATIONS

from the

NAVAL POSTGRADUATE SCHOOL
June 2014

Author: John E. DeMello

Approved by: Richard Olsen
Thesis Advisor

Susan Durham
Second Reader

Rudolph Panholzer
Chair, Department of Space Systems Academic Group

THIS PAGE INTENTIONALLY LEFT BLANK

ABSTRACT

LIDAR has widely been used to create very accurate 3-D models for use in a wide range of commercial, governmental and nonprofit applications. This thesis identifies how recent advancements in Nd:YAG fiber lasers and InGaAs GmAPDs could be applied to space-borne missions, enabling low-cost solutions that fulfill NASA's ICESat-2 and United States Geological Survey (USGS) objectives. An analysis of launch vehicles, standard spacecraft buses and payload technologies identified three potential low-cost solutions: one hosted aboard Iridium and two onboard a BCP2000 commercial bus. These systems were evaluated using NASA's mass-based and aperture-based cost models to provide a rough estimate of cost versus NASA's CALIPSO, ICESat-1 and ICESat-2 missions.

Preliminary analysis shows a potential for these new technologies to outperform any previous space-based LIDAR mission. At \$55M, the Iridium-hosted solution is 1/16th the cost of ICESat-2 at roughly one-third its capability. Two other solutions were estimated at \$216.6M and \$370.586M and provided over 3X and 10X the estimated capability of ICESat-2, respectively. Both systems are anticipated to fulfill NASA's ice sheet and vegetation objectives while delivering a return on investment of roughly \$1B per year based on USGS's analysis of advanced 3-D data for the United States.

THIS PAGE INTENTIONALLY LEFT BLANK

TABLE OF CONTENTS

I.	INTRODUCTION.....	1
A.	PURPOSE.....	1
B.	RESEARCH QUESTIONS	2
C.	BENEFITS OF STUDY.....	2
D.	TYPES OF LIDAR.....	2
II.	LIDAR OBJECTIVES AND REQUIREMENTS	5
A.	NASA OBJECTIVES.....	5
1.	Glacier, Sea Ice and Ice Sheet Thickness.....	8
2.	Vegetation and Biomass	9
3.	Topography	10
4.	Hydrology and Atmospheric Sensing	12
B.	USGS'S NATIONAL ENHANCED ELEVATION ASSESSMENT	12
III.	HISTORY OF LIDAR IN SPACE	19
A.	APOLLO LASER ALTIMETER.....	19
B.	CLEMENTINE	20
C.	LIDAR IN-SPACE TECHNOLOGY EXPERIMENT (LITE).....	22
D.	MARS ORBITER LASER ALTIMETER (MOLA)	25
E.	MESSENGER LASER ALTIMETER (MLA).....	27
F.	CLOUD-AEROSOL LIDAR AND INFRARED PATHFINDER SATELLITE OBSERVATIONS (CALIPSO)	29
G.	LUNAR ORBITER LASER ALTIMETER (LOLA)	31
H.	GEOSCIENCE LASER ALTIMETER SYSTEM (GLAS)	33
I.	ICESAT-2	35
IV.	SPACE-BASED LIDAR COST CONSIDERATIONS.....	41
A.	HISTORICAL COSTS AND ICESAT-2 ESTIMATES.....	41
B.	SATELLITE COST MODELS.....	43
1.	Cost Estimation Methodologies	43
2.	NASA Small Satellite Cost Breakdown	44
3.	NASA's Weight-Based Cost Model	45
4.	Optical Telescope Assembly-Based Cost Model	48
C.	STANDARD SPACECRAFT BUSES AND LAUNCH VEHICLES....	49
D.	HOSTED PAYLOAD	52
V.	LIDAR PAYLOAD DESIGN OPTIONS.....	55
A.	TRANSMITTER DESIGN	55
1.	MOPA Transmitter Overview	56
2.	Master-Oscillator Design Options	57
3.	Power Amplifier Design Options	58
4.	Beam Steering and Shaping Design Options.....	59
B.	RECEIVER DESIGN	61
VI.	LIDAR MISSION DESIGN	65

A.	LINK BUDGET	65
B.	ASSUMPTIONS	69
1.	Transmitter Assumptions	70
2.	Receiver Assumptions	71
3.	Thermal Assumptions	73
4.	Telescope Mass Assumptions.....	73
5.	Mission Assumptions.....	73
VII.	LIDAR SYSTEM DESIGN AND COSTS.....	77
A.	IRIDIUM HOSTED PAYLOAD DESIGN.....	77
1.	32x32 Array Detector-Based Payload Design	77
2.	10X10 Array Detector-Based Payload Design	79
3.	Estimated Mission Cost and Collection Rate	83
B.	FREE-FLIER SATELLITE DESIGNS.....	87
1.	Low Cost: Less than \$250M Satellite Design	87
2.	Mid Cost: Less than \$500M Satellite Design	93
VIII.	CONCLUSIONS.....	101
LIST OF REFERENCES.....		105
INITIAL DISTRIBUTION LIST		111

LIST OF FIGURES

Figure 1.	NASA's ICESat-2 Implementation Requirements Flowdown (from Abdalati et al., 2010).....	7
Figure 2.	DEM Comparison of California's Salinas River (from National Research Council, 2007).....	11
Figure 3.	1971 Apollo Laser Altimeter (from Abshire, 2010).....	20
Figure 4.	Clementine LIDAR Topographic Map of the Lunar Surface (from Spudis, 1994)	22
Figure 5.	LITE Instrument in Flight Configuration (from Winker, Couch, & McCormick, 1996)	23
Figure 6.	LITE Instrument On-orbit (from Winker, Couch, & McCormick, 1996)	23
Figure 7.	LITE Return Signal at 532nm over the Atlas Mountains and the Atlantic Coast of Morocco (from Winker, Couch, & McCormick, 1996)	25
Figure 8.	MOLA's Collection of Olympus Mons (from Abshire, 2010).....	26
Figure 9.	MLA Payload Assembly (from Abshire, 2010)	27
Figure 10.	Profile of the Atget crater from MLA (from Zuber, et al., 2012).....	28
Figure 11.	CALIOP observations from 9 June 2006 from Northern Europe across Africa into the south Atlantic. Shown are (top) total 532 nm return, (middle) 532 nm perpendicular return, and (bottom) total 1064 nm return. (from Winker, Hunt, & McGill, 2007).....	29
Figure 12.	CALIOP transmitter and receiver subsystems (from Winker, Hunt, & Hostetler, 2004)	31
Figure 13.	LOLA Redundant Transmitters (from Riris et al., 2010).....	32
Figure 14.	LOLA Payload Five Spot Ground Pattern (from Riris et al., 2010)	33
Figure 15.	GLAS Instrument Cut-Away View (from Abshire, 2010)	34
Figure 16.	ICESat-2 Instrument Overview (from NASA: ICESat-2, 2013)	36
Figure 17.	ICESat-2 Mission Overview (from NASA: ICESat-2, 2013)	37
Figure 18.	Parametric Cost Model Development Process (from Guerra, 2008)...	44
Figure 19.	Average NASA Small Spacecraft Mission Cost Breakout (from Guerra, 2008)	45
Figure 20.	NASA's Small Satellite Weight-Based Cost Model Inputs (from Guerra, 2008)	46
Figure 21.	NASA's Weight-Based Cost Curves (from Guerra, 2008)	47
Figure 22.	MOPA Laser Architecture in Development for ATLAS (from Yu et al., 2010)	57
Figure 23.	LOLA Diffractive Optical Element (from Ramos-Izquierdo et al., 2009)	60
Figure 24.	Fast Steering Mirror Exploded View (from Applied Technology Associates, 2011).....	60
Figure 25.	Solar Background Irradiance	63

Figure 26.	Pre and Post-Irradiation Curves for Spectrolab GmAPD (from Becker et al., 2007)	64
Figure 27.	LIDAR Link Budget Variables (from Burton, 2002)	66
Figure 28.	Iridium NEXT 32x32 Array Payload Power Design Trades.....	78
Figure 29.	Iridium NEXT 32x32 Array Payload Mass Design Trades	78
Figure 30.	Iridium NEXT 32x32 Array Payload Mass Versus Aperture Diameters	79
Figure 31.	10% Duty Cycle Iridium NEXT 10x10 Array Payload Power Design Trades	80
Figure 32.	10% Duty Cycle Iridium NEXT 10x10 Array Payload Mass Design Trades	80
Figure 33.	10% Duty Cycle Iridium NEXT 10x10 Array Payload Mass Versus Aperture Diameters	81
Figure 34.	10% Duty Cycle Iridium NEXT 10x10 Array Payload Mass Versus Volume Designs	82
Figure 35.	Low-Cost Payload 32x32 Array Mission Cost Versus Number of Transmitters (Aperture-Based Cost Estimate).....	89
Figure 36.	Low-Cost Payload 32x32 Array Mission Cost Versus Number of Transmitters and Standard Buses	90
Figure 37.	Mid-Cost Payload 32x256 Array Mission Cost Versus Number of Transmitters (Aperture-based Cost Estimate)	94
Figure 38.	Mid-Cost Payload 32x128 Array Mission Cost Versus Number of Transmitters (Aperture-based Cost Estimate)	95
Figure 39.	Mid-Cost Payload 32x128 Array Mission Cost Versus Number of Transmitters and Standard Buses	96

LIST OF TABLES

Table 1.	Estimated Annual Dollar Benefit from Enhanced Elevation Data (from Dewberry, 2012).....	13
Table 2.	Topographic Data Quality Levels (from Dewberry, 2012).....	14
Table 3.	Average Cost of Airborne LIDAR (from Dewberry, 2012).....	15
Table 4.	Cost-Benefit Ratios and Benefits for USGS LIDAR at Varying Quality Levels and Frequencies (from Dewberry, 2012).....	16
Table 5.	Combined NASA and USGS LIDAR Objectives	17
Table 6.	532-nm Single Photon Sensitive Detectors (from Krainak et al., 2010)	38
Table 7.	1064-nm Single Photon Sensitive Detectors (from Krainak et al., 2010)	39
Table 8.	NASA's Complexity Factors for Cost Modeling (from Guerra, 2008) ..	48
Table 9.	Standard Bus Providers for NASA.....	50
Table 10.	Standard Bus Providers for NASA Continued	51
Table 11.	Launch Vehicle Costs.....	52
Table 12.	Previous Commercially Hosted Payloads (from Andraschko, Antol, Horan, and Neil, 2011)	53
Table 13.	Iridium NEXT Hosted Payload Parameters (after Richard, Le Roy, Thouvenot, and Escudier, 2008)	54
Table 14.	Yb-Doped Tiled and Tapered Fiber Lasers Predicted Performance...	70
Table 15.	Utah State University's FSM Performance Characteristics (after Wassam et al., 2006).....	71
Table 16.	Estimated GmAPD Receiver Performance Characteristics	72
Table 17.	Iridium NEXT Payload Options Performance and Margin.....	83
Table 18.	Iridium Fulfillment of NASA and USGS LIDAR Objectives	85
Table 19.	Low-Cost Satellite Payload and Bus Performance and Margin	91
Table 20.	Low-Cost Free-Flyer Fulfillment of NASA and USGS LIDAR Objectives.....	92
Table 21.	Mid-Cost Satellite Payload and Bus Performance and Margin	97
Table 22.	Mid-Cost Free-Flyer Fulfillment of NASA and USGS LIDAR Objectives.....	98
Table 23.	Hosted, Low-Cost and Mid-Cost LIDAR Payload Parameters.....	102

THIS PAGE INTENTIONALLY LEFT BLANK

LIST OF ACRONYMS AND ABBREVIATIONS

3-D	Three Dimensional
AlGaAs	Aluminum Gallium Arsenide
ALIRT	Airborne Ladar Imaging Research Testbed
ATLAS	Advanced Topographic Laser Altimeter System
BMDO	Ballistic Missile Defense Organization
CALIPSO	Cloud-Aerosol Lidar and Infrared Pathfinder Satellite Observations
CALIOP	Cloud-Aerosol Lidar with Orthogonal Polarization
CE90	Circular Error 90th Percentile
CHIRP	Commercially Hosted Infrared Payload
Cr	Chromium
DDT&E	Design, Development, Test and Evaluation
DEM	Digital Elevation Model
DOE	Diffractive Optical Element
FSM	Field Steering Mirror
GaInAsP	Gallium Indium Arsenide Phosphide
GAO	Government Accountability Office
GEO	Geostationary Equatorial Orbit
GLAS	Geoscience Laser Altimeter
GmAPD	Geiger-Mode Avalanche Photo-Detector
HALOE	High Altitude Lidar Operations Experiment
Hz	Hertz
ICESat	Ice, Cloud and Land Elevation Satellite
IFOV	Instantaneous Field of View
InP	Indium Phosphide
Kg	Kilograms
LASER	Light Amplification by Stimulated Emission
LE90	Linear Error 90 th Percentile
LIDAR	Light Detection and Ranging

LITE	LIDAR In-Space Technology Experiment
LOLA	Lunar Orbiter Laser Altimeter
MABEL	Multiple Altimeter Beam Experimental Lidar
MGS	Mars Global Surveyor
MESSENGER	Mercury Surface, Space Environment, Geochemistry and Ranging
MLA	Mercury Laser Altimeter
MOLA	Mars Orbiter Laser Altimeter
MOPA	Master-Oscillator Power Amplifier
NASA	National Aeronautics and Space Administration
Nd:YAG	Neodymium-Doped Yttrium Aluminum Garnet
Nd:YVO ₄	Neodymium-Doped Yttrium Orthovanadate
NAS	National Academy of Sciences
NEAR/ELR	Near Earth Asteroid Rendezvous
NEEA	National Enhanced Elevation Assessment
NOAA	National Oceanic and Atmospheric Administration
NRC	National Research Council
OTA	Optical Telescope Assembly
PAMELA	Payload for Antimatter Matter Exploration and Light-nuclei Astrophysics
PDR	Preliminary Design Review
PMT	Photon Multiplier Tube
SBIRS	Space-Based Infrared System
SiAPD	Silicon Avalanche Photodiode
SPCM	Single Photon Counting Module
SRTM	Shuttle Radar Topography Mission
TRL	Technology Readiness Level
USGS	United States Geological Survey
W	Watts

ACKNOWLEDGMENTS

Disce quasi semper victurus vive quasi cras moriturus.

—Mohandas Gandhi

Thank you. Thank you to all of the people that helped me through the better part of a decade it took to get to this point. To the U.S. Air Force for sponsoring me and all the amazing professors at the Naval Postgraduate School, thank you for expanding my mind and experiences. To all my bosses, thank you for putting up with some of the missed days and late mornings while I worked through this degree. A special thanks to the department, which was understanding though the multiple extensions and extenuating circumstances. To my advisors, Dr. Olsen and Dr. Durham, thank you for taking the time to guide me through this process. Your knowledge and insight has been invaluable.

To my mother and father, thank you for getting me to this point. You have instilled such great values into me. I could not have asked for any greater parents. You were THE driving factor throughout my life, pushing me to be the best person I could be. At times it was frustrating, since I know I was a stubborn child, but much of this is thanks to you.

And to my love, my wife, Nikki, thank you for putting up with my procrastination, the long weekends and for pushing me through the finish line. I cannot express how grateful I am for what you have done for me day in and day out. Your motivating spirit and help through the editing and occasional dry spell has led to this point. ...I know, finally.

And with that being said, it is on to the next challenge. For if there is anything that you all have taught me, it is to not stop learning, to not stop questioning, to not stop striving to be better than I am today. Thank you.

THIS PAGE INTENTIONALLY LEFT BLANK

I. INTRODUCTION

A. PURPOSE

Optical remote sensing can be divided into a number of different categories to include active and passive systems. Passive systems collect light from uncontrolled and often natural sources such as the sun or other lighting elements at the focus of the system. Active systems produce their own light through diodes, lasers or other apparatus that are controlled by the user. Light Detection and Ranging (LIDAR) is a form of optical remote sensing that has existed for roughly 50 years, having been used for ranging, spectroscopy and a host of other purposes. LIDAR has also been widely used to create very accurate 3-D models and provide direct vertical measurements with low circular and linear error (CE90/LE90). This thesis identifies how recent advancements in lasers and sensitive photon counting sensors, which have been demonstrated in airborne platforms, may be applied to space-borne missions to enable low-cost solutions for global 3-D mapping. In the NASA sponsored decadal survey produced by the National Academy of Sciences, LIDAR was highlighted as a key area that provides data for a number of high priority Earth Sensing Missions. Beyond NASA's requirements, LIDAR from airborne platforms has provided key data for earthquake response, urban planning, flood plain analysis and a variety of other disaster planning and relief efforts. New technologies may decrease the cost enough to allow for a number of viable platforms that can provide consistent and continuous monitoring of the effects of climate change on ice sheet elevation seasonal variations, forest density changes for assessing carbon sequestration values, and would enable the creation of more detailed 3-D maps of the world that can aid in planning and disaster response.

This thesis will provide analysis of launch vehicles, standard buses, optical and payload technologies to determine a number of low cost options for a space-based LIDAR mission. Tradeoffs will be made to determine minimum achievable

links depending on mission duration, orbital regimes and area coverage rates with an eye towards mission utility.

B. RESEARCH QUESTIONS

What low- and mid-cost (<\$250M & <\$500M) LIDAR satellite options are possible while still able to close a low-earth orbit link with a lifetime of five years or greater?

What are the capabilities of these systems and can they fulfill the NASA's ICESat-2 requirements?

Could the LIDAR satellite provide useful data for other missions such as USGS's 3D Elevation Program?

C. BENEFITS OF STUDY

This thesis examines three low-cost options for a space-based 3D LIDAR as the follow-on to National Aeronautics and Space Administration's (NASA) ICESat-2 Mission. These low-cost options will examine tradeoffs in advanced transmitter and receiver technologies paired with low-cost standard buses and launch vehicles to address the need for advanced elevation models, foliage penetration measurements and other requirements outlined in NASA and United States Geological Survey's (USGS) processes. These options will help identify recent advancement in receiver and transmitter technology and perform trades to enable a lower cost and potentially more capable ICESat-2 follow-on to address a number of missions of benefit to the remote sensing scientific community.

D. TYPES OF LIDAR

LIDAR refers to a broad area of active remote sensing that relies on the manipulation of light to remotely interrogate a material. Under this umbrella are a number of sub-categories that address different areas of study and rely on a different property of light. The main interactions materials have with light are absorption, fluorescence and scattering and are wavelength dependent.

Absorption is the attenuation of light by a material, whereas a portion of light is absorbed and not re-emitted. Fluorescence occurs when a material absorbs light but a portion of that light is re-emitted at a different frequency due to material properties. Scattering is a process where light is reflected from a material and is dependent on the material size, composition and roughness. The scattering process may be elastic with no change in wavelength after scattering or inelastic where a change in wavelength occurs due to the material's properties. This paper will rely on the properties of elastic scattering for an elastic LIDAR payload build and design. This is due to the size of objects being imaged (equal to the wavelength of the laser), the high reflected signal needed to achieve a link from space, and the inclusion of only an altimetry mission vice material identification.

Elastic LIDAR is based upon Mie scattering properties that involve objects equal in wavelength to the light source. These objects also do not change the wavelength of the reflected light. "Since Mie scattering has the largest cross section and a narrow bandwidth, this technique is the most sensitive and thus has the longest detection range" (Burton, 2002, p. 12). Using time gating, as most laser altimetry systems do, an elastic LIDAR system can measure the time-of-flight for a set of photons and determine a very accurate range estimate. With light being a much shorter wavelength than the radio frequencies in RADAR, LIDAR also has the advantage of being able to penetrate dense foliage through the spaces between leaves and return photons and multiple range gates, allowing for vertical measurement of objects under canopy. With these advantages elastic LIDARs have been flown on multiple airborne and space-borne platforms to demonstrate their ability to efficiently collect altimetry measurements for a variety of missions.

THIS PAGE INTENTIONALLY LEFT BLANK

II. LIDAR OBJECTIVES AND REQUIREMENTS

Direct Detect LIDAR systems provide a unique dataset due to their very short wavelengths in comparison to RADAR, interferometric synthetic aperture RADAR and other modes of collecting elevation data. While LIDAR remains a lower area collection rate platform in comparison to other modalities, the need for high fidelity elevation measurements has garnered both national and international government, nonprofit and for-profit support. The National Academies of Science (NAS) and the United States Geological Survey (USGS) both commissioned studies that pointed towards the benefits of high fidelity elevation measurements beyond what is currently available. The NAS performed the survey in support of future NASA Earth observing satellites, while the USGS looked at the benefits of terrain elevation data for the nation and its cost saving capabilities for government, non-government organizations and commercial applications. This chapter is divided into two sections that cover objectives levied on NASA by NAS's Decadal Survey and the USGS's objectives.

A. NASA OBJECTIVES

Understanding the complex, changing planet on which we live, how it supports life, and how human activities affect its ability to do so in the future is one of the greatest intellectual challenges facing humanity. It is also one of the most important for society as it seeks to achieve prosperity and sustainability. (National Research Council, 2007, p. 1)

In 2004, NASA, NOAA, and the USGS asked the National Research Council to conduct a decadal survey of the Earth sciences community. The charge was to recommend a prioritized list of flight missions and supporting activities for space-based Earth observation over the next decade (through the 2010s) and to identify key factors in planning for the decade beyond (into the 2020s). (Henson, 2008, p. 1)

In the decadal survey, the National Research Council (NRC) came to consensus on a number of key issues the next generation of Earth observing satellites should tackle, of which LIDAR was slated as a key technology to

provide insight into many of these issues. The scientific questions and requirements posed to future LIDAR systems centered around five major themes: glacier and sea ice thickness, vegetation and biomass measurements, topography, hydrology and atmospheric measurements.

Science Goals	Science Requirements	Measurement Requirements	Instrument Functional Requirements	Mission Functional Requirements
<u>Ice Sheets</u> Quantify polar ice sheet mass balance to determine contributions to current and recent sea level change and impacts on ocean circulation Determine seasonal cycle of ice sheet changes Determine topographic character of ice sheet changes to assess mechanisms driving that change and constrain ice sheet models	Annual elevation change of 0.2 cm/yr over entire ice sheet Surface elevation change of 25 cm/yr annually in 100 km ² areas and along linear distances of 1 km Resolve winter and summer ice sheet elevation change to 2.5 cm over 25x25 km ² areas Continuous observations through for at least 5 years Direct comparability to ICESat-I measurements for 15-year dh/dt	Ability to penetrate optically thin clouds Precise repeatability of ground tracks Repeat sampling 4x per year, uniformly spaced in time Slope information in the cross-track direction Continuous measurements for no less than 5 years	4.5 m pointing knowledge 5 years continuous operation with 7-year goal Measurement capability in the cross-track direction within the vicinity of the primary beam Surface reflectivity capability of 5% to enable characterization of snow conditions for gain and range corrections Telescope FOV of 100 m (160 µrad) or better to minimize atmospheric forward-scattering effects Atmospheric vertical resolution of 75 km to enable atmospheric corrections plus studies of clouds	Orbit parameters comparable to those of ICESat (600 km altitude; 94 deg. incl., 91-day repeat). 10 arcsec (30-m) pointing control 1.5 arcsec (4.5-m) pointing knowledge 2 cm radial orbit accuracy requirement 5 year continuous operation with 7-year goal
<u>Sea Ice</u> Estimate sea ice thickness to examine ice/ocean/atmosphere exchanges of energy, mass and moisture	Discriminate freeboard from surrounding ocean level to within 3 cm Capture seasonal evolution of sea ice cover on 25 x 25 km scales	Vertical precision of <2 cm between leads and sea ice freeboard height Monthly near-repeat coverage of Arctic and Southern Oceans at 25 x 25 km scales Coverage up to at least 86 deg. latitude		91 day repeat orbit to capture seasonal effects and maximize comparability to ICESat for trend detection
<u>Vegetation</u> Estimate Large Scale Biomass in Support of DESDynI Science Requirements	Produce a global vegetation height surface with 3-m accuracy at 1-km resolution	Ability to point between nadir ground tracks on every ascending and descending pass to fill in gaps between tracks every km over non-ice-covered land		

Figure 1. NASA's ICESat-2 Implementation Requirements Flowdown (from Abdalati et al., 2010)

1. Glacier, Sea Ice and Ice Sheet Thickness

Mass balance of Earth's great ice sheets and their contributions to sea level are key issues in climate variability and change. The relationships between sea level and climate have been identified as critical subjects of study in the Intergovernmental Panel on Climate Change assessments, the Climate Change Science Program strategy, and the U.S. International Earth Observing System. Because much of the behavior of ice sheets is manifested in their shape, accurate observations of ice elevation changes are essential for understanding ice sheets' current and likely contributions to sea-level rise. (National Research Council, 2007, p. 271)

The launch of ICESat-1 in 2003 in addition to other missions over the polar cryosphere have helped inform the scientific community about the impact of climate change over the past decade. With nearly 75% of the Earth's freshwater contained in ice sheets and glaciers, scientists and climatologists have examined the extent of ice loss and potential effects on the environment and society. Past data suggests that "The Greenland and Antarctic ice sheets are losing mass at an increasing rate [1]–[3]... The sea ice that covers the Arctic Ocean has decreased in areal extent far more rapidly than climate models have predicted [8] and has thinned substantially [9], suggesting that a summertime ice-free Arctic ocean may be imminent" (Abdalati et al., 2010, p. 736).

The requirements placed on ICESat-2 build upon lessons learned from measurements taken from the ICESat-1 mission. An assessment of the ICESat-1 data showed that the accuracy of its thickness measurements were within half a meter of measurements based upon submarine sonar and ocean moorings (Abdalati et al., 2010). To improve this even further scientists gathered for the ICESat-2 Workshop where they set priorities in three major sea ice areas: "Improve current knowledge of mean and variability of the ice thickness distribution of the polar oceans, provide long-term monitoring to determine trends in ice thickness, and refine the estimates of sea ice outflow into the Northern Atlantic" (NASA, 2007, p. 12). To accomplish these missions, more stringent requirements were needed, driving the ICESat-2 mission to a 2-cm range

precision (satellite-to-surface) and a pointing knowledge of less than 2 arcseconds (equating to roughly six meters horizontally). The added pointing and range precision combined with a longer expected lifetime and continuous campaigns (versus the 33-day campaigns on ICESat-1 due to laser issues) will enable seasonal ice sheet measurement accuracies of ± 2 cm and yearly accuracies of ± 1 cm/year. Overall, these numbers equate to an uncertainty of about ten percent of the annual ice sheet mass interchange with the ocean, resulting in an accuracy of ± 1 mm/year of sea level rise (NASA, 2007).

2. Vegetation and Biomass

The horizontal and vertical structure of ecosystems is a key feature that enables quantification of carbon storage, the effects of disturbances such as fire, and species habitats. The above ground woody biomass and its associated below ground biomass store a large pool of terrestrial carbon. Quantifying changes in the size of this pool, its horizontal distribution, and its vertical structure resulting from natural and human-induced perturbations such as deforestation and fire, as well as the recovery processes, is critical for quantifying ecosystem change. (National Research Council, 2007, p. 191)

In addition to studying the cryosphere, NASA's Decadal Survey and the ICESat-2 Workshop identified the need to study changes in biomass ecosystem structure to estimate land carbon storage. The carbon contained in Earth's forest canopies account for roughly 85% of all aboveground biomass, playing a significant role in terrestrial carbon stocks. Due to the dynamic nature of forest carbon stocks (e.g., fire, logging, regrowth, disease), three-dimensional measurements of the structure of forests and their canopy heights are needed to accurately estimate varying biomass and carbon stocks and better understand the carbon cycle. "These measurements include vegetation height; the vertical profile of canopy elements (i.e., leaves, stems, and branches); and/or the volume scattering of canopy elements. Such measurements are critical for reducing uncertainties in the global carbon budget" (NASA, 2007, p. 14). Three-dimensional measurements of vegetation are also important for the mapping of

forest disease and pest outbreaks, and to characterize animal habitats and biodiversity changes due to anthropogenic disturbances. Requirements for the ICESat-2 mission have been increased over those of ICESat-1 to help answer many of the questions surrounding these issues. The specific vegetation requirement of a three-meter vertical accuracy with a 1 km spatial resolution of the Earth's canopy was taken from a more stringent set of requirements from the Vegetation Structure Science Working Group:

...statistically rigorous sampling of height and profiles and/or contiguous global coverage over a 3-year period ... maximum vertical height measurement accuracy ~1m, vertical resolution of canopy profile, 2–3 m, 25 m spatial resolution or better in a sampling mode; aboveground biomass and changes including disturbance; spatial resolution ~100 m to 1 km for contiguous biomass." (NASA, 2007, p. 15)

3. Topography

Earth's surface is dynamic in the literal sense: it is continually being shaped by the interplay of uplift, erosion, and deposition as modulated by hydrological and biological processes. Surface topography influences air currents and precipitation patterns and controls how water and soil are distributed across the landscape... And it influences how natural hazards, such as landslides, floods, and earthquakes, are distributed across the landscape. (National Research Council, 2007, p. 119)

While only a tertiary mission for the ICESat-2 spacecraft, advanced topographic information from LIDAR systems is valued due to the lack of high-resolution data currently available. Worldwide topographical maps generated by the Shuttle Radar Topography Mission remain the main dataset for terrain maps and only have post-spacing of 30 to 90 meters. At this resolution, multiple features are obscured that are beneficial to understanding and calculating surface topographic effects for a number of phenomena (as can be seen in Figure 2). Higher resolution data at 5-m post-spacing and sub-10cm precision would enable advanced analysis of a number of geological, topographical and geomorphological processes to include prediction of potential landslides, floods, tsunami effects, volcanic and mud flows and earthquakes. These predictions,

informed by advanced topographic data, would help in disaster mitigation, planning and relief operations that could save lives and money (National Research Council, 2007).

The events of the past few years, for example, the volcanic unrest of Mt. Saint Helens in 2004, the devastation of the December 26, 2004, Sumatra earthquake and resulting tsunami, the loss of life and destruction from the great Pakistan earthquake and associated landslides of 2005, and the chaos following Hurricane Katrina... demonstrate humankind's vulnerability to naturally occurring disasters. These events highlighted the costs associated with inadequate information and the consequences of inadequate planning for the dissemination of available or obtainable information. (National Research Council, 2007, pp. 223–4)

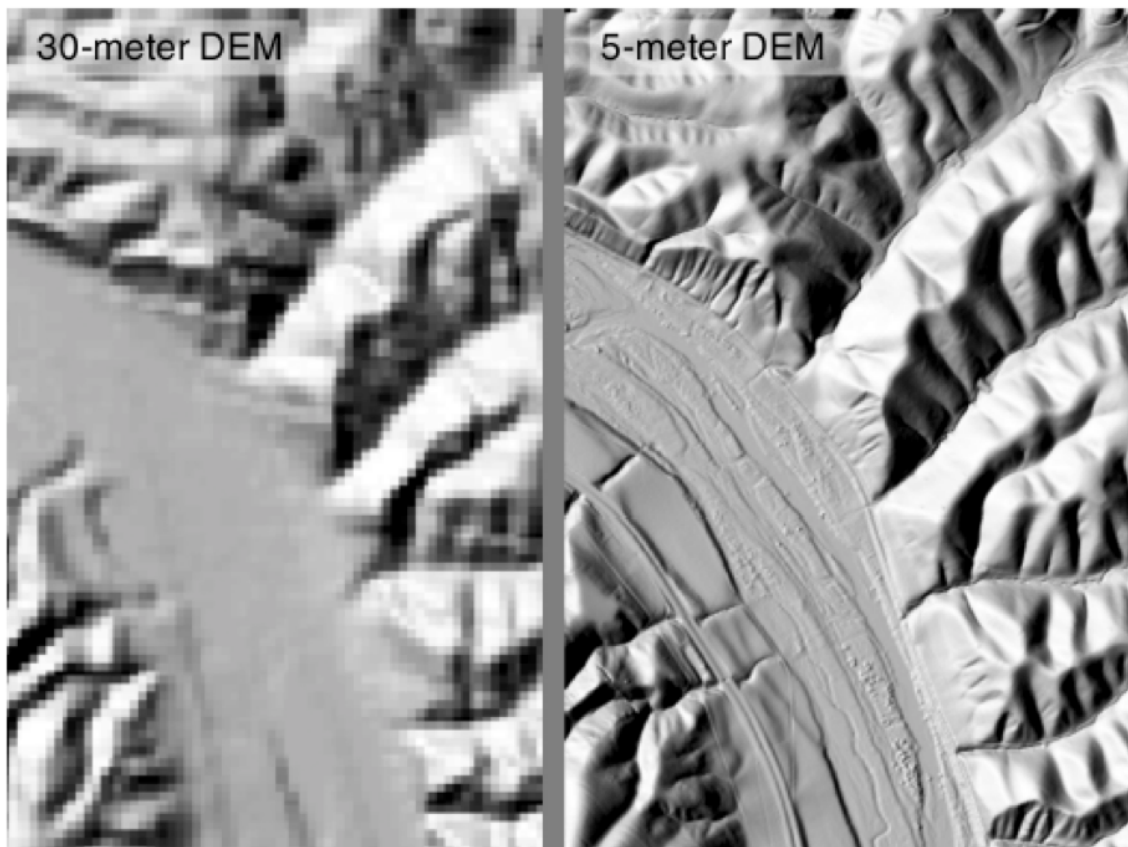


Figure 2. DEM Comparison of California's Salinas River (from National Research Council, 2007)

4. Hydrology and Atmospheric Sensing

Two additional missions for ICESat-2 that have also been levied on past and future LIDAR systems are the monitoring of hydrological and atmospheric phenomenon. Specifically, measurements of lakes and reservoirs at 10-cm vertical accuracy in 1-week intervals would generate “improved knowledge of global water cycle science and also enhance decision making in a number of applications including water resources, agriculture, disaster management, and public health” (NASA, 2007, p. 18). For atmospheric science, ICESat-1 demonstrated the utility of the 1064-nm channel at detecting a number of important characteristics to include: “polar clouds and haze, global pollution aerosols, planetary boundary layer height, [and] global cloud change monitoring” (NASA, 2007, p. 18). While the ICESat-II Workshop and other groups provided no requirements in regards to atmospheric monitoring, it remains a potential capability for future LIDAR-based system to include ICESat-2.

B. USGS'S NATIONAL ENHANCED ELEVATION ASSESSMENT

For much of the nation, professionals in a broad range of critical fields find themselves lacking the right data to perform their missions. Today, federal agencies, states, local governments, tribes and nongovernmental users (not-for-profit and private businesses) are grappling with maps created from elevation data that are mostly 30–50 years old and far less detailed than is needed. (Dewberry, 2012, p. 34)

In December of 2011, the USGS sponsored the National Enhanced Elevation Assessment (NEEA) “[t]o develop strategies to better meet national elevation data needs... (1) document national-level requirements for improved elevation data, (2) estimate the benefits and costs of meeting those requirements, and (3) evaluate new, national-level elevation program models” (Snyder, 2013, p. 105). The study reached a number of conclusions about the benefits of enhanced elevation data to public, private and nonprofits, having determined a potential benefit of \$13 billion annually. The participants included a variety of government and non-governmental organizations that documented 602

mission-critical activities that require more accurate data than is available today. Among these activities are optimized precision agriculture, flood risk analysis, improved navigation for airborne and terrestrial assets, wildfire prevention and mitigation, wind farm planning and optimization and fuel consumption reduction for vehicles. Table 1 describes the top 27 business uses for enhanced elevation data aligned with these mission-critical activities surveyed, describing both the conservative and potential annual benefits.

BU#	BU Name	Enhanced Elevation Data Annual Benefits	
		Conservative Benefits	Potential Benefits
14	Flood Risk Management	\$294.706M	\$501.576M
21	Infrastructure and Construction Management	\$206.212M	\$941.951M
1	Natural Resources Conservation	\$159.225M	\$335.152M
8	Agriculture and Precision Farming	\$122.330M	\$2,011.330M
2	Water Supply and Quality	\$85.288M	\$156.351M
16	Wildfire Management, Planning and Response	\$75.700M	\$158.950M
9	Geologic Resource Assessment and Hazard Mitigation	\$51.750M	\$1,066.750M
5	Forest Resources Management	\$43.949M	\$61.655M
3	River and Stream Resource Management	\$38.422M	\$86.582M
20	Aviation Navigation and Safety	\$35.000M	\$56.000M
4	Coastal Zone Management	\$23.785M	\$41.740M
11	Renewable Energy Resources	\$10.050M	\$100.050M
12	Oil and Gas Resources	\$10.000M	\$100.000M
17	Homeland Security, Law Enforcement, Disaster Response	\$9.975M	\$126.469M
15	Sea Level Rise and Subsidence	\$5.780M	\$21.660M
22	Urban and Regional Planning	\$4.197M	\$68.569M
10	Resource Mining	\$1.686M	\$4.864M
7	Wildlife and Habitat Management	\$1.510M	\$4.020M
25	Education K-12 and Beyond	\$0.264M	\$2.264M
18	Land Navigation and Safety	\$0.191M	\$7,124.875M
27	Telecommunications	\$0.185M	\$1.850M
26	Recreation	\$0.050M	\$0.050M
13	Cultural Resources Preservation and Management	\$0.000M	\$7.000M
23	Health and Human Services	\$0.000M	\$1.000M
19	Marine Navigation and Safety	\$0.000M	\$0.000M
24	Real Estate, Banking, Mortgage, Insurance	\$0.000M	\$0.000M
6	Rangeland Management	\$0.000M	\$0.000M
Total Estimated Annual Dollar Benefits		\$1,180.224M	\$12,980.707M

Table 1. Estimated Annual Dollar Benefit from Enhanced Elevation Data
(from Dewberry, 2012)

“For most of the past century, Americans have relied upon paper topographic quadrangle maps from USGS to visualize the 3-D shape of the

topography by human interpretation of contour lines manually compiled by labor-intensive photogrammetric processes" (Dewberry, 2012, p. 1). LIDAR has significantly changed the way USGS has derived high-resolution elevation data for public use. Currently the National Elevation Dataset (NED) contains LIDAR over roughly 28 percent of the lower 49 states and continues at a rate of 2–3 percent per year. At this rate, full U.S. coverage is anticipated to take 35 years, negating the full benefits outlined in the study and spurring on the need for a comprehensive plan to address the nation's enhanced elevation needs.

Airborne LIDAR and Interferometric Synthetic Aperture RADAR (IFSAR) are the most widely used methods used to collect high-resolution elevation data. In Table 2 the quality levels defined in the USGS NEEA are shown to describe post spacing, vertical resolution and contour accuracy. These quality levels (QLs) were then used to determine average costs for LIDAR collection over rectangular blocks greater than 5,000 square miles. The average cost (in FY11 dollars) per square mile can be seen in Table 3. Extrapolating from these numbers, the estimated total cost to cover the lower 48 states plus Hawaii would be: \$1.653B for QL1 LIDAR, \$1.01B for QL2 LIDAR, \$763M for QL3 LIDAR, \$487.8M for QL4 Imagery Digital Elevation Models (DEMs) and \$241M for QL5 IFSAR.

Elevation Quality Levels (QL)	Source	Horizontal Resolution Terms			Vertical Accuracy Terms	
		Point Density	Nominal Pulse Spacing (NPS)	DEM Post Spacing	Vertical RMSEz	Equivalent Contour Accuracy
QL 1	LiDAR	8 pts/m ²	0.35 m	1/27 arc-sec ~1 meter	9.25 cm	1-ft
QL 2	LiDAR	2 pts/m ²	0.7 m	1/27 arc-sec ~1 meter	9.25 cm	1-ft
QL 3	LiDAR	1 – 0.25 pts/m ²	1 – 2 m	1/9 arc-sec ~3 meters	≤18.5 cm	2-ft
QL 4	Imagery	0.04 pts/m ²	5 m	1/3 arc-sec ~10 meters	46.3 cm – 139 cm	5 – 15 ft
QL 5	IFSAR	0.04 pts/m ²	5 m	1/3 arc-sec ~10 meters	92.7 cm – 185 cm	10 – 20 ft

Table 2. Topographic Data Quality Levels (from Dewberry, 2012)

Per USGS LiDAR v13 Specifications	\$/mi ² for 500-1000 mi ²	\$/mi ² for 1000-5000 mi ²	\$/mi ² for >5000 mi ²
QL1 LiDAR per upgraded v13 specs	\$602.50	\$497.00	\$453.25
QL2 LiDAR per upgraded v13 specs	\$374.50	\$310.75	\$277.00
QL3 LiDAR per current v13 specs	\$291.50	\$238.00	\$209.25

Table 3. Average Cost of Airborne LIDAR (from Dewberry, 2012)

With the relatively high initial cost of LIDAR for high-quality DEMs and the additional recurring cost due to geological and anthropogenic changes, the NEEA examined multiple collection scenarios with varying benefits (Table 4). Furthermore, a cost-benefit ratio was calculated to determine the greatest return on investment aligned with varying quality levels and update frequencies. All annual update scenarios, regardless of the quality level, resulted in a net loss and negative cost-benefit ratio. High quality LIDAR with modest update rates have high net benefits but require large per year investments for airborne LIDAR collection, creating a lower cost-benefit ratio of 3 to 4. Only three collection scenarios have a high cost-benefit ratio of above 5 with a modest net benefit ranging from \$272M to \$548M. These scenarios suggest that a Quality Level of 2 or 3 (1-3 meter post spacing) with an update frequency of 6–10+ years is of the greatest benefit with the least investment (\$67M-\$126M per year).

The NEEA goes on to describe alternative scenarios with non-uniform quality levels and update frequencies in different sections of the U.S. but this coarse estimate provides enough top-level detail to determine potential requirements for a space-based system and the annual cost/area collection rate needed to realize these benefits. Extrapolating from the data, the requirements to map all 50 states with 6- or 10-year update frequencies would require annual collection rates of roughly 600,000 square miles per year and 360,000 square miles per year, respectively. This equates to 986 square miles per day at QL2 to realize a \$272M net benefit, 1,644 square miles per day at QL2 to realize a \$548M net benefit and 1,644 square miles per day at QL3 to realize a \$406M net benefit.

Option	Quality Level	Update Frequency	Annual Total Costs	Annual Total Benefits	Benefit/Cost Ratio	Net Benefits (Benefits - Costs)
1	1	Annual	\$1,646M	\$1,111M	0.674	(\$536M)
2	1	2-3 years	\$659M	\$1,110M	1.685	\$451M
3	1	4-5 years	\$366M	\$1,066M	2.914	\$700M
4	1	6-10 years	\$206M	\$800M	3.887	\$594M
5	1	>10 years	\$110M	\$403M	3.671	\$293M
6	2	Annual	\$1,006M	\$923M	0.917	(\$84M)
7	2	2-3 years	\$402M	\$922M	2.291	\$520M
8	2	4-5 years	\$224M	\$888M	3.970	\$664M
9	2	6-10 years	\$126M	\$674M	5.356	\$548M
10	2	>10 years	\$67M	\$339M	5.049	\$272M
11	3	Annual	\$760M	\$697M	0.917	(\$63M)
12	3	2-3 years	\$304M	\$696M	2.291	\$392M
13	3	4-5 years	\$169M	\$673M	3.983	\$504M
14	3	6-10 years	\$95M	\$501M	5.278	\$406M
15	3	>10 years	\$51M	\$252M	4.970	\$201M
16	4	Annual	\$487M	\$361M	0.741	(\$126M)
17	4	2-3 years	\$195M	\$360M	1.851	\$166M
18	4	4-5 years	\$108M	\$346M	3.198	\$238M
19	4	6-10 years	\$61M	\$256M	4.204	\$195M
20	4	>10 years	\$32M	\$129M	3.962	\$96M
21	5	Annual	\$241M	\$190M	0.788	(\$51M)
22	5	2-3 years	\$96M	\$190M	1.970	\$93M
23	5	4-5 years	\$53M	\$180M	3.365	\$126M
24	5	6-10 years	\$30M	\$131M	4.369	\$101M
25	5	>10 years	\$16M	\$66M	4.118	\$50M

Table 4. Cost-Benefit Ratios and Benefits for USGS LIDAR at Varying Quality Levels and Frequencies (from Dewberry, 2012)

The objectives and benefit analysis for both NASA and the USGS highlight the large impacts LIDAR data can have for the U.S. and the world. NASA's objectives are focused on challenges that affect the world from a climatology, hydrology and topography standpoint and do not contain cost benefit numbers. The objectives outlined for ICESat-2 describe the desired attributes of a space-based LIDAR system and are summarized in Table 5. USGS's objectives are based upon government, industry and nonprofit feedback on the benefits of enhanced elevation data, with an airborne cost-benefit analysis attached to differing quality levels and update frequencies. A subset of this is also summarized in Table 5 and will be used to evaluate the space-based LIDAR

systems described in this Thesis. Of note, an objective system for NASA would have 5-m post spacing (with at least 1 post-processed point per 5 m² area) and a 2-cm range resolution while maintaining a five-year mission lifetime. The objective refresh rate would be bi-annual for ice sheets, every three years for vegetation, variable for topography and weekly for hydrology measurements. For the USGS, the annual benefits vary with update frequencies and quality levels.

NASA Objectives				
Area of Study	Post-Spacing	Range Resolution	Refresh Rate / Area per year	Other Requirements
Ice Sheets	25 km	2 cm	.5 Years / 31.4M km ²	Pointing Control – 10 arcsec
Vegetation	25 m	1 m	3 Years / 13.17M km ²	Pointing Knowledge –
Topography	5 m	<10 cm	Unknown	1.5 arcsec
Hydrology	N/A	10 cm	Weekly / Negligible	5 Year Mission Lifetime
USGS Objectives				
Quality Level / Update Frequency	Post-Spacing	Range Resolution	Airborne Annual Cost	Estimated Annual Benefit
1 (Yearly)	5 m	46.3 cm	\$1,646 M	\$1,111 M
1 (2-3 Years)	5 m	46.3 cm	\$659 M	\$1,110 M
1 (4-5 Years)	5 m	46.3 cm	\$366 M	\$1,066 M
1 (6-10 Years)	5 m	46.3 cm	\$206 M	\$800 M
1 (>10 Years)	5 m	46.3 cm	\$110 M	\$403 M
2 (Yearly)	1 m	18.5 cm	\$1,006 M	\$923 M
2 (2-3 Years)	1 m	18.5 cm	\$402 M	\$922 M
2 (4-5 Years)	1 m	18.5 cm	\$224 M	\$888 M
2 (6-10 Years)	1 m	18.5 cm	\$126 M	\$674 M
2 (>10 Years)	1 m	18.5 cm	\$67 M	\$339 M
3 (Yearly)	0.7 m	9.25 cm	\$760 M	\$697 M
3 (2-3 Years)	0.7 m	9.25 cm	\$304 M	\$696 M
3 (4-5 Years)	0.7 m	9.25 cm	\$169 M	\$673 M
3 (6-10 Years)	0.7 m	9.25 cm	\$95 M	\$501 M
3 (>10 Years)	0.7 m	9.25 cm	\$51 M	\$252 M

Table 5. Combined NASA and USGS LIDAR Objectives

THIS PAGE INTENTIONALLY LEFT BLANK

III. HISTORY OF LIDAR IN SPACE

A number of methods have historically been developed and used to measure the distance to an object. Initial technologies included RADAR and research into microwave technologies. Limitations were identified due to the wavelength used and the need for higher frequencies to increase resolution and distance accuracy. As scientists and engineers continued to press to find solutions in the microwave domain, a key contribution to the field came on 6 August 1960 when Theodore Maiman “proposed a technique for the generation of very monochromatic radiation in the infra-red optical region of the spectrum” (Maiman, p. 494). The ability to generate narrow wavelengths of light led to the invention of the LASER or “Light Amplification by Simulated Emission of Radiation.” Shortly thereafter, Hughes Laboratories introduced the first LASER rangefinder, increasing the accuracy of the measurement of an object’s three dimensional position nearly 1000 times over radar systems of the same time period. Since then, these rangefinders have found their way into defense systems, video game consoles and golf pro shops around the world, and have paved the way for LIDAR mapping technologies.

With the invention of LIDAR for laser altimetry, LIDAR systems have found their way into multiple applications aboard ground vehicles, aircraft, helicopters, ships and even satellites. In the space environment, NASA has been a pioneer in developing laser rangefinders for docking and laser altimeters for measuring surface characteristics of different celestial bodies. NASA’s accomplishments in space-based LIDAR are numerous and range from Apollo 15 through the present day.

A. APOLLO LASER ALTIMETER

While ground, land and airborne LIDAR payloads were operated throughout the 1960s, it wasn’t until 1971 when the first laser altimeter was launched into space aboard Apollo 15. At a mass of 23 kg, the laser transmitter

utilized a mechanically Q-switched and flash pumped ruby laser. The design was based upon a military qualified rangefinder for tank applications and adapted to the rigors of space. With a pulse repetition frequency of 0.05 Hz, the payload mapped portions of the moon with a post spacing of 30 kilometers and accuracy of nearly 10 meters. The full collection only lasted for roughly 5,000 shots, but the Apollo laser altimeter proved the worth of lasers for topographic applications (Masursky, Colton, El-Baz, & Doyle, 1978).



Figure 3. 1971 Apollo Laser Altimeter (from Abshire, 2010)

B. CLEMENTINE

The laser community continued to make advances in advanced lasing mediums, eventually replacing the ruby laser with a number of other solid-state and new chemical vapor lasers. Due to the difficulty of ruggedizing a chemical vapor laser for space due to launch survival and outgassing issues, solid-state lasers (primarily Nd:YAG) gained greater traction in the space LIDAR community. The Nd:YAG laser continues to be the standard for space-based solid-state LIDAR lasers, introduced during the Clementine and NEAR missions and having demonstrated roughly 600,000 and 11 million shots, respectively (Neumann, 2001).

The first space-based use of Nd:YAG lasers occurred on the Clementine mission, launched on 25 January 1994. The mission was a joint venture between Ballistic Missile Defense Organization (BMDO) and NASA, and sought to demonstrate new spacecraft systems and technologies in a high-radiation, lunar orbit, as well as provide detailed topographic, altimetry and multispectral data of the moon. One of the new technologies on-board was the Nd:YAG miniature LIDAR. Clementine's laser altimeter performed substantially better than Apollo missions 15, 16, and 17, whose ruby laser only lasted roughly 7,080 shots over all three missions. Clementine saw a two orders of magnitude improvement over Apollo's ruby lasers, firing for roughly 600,000 shots (Neumann, 2001).

Clementine's LIDAR payload consisted of a diode-pumped Cr:Nd:YAG laser operating at both 1064nm (ranging) and 532nm (active imaging) and a silicon avalanche photodiode (SiAPD). In a 425km x 8300 km highly elliptical polar orbit, the 1.1 kg payload collected data every 2 km along-track (Spudis, 1994). The spot size or instantaneous field of view (IFOV) was 100 meters with a 90-meter vertical accuracy and 40-meter range resolution (Neumann, 2001). The laser operated at 1 Hz with a 10-nanosecond pulse-width providing 180 mJ per pulse or with a thermal-limited burst rate of 400 pulses at 8 Hz. Though the vertical precision and accuracy of the Clementine LIDAR system was relatively poor, the improvement of Nd:YAG laser lifetimes and reduced mass over that of the Apollo ruby lasers paved the way for future Nd:YAG-based LIDAR systems in space (Sorensen & Spudis, 2005).

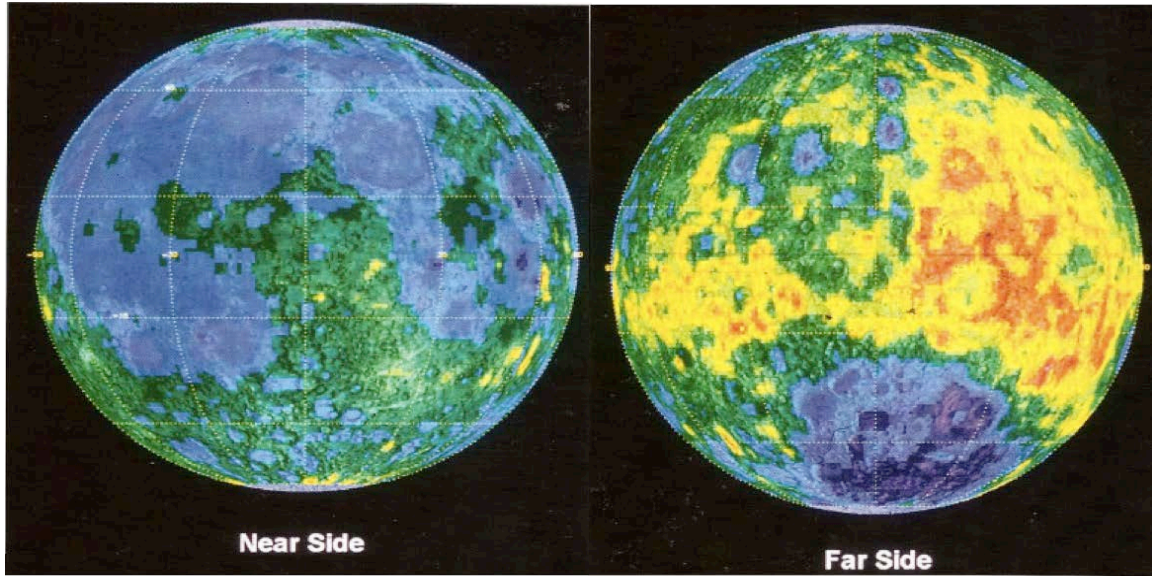


Figure 4. Clementine LIDAR Topographic Map of the Lunar Surface (from Spudis, 1994)

C. LIDAR IN-SPACE TECHNOLOGY EXPERIMENT (LITE)

The same year Clementine launched on a mapping mission of the moon, NASA launched the LIDAR In-space Technology Experiment to validate key technologies for space-based LIDAR missions and investigate Earth's atmosphere. The LITE development effort was started in 1985 and launched aboard the Space Shuttle on the STS-64 mission, operating between 9 and 20 September 1994. The LITE payload operated at three wavelengths (1064 nm, 532 nm and 355 nm) to detect and profile cloud and aerosol layers. After 53.6 hours of operation, 1.93 million shots were fired between two redundant lasers, providing unprecedented detail of the vertical structure of cloud layers and aerosols (Winker, D., Couch, R., & McCormick, P., 1996).

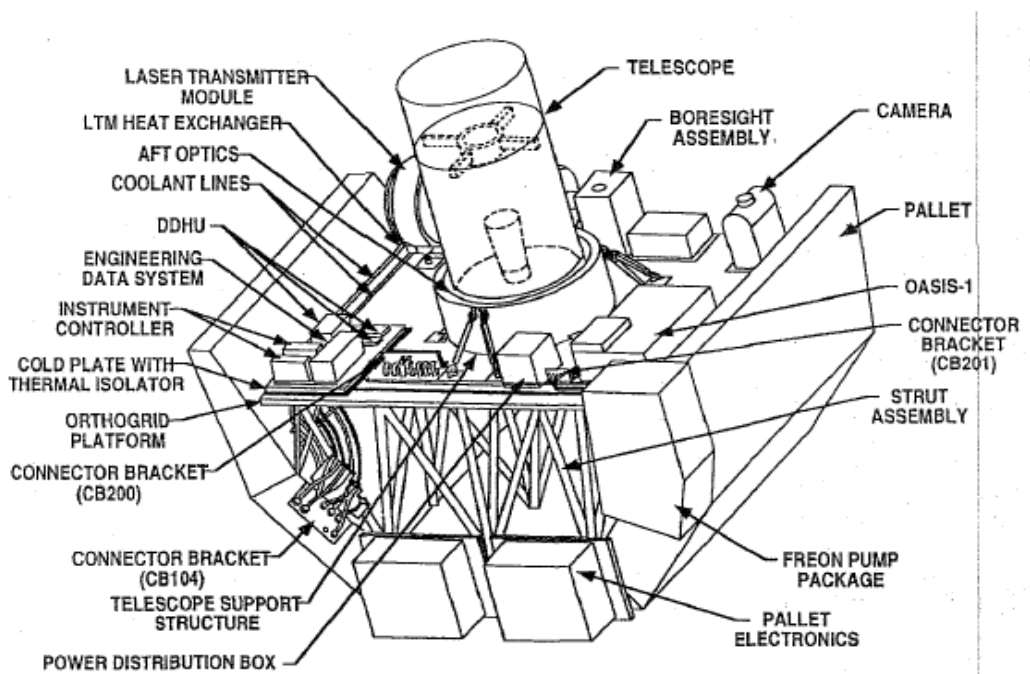


Figure 5. LITE Instrument in Flight Configuration (from Winker, Couch, & McCormick, 1996)

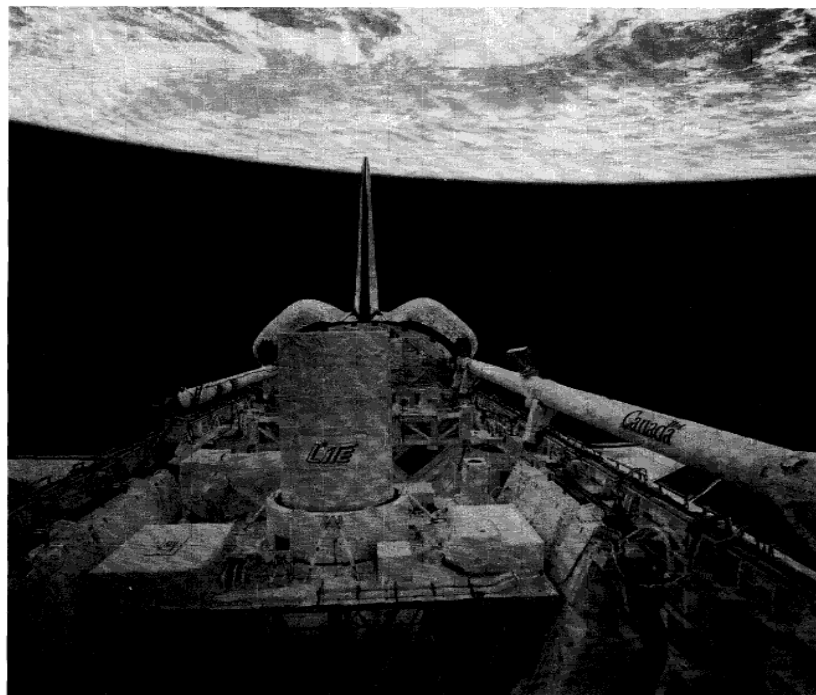


Figure 6. LITE Instrument On-orbit (from Winker, Couch, & McCormick, 1996)

The LITE payload consisted of two redundant Q-switched Nd:YAG flash lamp-pumped lasers that are frequency doubled and tripled to provide three distinct wavelengths for measurement. Three separate receivers collect photons through dichroic beam-splitter and a 1-meter parabolic aperture. In a 260-km circular orbit, the 990-kg, 3,100-W payload collected data every 740 meters along-track. The spot size or IFOV was 470 meters with a 15-meter range resolution. The transmitter design was a two stage Nd:YAG slab amplifier pumped by a flashlamp. This laser was then split and fed into a deuterated cesium dihydrogen arsenate and deuterated potassium dihydrogen phosphate crystal for frequency doubling and tripling, respectively. The laser operated at 10 Hz with a 27-ns pulse-width providing 470 mJ at 1064 nm, 530 mJ at 532 nm and 170 mJ at 355 nm per pulse for laser A. Laser B provided slightly different values of 440 mJ at 1064 nm, 560 mJ at 532 nm, 160 mJ at 355 nm. Lasers A and B successfully provided 1.16 million shots and 0.77 million shots, respectively, but did experience unanticipated degradation due to the outgassing and coating of optical components. Three receivers were used, each for a different frequency. Two PMTs were used to collect the 532 nm and 355 nm returns while an avalanche photodiode (APD) collected the 1064 nm returns. As the first LIDAR used solely for Earth observation, albeit temporary, the LITE mission provided considerable atmospheric and LIDAR hardware data for the scientific community, effectively maturing these technologies along with the Clementine mission (Winker et al., 1996).

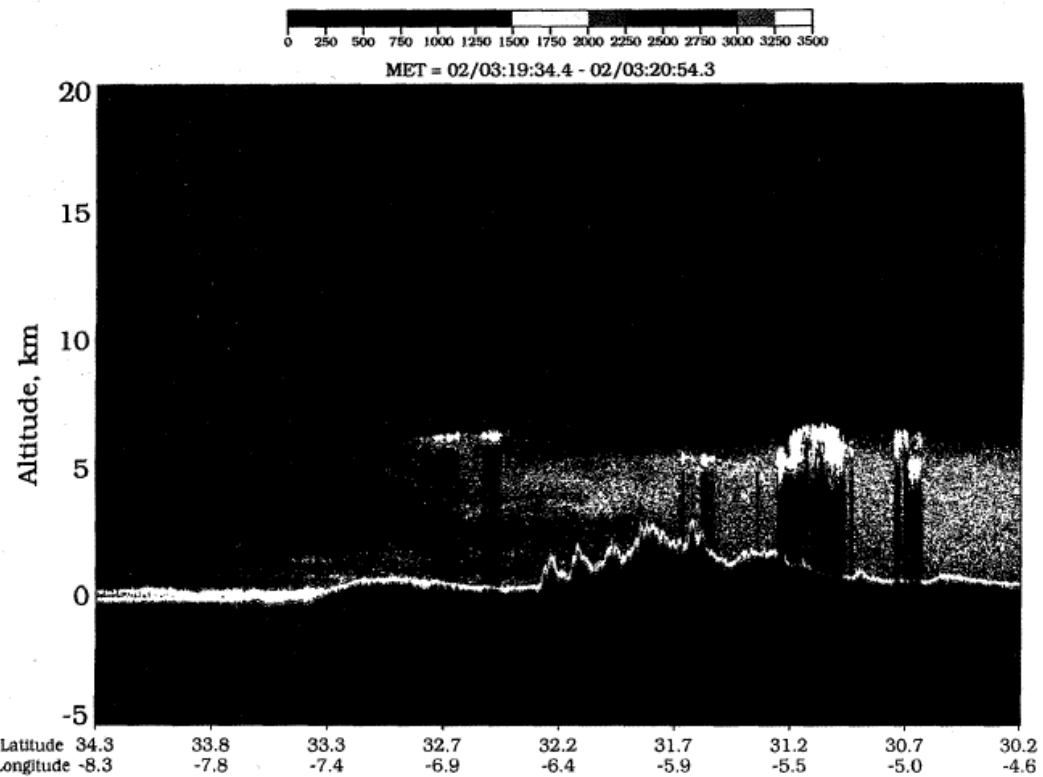


Figure 7. LITE Return Signal at 532nm over the Atlas Mountains and the Atlantic Coast of Morocco (from Winker, Couch, & McCormick, 1996)

D. MARS ORBITER LASER ALTIMETER (MOLA)

Continuing the fledgling tradition of Nd:YAG lasers for space-based LIDAR, their use was again demonstrated on the Mars Global Surveyor (MGS) on 7 November 1996. The mission of the MGS was to study the Martian surface and produce detailed topographical and atmospheric measurements to support future unmanned missions to and a better understanding of Mars. On-board the satellite was the Mars Orbiter Laser Altimeter, which provided detailed measurements of the “topography, surface roughness, and 1.064- μm reflectivity of Mars and the heights of volatile and dust clouds” (Smith et al., 2001, p. 23689). MOLA provided roughly four and a half years of mapping data when it was declared mission complete on 30 June 2001.

The MOLA payload consisted of a Q-switched Cr:Nd:YAG diode-pumped laser and a SiAPD collecting photons through a 0.5-meter parabolic aperture. In a 400-km circular orbit, the 23.8-kg, 34.2-W payload collected data every 330 meters along-track with an across-track spacing of 4 kilometers. The spot size or IFOV was 168 meters with a 1-meter vertical accuracy and 38-centimeter range resolution. The transmitter design was a single stage Cr:Nd:YAG zigzag slab amplifier pumped by a 36-bar array each with 80 aluminum gallium arsenide (AlGaAs) diodes. The laser operated at 10 Hz with an 8-ns pulse-width providing 40 mJ per pulse and effectively performed for 671,121,600 pulses. The receiver, an RCA manufactured SiAPD, had a gain of roughly 150 and quantum efficiency of 30%, requiring 230 photons to trigger an avalanche (Abshire, 2010). While relatively inefficient with a large post-spacing, the MOLA payload nevertheless continued to pave the way for future LIDAR payloads due to its success beyond initial requirements, an example of which can be seen below.

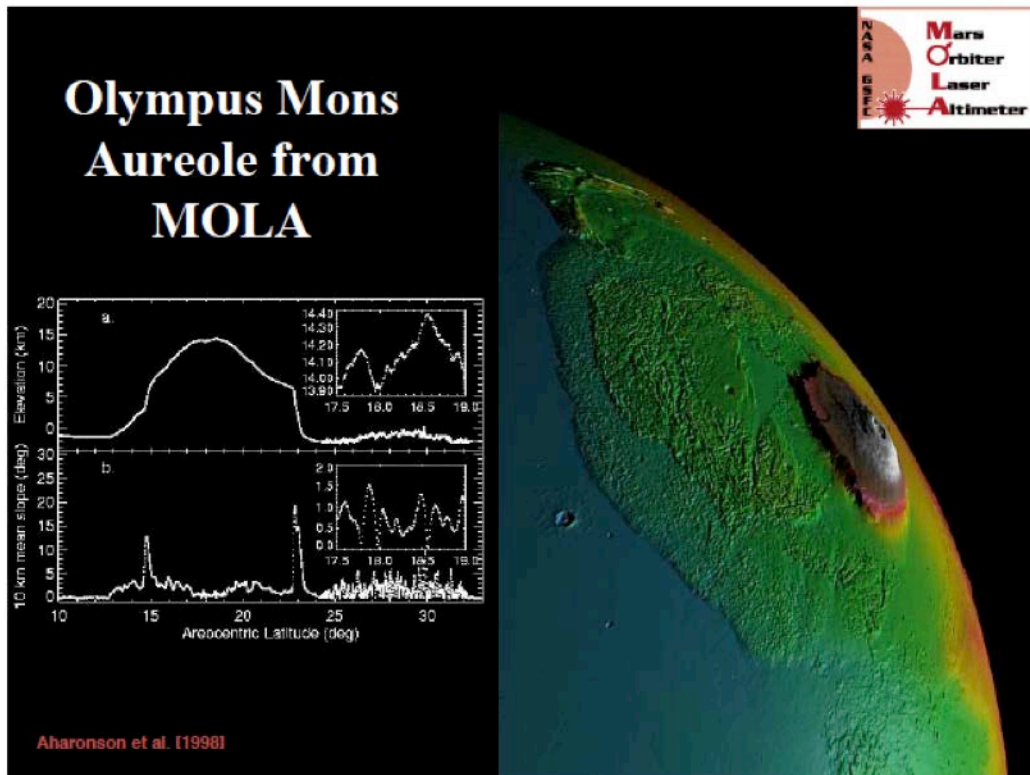


Figure 8. MOLA's Collection of Olympus Mons (from Abshire, 2010)

E. MESSENGER LASER ALTIMETER (MLA)

The MESSENGER spacecraft followed on the heels of MOLA's successes, having launched on 3 August 2004 from Kennedy Space Center. As the first spacecraft to orbit Mercury, MESSENGER's mission was to characterize the geological composition and history of the innermost planet, as well as answer fundamental questions of how the planet was formed. The MLA was one of seven instruments on-board the spacecraft, which provided detailed topographic and reflectivity measurements of Mercury. MESSENGER continues to provide data on Mercury since its orbital insertion on 17 March 2011 to present day operations with over 26,716,501 laser shots to date (C. Ernst, personal communication, November 5, 2013).



Figure 9. MLA Payload Assembly (from Abshire, 2010)

The MLA payload, having built upon the MOLA design, consists of a two-pass, passively Q-switched Cr:Nd:YAG diode-pumped laser and a SiAPD collecting photons through four 14-cm refractive telescopes. In a 15,000-km by 300-km highly elliptical orbit, the 7.4-kg, 25-W payload collects data for 30

minutes each orbit (on average) as the spacecraft passes within 1,800 km of Mercury. The along-track spacing is roughly 400 meters but remains variable due to changes in orbital altitude (Zuber, M. T., et al., 2012). The spot size is also variable due to the elliptical orbit, with a 23-meter spot size at the periapsis to 134 meters at the payload's maximum operating range. The vertical accuracy varies with signal strength and altitude with an accuracy of less than 15 cm at periapsis and 6-cm range resolution (Zuber M. T., et al., 2008). The transmitter design is a single-stage, double-pass Cr:Nd:YAG zigzag slab amplifier pumped by two four-bar stacks of GaInAsP diodes. The laser operates at 8 Hz with a 6 ns pulse-width providing 18 mJ per pulse. The receiver, an RCA manufactured SiAPD similar to MOLA's, has a gain of rough 150 and quantum efficiency of 30% (Cavanaugh, J. F., et al., 2007). The MLA continues to demonstrate the robustness of the LIDAR design inherited from MOLA in the harsh Mercury environment.

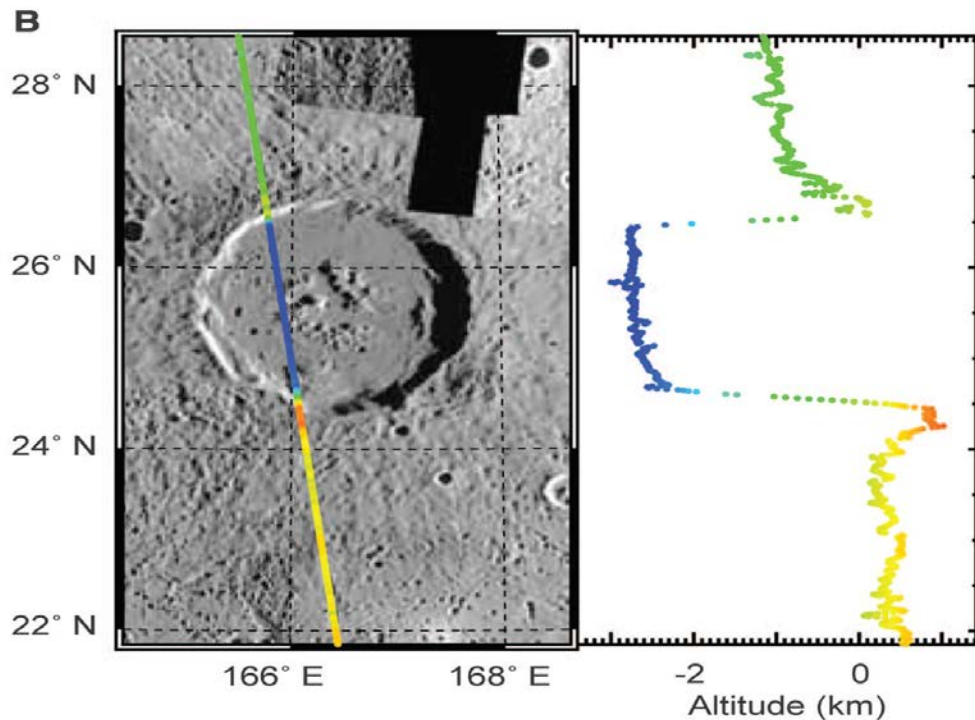


Figure 10. Profile of the Atget crater from MLA (from Zuber, et al., 2012)

F. CLOUD-AEROSOL LIDAR AND INFRARED PATHFINDER SATELLITE OBSERVATIONS (CALIPSO)

The Cloud-Aerosol LIDAR with Orthogonal Polarization (CALIOP) is the primary payload on-board NASA's CALIPSO spacecraft, which continues the heritage of Nd:YAG lasers in space. CALIPSO was launched on 28 April 2006 with an Earth-centric mission: "to provide the observations necessary to improve our understanding of the effects of clouds and aerosols on the climate system" (Winker, D., Hunt, W., & Hostetler, C., 2004, p. 1). CALIOP has operated for over seven years with over two billion shots collected, detecting and characterizing cloud and aerosol heights and layers with the highest level of detail and accuracy.

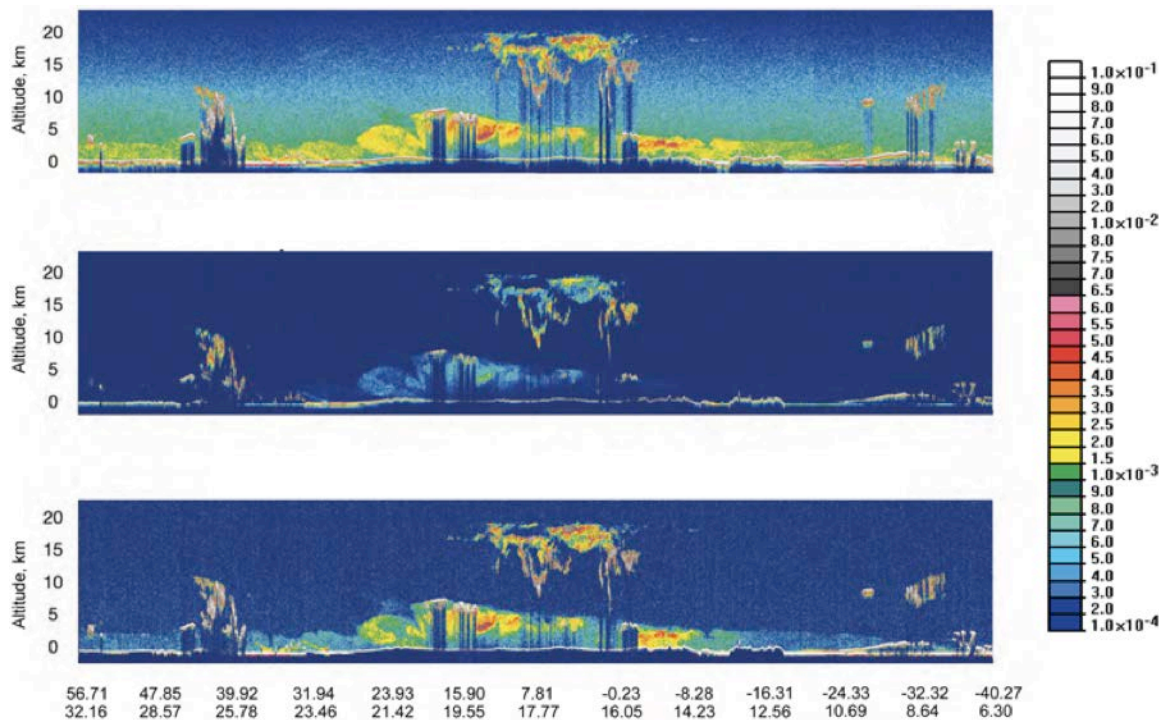


Figure 11. CALIOP observations from 9 June 2006 from Northern Europe across Africa into the south Atlantic. Shown are (top) total 532 nm return, (middle) 532 nm perpendicular return, and (bottom) total 1064 nm return. (from Winker, Hunt, & McGill, 2007)

The CALIOP payload consists of two redundant Q-switched Nd:YAG diode-pumped lasers and one SiAPD and two photon multiplier tubes (PMTs) collecting photons through a 1-meter aperture. In a 705-km circular orbit, the 172-kg, 197-W payload collects data with a one-third kilometer post spacing. The CALIOP payload has substantially larger post spacing than many of the other LIDAR packages due to an atmospheric sensing versus a topographic mapping mission, sacrificing resolution for area coverage rates. The Cr:NdYAG slab is pumped by 192 diode bars capable of producing 400 mJ per pulse for each of the two lasers. Each laser's actual operating energy was de-rated to 220 mJ per pulse, however, to increase the reliability and mission lifetime. This high pulse energy can either be transmitted through the beam expanders at 1064 nm or frequency-doubled to provide 110 mJ of 532 nm light per pulse, enabling two different wavelengths for aerosol and cloud characterization. Both lasers operate with a pulse repetition rate of 20.16 Hz and a pulse length of roughly 20 ns (Winker, D. M., Hunt W., & McGill M., 2007). With these high pulse energies, the CALIOP lasers represented a new generation of high energy Nd:YAG transmitters for Earth remote sensing applications and continues to demonstrate its robust design through current day operations.

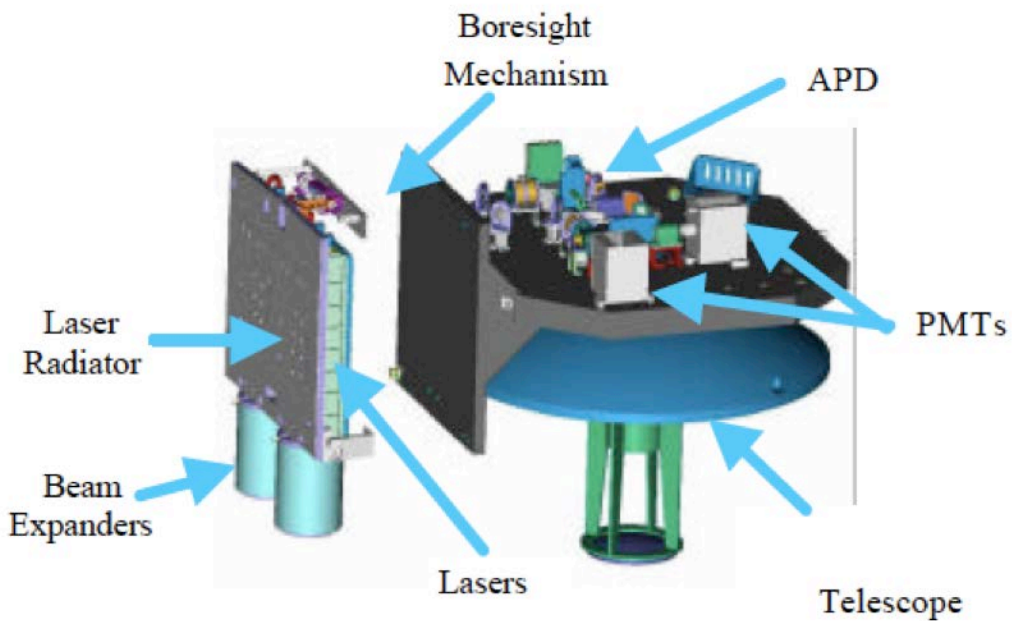


Figure 12. CALIOP transmitter and receiver subsystems (from Winker, Hunt, & Hostetler, 2004)

G. LUNAR ORBITER LASER ALTIMETER (LOLA)

The Lunar Orbiter Laser Altimeter builds on the work of Apollo 15 to characterize the lunar surface, but this time with advanced equipment developed throughout the MOLA and Near Earth Asteroid Rendezvous (NEAR) missions. The LOLA payload was launched on 18 June 2009 aboard the Lunar Reconnaissance Orbiter with the goal of “assist[ing] in the selection of landing sites on the moon for future robotic and human exploration missions and... to detect the presence of water ice on or near the surface...” (Riris et al., 2007, p. 1). LOLA has operated for over three years with roughly 6 billion shots collected from its LIDAR system, doing “at the moon what MOLA did at Mars, but with 3–5 times greater accuracy and 32 times more frequent measurements along track” (Smith & Zuber, p. 1).

The LOLA payload consists of two redundant Q-switched Nd:YAG diode-pumped laser (Figure 13) and five SiAPD collecting photons through a 0.14-

meter aperture. In a 40-km circular orbit, the 9.6-kg, 26.2-W payload collects data with a 10 to 15-meter post spacing and 30-cm vertical accuracy. The LOLA payload differs from the MOLA payload due to its use of the first diffractive optical element (DOE) to split a single beam into five separate beams. The DOE follows a diode-pumped Nd:YAG amplifier operating at 28 Hz with a 5-nanosecond pulse-width providing 3.2 mJ per pulse. The receiver follows the design of that flown on MOLA but consists of five SiAPDs fiber-coupled to the receive optics to provide a 20-meter IFOV while the laser illuminates a 5-meter target within each IFOV (Riris & Cavanaugh, 2010). LOLA remains relatively inefficient compared to current technology but due to the new design and the near-zero lunar atmosphere, improvements in post-spacing and reliability were realized, successfully implemented and enable operation to this day.

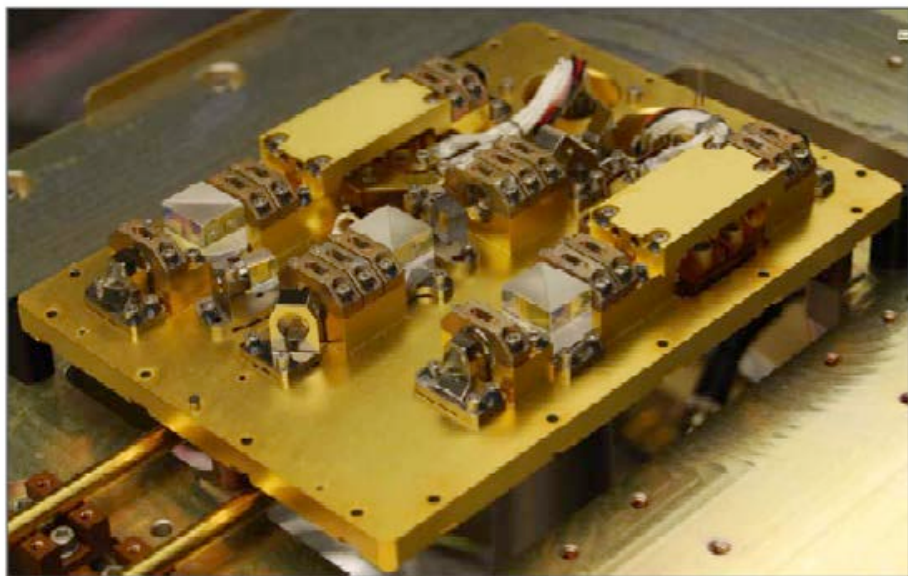


Figure 13. LOLA Redundant Transmitters (from Riris et al., 2010)

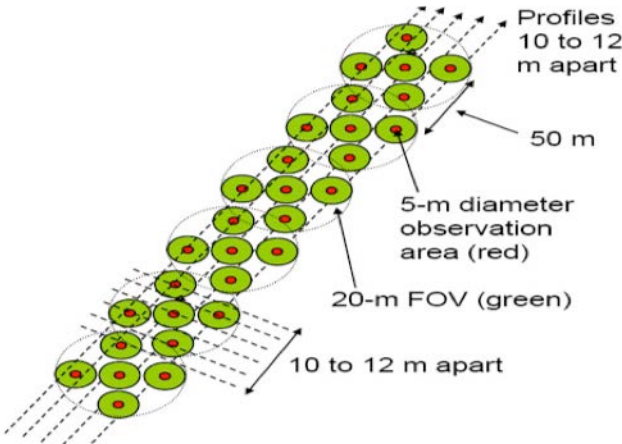


Figure 14. LOLA Payload Five Spot Ground Pattern (from Riris et al., 2010)

H. GEOSCIENCE LASER ALTIMETER SYSTEM (GLAS)

The Geoscience Laser Altimeter was the first continuous Earth observing laser altimeter payload launched aboard the ICESat satellite on 12 January 2003. “The GLAS instrument on ICESat was the sole instrument on the satellite, and provided unprecedented science data on global surface elevation of ice and land, sea ice freeboard heights, vertical cloud height distributions, and vegetation canopy heights, despite issues with laser lifetime” (Yu et al., 2010, p. 757809-2). ICESat operated for seven and a half years through multiple failed lasers, eventually accumulating over 1.8 billion laser pulses before its decommissioning on 14 August 2010 (NASA ICESat, 2013). The mission was hailed as a success despite its shortened lifetime, providing key insights into the melting of ice sheets in the cryosphere.

To accomplish the mission, the GLAS instrument utilized three redundant Q-switched Nd:YAG diode-pumped lasers in a master oscillator – power amplifier configuration (MOPA) and eight SiAPDs collecting photons through a one-meter aperture. The MOPA configuration consisted of a master oscillator operating at roughly 2.2 mJ per pulse feeding a 10X pre-amplifier (bringing the power to about 22 mJ) and a 5X power amplifier that brought the total power to about 110 mJ per pulse (Abshire, 2010). In a 600-km circular orbit, the payload collects data with a 70-m spot size, 170-m along-track spacing and 3-cm range accuracy.

GLAS uses an optical expander to bring the spot beam to the proper size and follows the amplifier configuration operating at 40 Hz with a less than 6-ns pulse-width. The receivers are also similar to those flown on previous LIDAR missions to include MOLA, except with a one-gigahertz waveform recorder on the backend to increase vertical resolution and accuracy (Yu et al., 2010).

The ICESat mission's laser transmitter assembly experienced a number of issues in the initial checkout period. Each of GLAS's lasers was designed "to operate continuously for approximately 18 months to enable a nearly five-year mission" (Abdalati et al., 2010, p. 736). The first laser failed after just "74 days of pre-launch operations plus 36 days of on-orbit operations" (Kichak, 2003, p. 2). The cause of this failure was poor indium solder bonds in the laser diode arrays compounded by a current short in the same array, causing them to fuse open. The decision was then made to prolong the lifetime of the second and third laser by reducing the duty cycle, allowing ICESat to continue successful observations over its lifetime (Kichak, 2003).

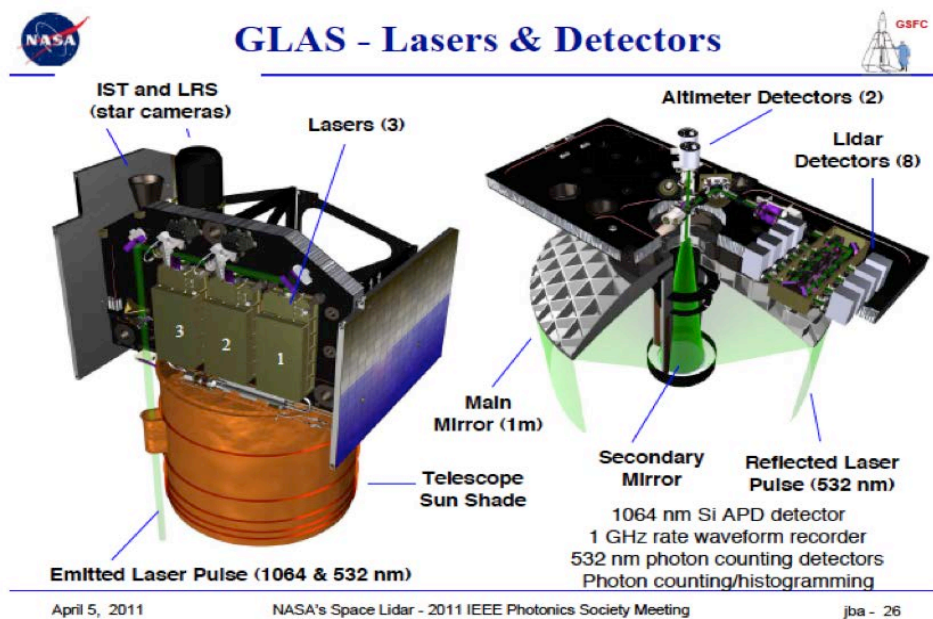


Figure 15. GLAS Instrument Cut-Away View (from Abshire, 2010)

I. ICESAT-2

NASA's ICESat-2 mission, slated for launch in July 2016, is the follow-on to ICESat-1 and will carry the ATLAS payload. The payload and space vehicle for ICESat-2 are in the Phase C or "Design and Development" stage according to NASA's ICESat-2 website, with technologies and conceptual designs selected for flight (NASA: ICESat-2, 2013). The mission of ICESat-2 will be similar in scope to ICESat-1's, which prematurely ended in 2010 due to laser transmitter anomalies.

In particular, ICESat-2 will measure the temporal and spatial character of ice sheet elevation change to enable assessment of ice sheet mass balance and examination of the underlying mechanisms that control it. The precision of ICESat-2's elevation measurement will also allow for accurate measurements of sea ice freeboard height, from which sea ice thickness and its temporal changes can be estimated. ICESat-2 will provide important information on other components of the Earth System as well, most notably large-scale vegetation biomass estimates through the measurement of vegetation canopy height. When combined with the original ICESat observations, ICESat-2 will provide ice change measurements across more than a 15-year time span. Its significantly improved laser system will also provide observations with much greater spatial resolution, temporal resolution, and accuracy than has ever been possible before. (Abdalati et al., 2010, p. 735)

To accomplish this mission, Advanced Topographic Laser Altimeter System (ATLAS) will depart from many of the historical planetary LIDARs including ICESat-1's GLAS design, which primarily used an analog detection scheme and 1064 nm lasers (although ICESat-1 did have a secondary laser and detectors at 532 nm). Instead, ATLAS will employ single-photon sensitive receivers operating with much higher gain and a laser transmitter operating at 532nm, similar to GLAS's secondary system. The full laser and receiver designs have yet to be completed at this time, but NASA's "snapshot" documents offer a preview of the instrument. ATLAS's transmitter is a frequency doubled Nd:YVO₄ Q-switched MOPA laser. The 1064-nm light is then passed through a second harmonic generator, in this case a lithium triborate crystal, to generate the frequency-doubled 532-nm beam with a laser wall-plug efficiency of greater than

5%. The laser design departs from other “traditional” space LIDARs by operating with a high pulse repetition frequency (PRF) of 10 kHz while maintaining tunable pulse energies between 250 and 900 μ J (Sawruk et al., 2013). ATLAS then uses a DOE that separates a single beam into nine beams of varying power (see Figure 16), “which aims to address issues of detector dynamic range when alternating between bright and dark surfaces such as ice and water” (Rosette, Field, Nelson, DeCola, and Cook, 2011, p. 3).

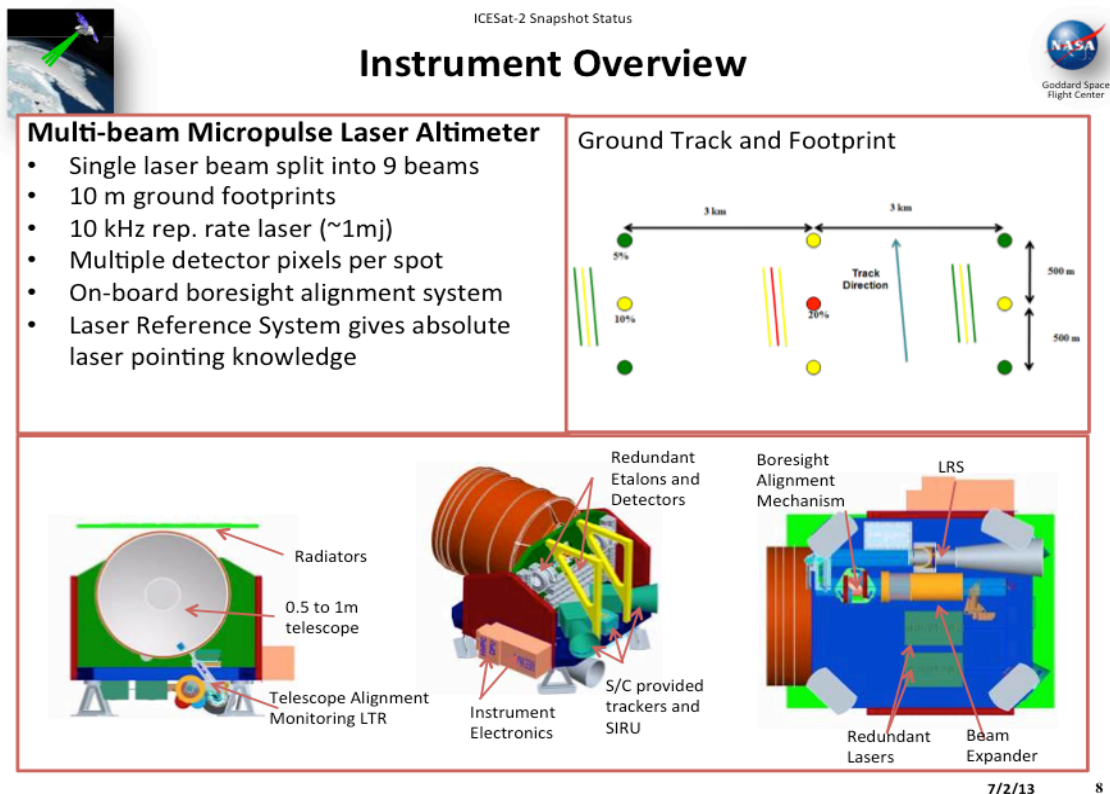
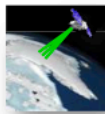


Figure 16. ICESat-2 Instrument Overview (from NASA: ICESat-2, 2013)



ICESat-2 Snapshot Status

ICESat-2 Mission Concept



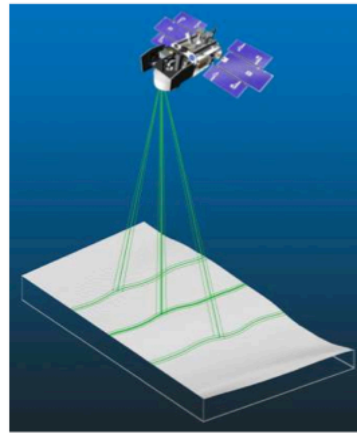
In contrast to the ICESat design, ICESat-2 will use micro-pulse multi-beam photon-counting approach.

Provides:

- Dense cross-track sampling to resolve surface slope on an orbit basis.
- High repetition rate generates dense along-track sampling.

Advantages:

- Improved elevation estimates over high slope areas and very rough (i.e., crevassed) areas.
- Improved lead detection in sea ice.

**ICESat-2 Key Facts:**

Orbit: 600km, 91-day repeat, with monthly Sub-cycles, ICESat orbit

Laser Rep. Rate: 10 kHz

Number of beams: 9, with unequal energy

Along-track sampling: 70 cm

Wavelength: 532 nm

Website: icesat.gsfc.nasa.gov/icesat2

7/2/13

3

Figure 17. ICESat-2 Mission Overview (from NASA: ICESat-2, 2013)

In a 600-km circular orbit, the ATLAS payload will collect data with a 10-m spot size, 70-cm along-track sampling, 3 km across-track spacing and better than 2-cm range accuracy. The range accuracy is improved due to the shortened 2-ns pulse-width, while sampling frequency is improved with a 10-kHz PRF. In addition to the transmitter changes, ICESat-2 seeks to address the multiple issues experienced on the ICESat-1 mission that led to a premature failure of its lasers. The indium solder used in the laser diode array will be eliminated and the housing will be pressurized to minimize outgassing and reduce the risk of contaminating the optics (Abdalati et al., 2010).

The receiver design for ATLAS has yet to be finalized, but the concept of using single-photon sensitive devices was demonstrated on both ICESat-1 and PAMELA (Payload for Antimatter Matter Exploration and Light-nuclei Astrophysics) in a limited fashion. ICESat-1 utilized the Perkin Elmer Single Photon Counting Modules (SPCMs) for atmospheric backscatter measurements and demonstrated the effectiveness and efficiency of this class of detectors.

Tables 6 and 7 show the variety of detectors being traded off for the ICESat-2 mission, the attributes of each detector and the ICESat-2 mission requirements. The decision to pursue the 532-nm wavelength for the ATLAS system versus previous 1064-nm Space LIDARs was due to advancements in technology (short pulse, high PRF lasers and radiation tolerant single photon sensitive receivers) for the shorter wavelength. At 1064 nm, single-photon detectors exist but had difficulty meeting requirements and technology readiness levels (TRLs) at that particular time in ICESat-2's design (Krainak, Yu, Yang, Li, and Sun, 2010).

Parameter	Requirements	GLAS SPCM-Perkin Elmer (16 per channel)	Hamamatsu PMT R5900	Hamamatsu HPMT H10777-40	Silicon APD microarray (8x8) (4 per channel)
TRL/Space flight heritage	TRL 6 by Preliminary Design Review	TRL 9 on ICESat/GLAS	TRL 9 on PAMELA	TRL 4	TRL 4
Photon Detection Efficiency	20%	65%	15%	40%	20%
Maximum count rate (MCPS)	300	200	200 (to be tested)	300 (to be tested)	30
Timing jitter (ps. FWHM)	230	300	300 (FWHM data sheet)	90	60
Multiple photon resolution	5	16 (multiple detector)	To be measured	Yes	Yes (multiple detector)
Dark Count (kHz)	30	500	<100 counts per second	<30	4
Lifetime (years) (at a solar background of 10^7 cps)	5	5	>5	4.7	>5
Diameter (μm)	200	170	1600	3000	800

Table 6. 532-nm Single Photon Sensitive Detectors (from Krainak et al., 2010)

Parameter	Requirements	IPD	GLAS SPCM – Perkin Elmer (8 per channel)	InGaAs APD microarray (16x16 with ROIC)
TRL/Space flight heritage	TRL 6 by Preliminary Design Review	TRL 4	TRL 9 on ICESat/GLAS	TRL 3
Photon Detection Efficiency	10%	20%	5%	15%
Maximum count rate (MCPS)	300	>200	100	>100 (to be verified)
Timing jitter (ps. FWHM)	230	150	300	200
Multiple photon resolution	5	Yes	8	Yes
Dark Count (kHz)	15	60	20	<10
Lifetime (years) (at a solar background of 10^7 cps)	5	4	5	No data, Solid stat device, radiation issues
Diameter (μm)	200	1000	170	50

Table 7. 1064-nm Single Photon Sensitive Detectors (from Krainak et al., 2010)

In order to demonstrate the new LIDAR approach of ICESat-2 in contrast to previous NASA missions, the Multiple Altimeter Beam Experimental LIDAR (MABEL) payload conducted airborne tests to verify the new methodology. MABEL does not completely mirror the ICESat-2 hardware, but mimics the expected space-based link budget through a high altitude ER-2 aircraft. According to NASA after the initial flights in 2010 and 2011, “MABEL demonstrates conclusively that the photon-counting altimetry concept is a valid measurement approach for the ICESat-2 mission...As a demonstrator for ICESat-2, the MABEL instrument has shown the measurement concept is sound” (McGill, 2011, p. 2). MABEL builds on a number of other demonstration aircraft operated by the military for single photon sensitive (or Geiger-mode) LIDAR terrain mapping, two of which are the National Geospatial Intelligence Agency’s (NGA) Airborne LIDAR Imaging Research Testbed (ALIRT) and Defense Advanced Research Projects Agency’s (DARPA) High Altitude LIDAR Operations Experiment (HALOE). These aircraft have mapped a significant portion of Afghanistan and Haiti in three dimensions, successfully demonstrating the use of

single-photon sensitive devices (these two specifically at 1064 nm) even prior to MABEL's test flights.

LIDAR has had a long and storied history in space, dating back to the Apollo missions that helped map the lunar surface in 1971. ICESat-2 is the latest generation of LIDAR sensors to be designed, having evolved from ruby lasers and analog receivers to high efficiency fiber lasers and single photon sensitive arrays. As the technology progresses, the missions continue to push towards more robust and higher resolution elevation measurements to tackle ever more challenging requirements.

IV. SPACE-BASED LIDAR COST CONSIDERATIONS

NASA's primary challenge in the next few years will be to complete a series of complex and expensive projects in the context of constrained budgets and sometimes competing priorities set by the Congress and the administration.

—*NASA Assessments of Selected Large-Scale Projects*, 2013, p. 23

Mission cost remains a key factor in determining the viability of a mission for government agencies, especially in the face of sequestration and a budget-constrained environment. Programs with high return-on-investment still require rigorous cost accounting procedures and independent cost estimates (ICE) to verify long-term program costs. These independent cost estimates involve multiple parametric models to calculate overall program costs and potential cost overruns with a high confidence level. This section does not provide a high fidelity ICE-like cost profile, but rather a first cut analysis on the main cost drivers for a space-LIDAR mission and historical cost knowledge.

A. HISTORICAL COSTS AND ICESAT-2 ESTIMATES

NASA has launched a number of space-based LIDAR missions in the past three decades to map and monitor the Moon, Mercury, and Mars and, with ICESat-1, Earth. The MESSENGER spacecraft was launched in 2004 and slated to study “Mercury’s mysterious magnetic field and unusual activity” (*Huffington Post*, 2011, p. 1). On-board MESSENGER was a number of instruments with one of the payloads consisting of a Nd:YAG LIDAR system to map the topography of Mercury. The 1000-kg spacecraft and payloads continues to operate successfully for over two years (with a six-year transit time) at a cost of \$446M.

The Lunar Reconnaissance Orbiter was launched in 2008 and continues operations with its LIDAR payload, a Nd:YAG system having cataloged over 1 billion shots. The mission, at a cost of \$504M, was “equipped with seven state-of-the-art cameras and other instruments... [looking] for suitable landing sites for

future manned missions while creating the most detailed lunar atlas ever assembled" (Harwood, 2009, p. 1). The 4,200-lbs spacecraft was launched on an Atlas V and has successfully mapped the topography of the moon in unprecedented detail.

While both the MESSENGER and LRO spacecraft demonstrated the utility and potential costs of a LIDAR system, it was not until 2003 when an Earth-observing LIDAR was specifically designed and launched into space for continuous operations. There are significant differences between the Earth observing mission and the inter-planetary missions due to atmospheric variables, the need for inter-planetary missions to transit to their location, radiation profiles and a multitude of other spacecraft differences. The inter-planetary costs provide a backdrop for both ICESat-1 and ICESat-2's cost profiles. ICESat-1 actual cost profiles are difficult to calculate due to the lack of full government cost accounting during the initial phases of ICESat-1, however, expert knowledge of the program has allowed for rough estimates of the final program cost. Cost estimates for the entire ICESat-1 system, excluding operations, total roughly \$462M. The cost breakout of the system includes launch costs at \$282M for the Delta II launcher, \$55M for the BCP2000 bus and roughly \$125M for the payload (Silverman, 2013; *USA Today*, 2003). ICESat-1 followed a similar technology path to previous missions but ended significantly early in its mission lifetime.

ICESat-2's initial cost estimate was roughly \$650M for the total mission to include formulation, development, launch and operations. Launch costs are still uncertain at this point, but the original value of Fibertek's ATLAS payload and Orbital's spacecraft bus and integration contracts were \$26M and \$135M, respectively (Leone, 2012). Most recently, the mission cost increased to \$860.3M with a cost breakout of \$248.8M for mission formulation, \$558M for development and \$52.9M for operations (Government Accountability Office, 2012).

Upon further examination of the limited cost and performance data for these space vehicles, it is difficult to draw any parallels between payload performance and spacecraft cost. Due to the limited amount of publically

available data and small number of space-borne missions with a LIDAR payload, any cost trending is inconclusive. Also, the number of variables including interplanetary versus Earth-observing, multi-payload versus single-payload, and other environmental conditions make a simple cost trending difficult to determine. Other non-LIDAR cost models need to be explored to determine a best first-order fit for a spacecraft cost estimation.

B. SATELLITE COST MODELS

A number of cost estimating methods and models have been developed over the years to accurately determine a satellite's cost throughout its development life-cycle. NASA's Space Systems Engineering Training's Cost Estimation Module describes a number of difficulties and considerations regarding spacecraft cost estimation. Cost estimation remains a blend of art and science due to the nature of the models and data that includes: small sample sizes, incomplete/cloudy historical data, multi-variable cost drivers and unique one-of-a-kind missions (Guerra, 2008). These challenges do not rule out effective cost estimation, but only provide a glimpse at the limitations for the aerospace community.

1. Cost Estimation Methodologies

Three main cost estimation methods exist with varying levels of complexity and accuracy. Detailed bottom-up estimating is time-consuming and requires detailed designs and work breakdown structures to calculate total spacecraft cost. Analogous estimation is based upon similar systems and their associated costs, but adjusted for differences in size and complexity. This method is fairly limited due to the inability to perform trade studies within this space. Parametric cost estimation is the third method available, and can account for a number of variables and is more easily extensible to trade studies while less time-consuming than bottom-up estimation. This method relies on historical data and a number of analogous data points to provide the best possible fit to the data, while keeping the number of variables manageable (Figure 18). Parametric

models also may include a “complexity factor” that allows new missions and technologies to be accounted for and estimated. The main detractors from this method include a strong reliance on limited historical data and an accuracy that is amenable to first-order or project inception-type estimating versus proposals and later, robust bottom-up cost estimation procedures.

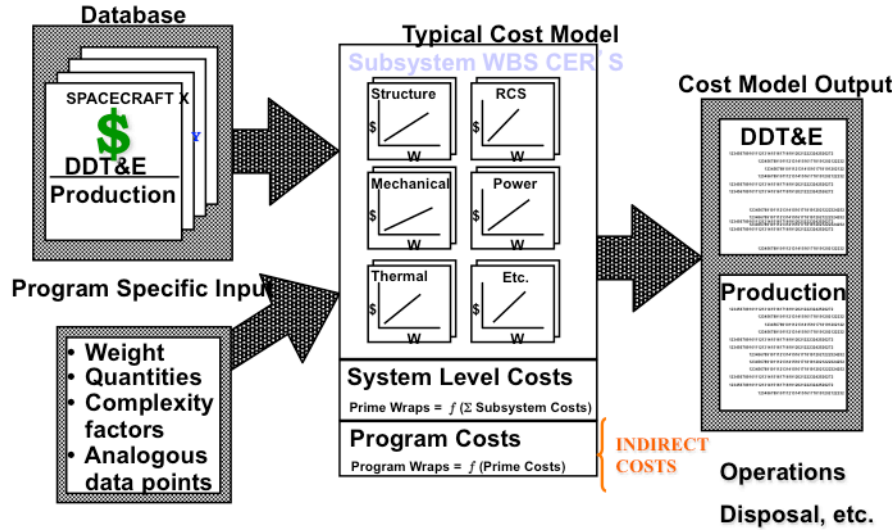


Figure 18. Parametric Cost Model Development Process (from Guerra, 2008)

2. NASA Small Satellite Cost Breakdown

The RAND Corporation, in 1998, attempted to categorize and provide one of the first cost analyses of small-satellites. Their analyses, while having a high standard deviation, focused on mass and mission complexity as the two main cost drivers. Based upon 13 NASA small-satellite missions, RAND also calculated an average total mission cost breakout as seen in Figure 19. For these small satellite missions the satellite bus is 41% of total mission cost, payload is 14.3% and launch is 21%.

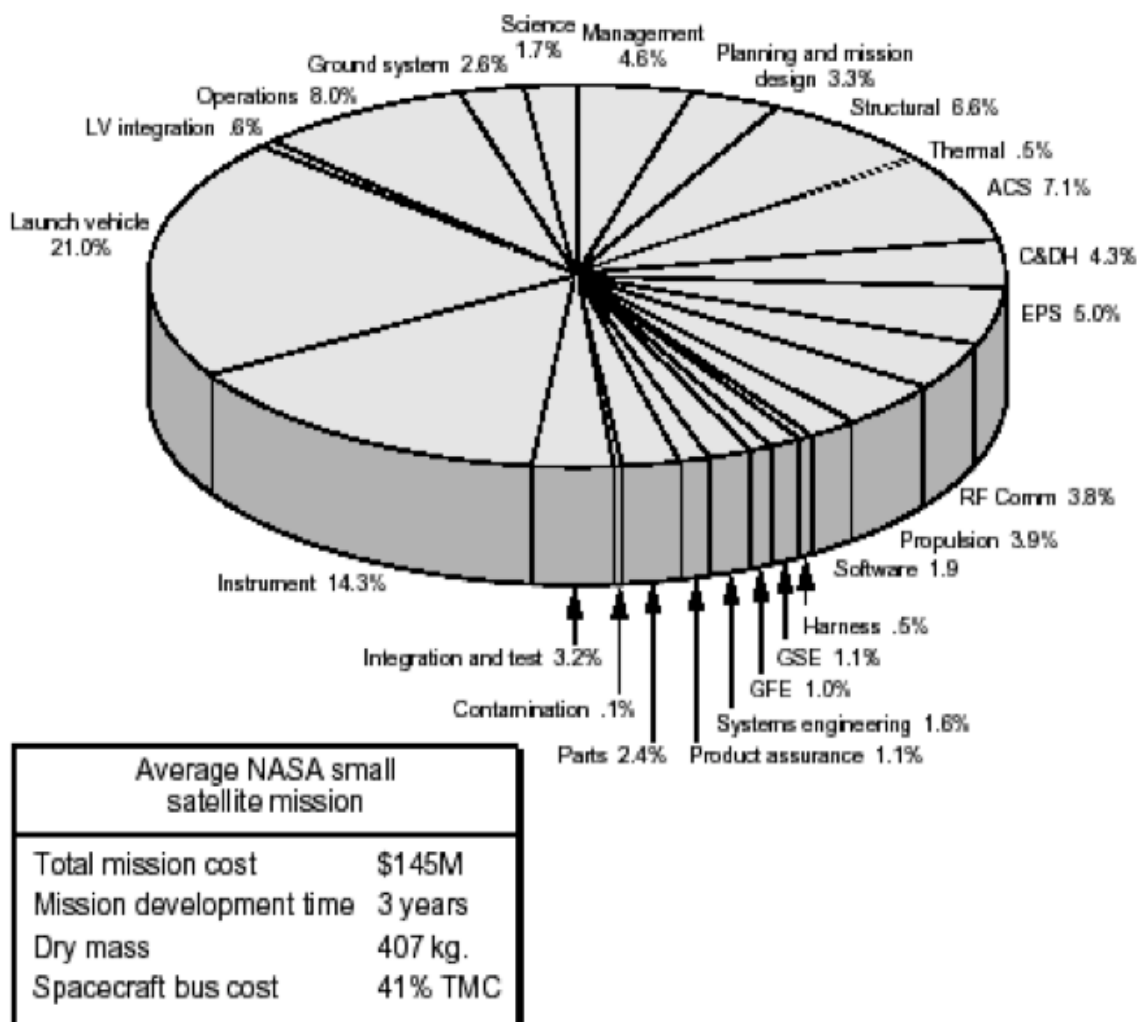


Figure 19. Average NASA Small Spacecraft Mission Cost Breakout (from Guerra, 2008)

3. NASA's Weight-Based Cost Model

Many attempts have been made to refine parametric cost estimation over the years as additional space platforms have been launched. One of NASA's parametric cost estimation models was outlined in a University of Texas seminar for Space Systems Engineering. Relying on 33 separate uncrewed Earth orbiting satellites as data inputs (Figure 20), the output of the parametric cost model has a weight-based cost dependency of:

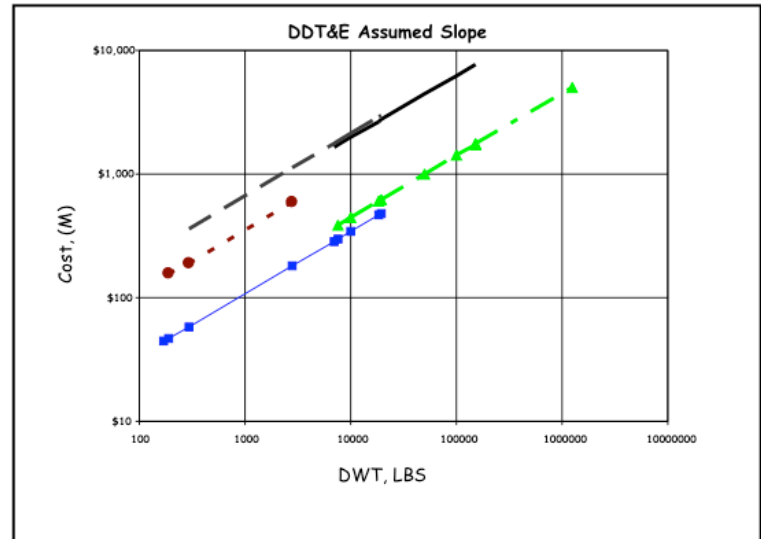
$$Cost_{SC} = 3.424 \square Wt^{0.5} \quad (1.1)$$

With applicability over a weight range of 163 to 19,513 lbs (or 74 to 8851 kg), the cost model provides first-order cost estimation accuracy commensurate with the mission concept stage this thesis is addressing. These numbers do not include launch costs or launch preparation but rather design, development, test and evaluation (DDT&E) costs that include everything prior to launch and operations. The numbers have also been adjusted for inflation due to the large time differences between the development of these spacecraft.

Uncrewed Earth Orbit			Uncrewed Planetary			Crewed		
<u>Program</u>	<u>Weight</u>	<u>DDT&E Cost</u>	<u>Program</u>	<u>Weight</u>	<u>DDT&E Cost</u>	<u>Program</u>	<u>Weight</u>	<u>DDT&E Cost</u>
AE-3	780	\$35	GALILEO	2,755	\$467	APOLLO-CSM	31,280	\$11,574
AEM-HCM	185	\$10	GAL. PROBE	671	\$97	APOLLO-LM	8,072	\$5,217
AMPT-E-CCE	395	\$20	SURVEYOR	647	\$1,179	GEMINI	7,344	\$2,481
COBE	4,320	\$55	VIKING LND	1,908	\$914	ORBITER	153,552	\$8,088
CRRES	6,164	\$35	VIKING ORB	1,941	\$417	SKYLAB-A/L	38,945	\$1,159
DE-1	569	\$14	PIONAERV. B.	758	\$91	SKYLAB-OW	68,001	\$1,786
DE-2	565	\$14	PIONERL	636	\$69	SPACELAB	23,050	\$1,671
DMSP-5D	1,210	\$69	PIONERS.	191	\$36	SUBTOTAL	330,244	\$31,976
ERBS	4,493	\$21	LUNARORB	394	\$430	AVERAGE	41,178	\$4,568
GPS-1	1,500	\$76	MAGELLAN	2,554	\$243	HIGH	153,552	\$11,574
HEAO-2	3,010	\$16	MARINER-4	532	\$286	LOW	7,344	\$1,159
HEAO-3	3,044	\$12	MARINER-6	696	\$420			
IDSCSP/A	495	\$59	MARINER-8	1,069	\$333			
LANDSAT-4	1,906	\$24	MARINER-10	1,037	\$241			
MAGSAT	168	\$9	PIONEER10	423	\$187			
SCATHA	1,194	\$27	VOYAGER	1,226	\$394			
TIROS-M	435	\$65	SUBTOTAL	17,438	\$5,804			
TIROS-N	836	\$26	AVERAGE	1,090	\$368			
VELA-IV	544	\$65	HIGH	2,755	\$1,179			
INTELSAT	237	\$77	LOW	191	\$36			
ATS-1	527	\$108						
ATS-2	406	\$99						
ATS-5	721	\$131						
ATS-6	2,532	\$201						
DSCS-11	1,062	\$158						
GRO	13,448	\$223						
HEAO-1	2,602	\$89						
LANDSAT-1	1,375	\$90						
MODEL-35	1,066	\$196						
SMS	1,038	\$76						
TACSAT	1,442	\$115						
OSO-8	1,037	\$71						
HUBBLE	19,514	\$968						
SUBTOTAL	78,820	\$3,254						
AVERAGE	2,388	\$99						
HIGH	19,514	\$968						
LOW	168	\$9						

	<u>Avg. Wt</u>	<u>Avg. \$</u>	<u># Data Points</u>
Uncrewed Earth Orbit	2,400	\$.10B	33
Uncrewed Planetary	1,100	\$.37B	16
Crewed	41,000	\$4.57B	9

Figure 20. NASA's Small Satellite Weight-Based Cost Model Inputs (from Guerra, 2008)



Program	Equation	Validity Range	No of Data Points
Liquid Rocket Engines	= 21.364 WT^.5	291 to 18,340	4
Crewed Spacecraft	= 19.750 WT^.5	7,000 to 153,552	9
Uncrewed Planetary S/C	= 11.279 WT^.5	191 to 2,755	16
Launch Vehicle	= 4.461 WT^.5	7,674 to 1,253,953	10
Uncrewed Earth Orbital S/C	= 3.424 WT^.5	168 to 19,513	33

Figure 21. NASA's Weight-Based Cost Curves (from Guerra, 2008)

In addition to the baseline weight-based parametric cost estimation module, there is a need to include complexity factors due to “unique features that aren’t accounted for in the CER historical data” (Guerra, 2008, p. 15). An overview of NASA’s complexity factors is listed in Table 8. These factors are applied post-parametric model to better accommodate design, development, test and integration of new components, technologies and unique mission features.

Description	Complexity Factor
System is “off the shelf”; minor modifications	.2
System’s basic design exists; few technical issues; 20% new design and development	.4
System’s design is similar to an existing design; some technical issues; 20% technical issues; 80% new design and development	.7
System requires new design, development, and qualification; some technology development needed (normal system development)	1.0
System requires new design, development, and qualification; <u>significant technology development; multiple contractors</u>	1.3
System requires new design, development and qualification; major technology development	1.7
System requires new design, development and qualification; major technology development; crash schedule	2.0

Table 8. NASA’s Complexity Factors for Cost Modeling (from Guerra, 2008)

4. Optical Telescope Assembly-Based Cost Model

In addition to the mass parametric model, more specific models also exist based upon classes of satellite payloads such as space telescopes. NASA has created a detailed parametric model for OTA cost (which includes only the primary, secondary and tertiary mirrors and supporting structure) based upon data on 59 different variables across 30 different space telescopes.

$$Cost_{OTA} \approx D_{OTA}^{1.5} \lambda^{-0.2} \quad (1.2)$$

The model (Equation 1.2) correlates highly with both the aperture diameter and the diffraction limited wavelength of the mirror design and accounts for 98% of data variability. This is not a surprise since the “aperture defines the observatory’s science performance (sensitivity and resolution) and determines the payload’s size and mass” (Stahl, Henrichs, Luedtke, and West, 2012, p. 5). Also of note is the aperture exponent, which is less than 2, and indicates that larger aperture telescopes cost less per area than smaller telescopes. Other variables were considered but those with high correlation were also multi-collinear with diameter (e.g., primary mirror focal length and pointing accuracy). Optical telescope assemblies, as part of NASA’s detailed bottoms-up analysis, have also shown correlation with total mission cost. “In fact, an analysis of

detailed WBS documents for 7 missions shows that the spacecraft accounts for approximately 34% of the cost, science instruments account for 28%, [and] OTAs account for 11%" (Stahl et al., 2012, p. 4).

C. STANDARD SPACECRAFT BUSES AND LAUNCH VEHICLES

Spacecraft buses are an integral piece of the cost and operational limitations of a space-based LIDAR system. While custom buses have been designed, in order to constrain costs, standard spacecraft buses should be used. In Tables 9 and 10, current standard buses are identified with their key operating parameters. These parameters are important as they provide payload constraints in terms of power, mass, volume, data storage, communication downlink rates, spacecraft lifetime and pointing.

These spacecraft buses predominantly constrain the size, mass and power of the payload options. Their size will also help determine the overall mass of the mission and mass-based cost. For comparison, two previous LIDAR buses for ICESat-1 and ICESat-2 are described in Table 9 as the BCP-2000 and LEOStar-3, respectively. The BCP-2000 is a low-cost, lightweight bus that provides moderate capability and was used on ICESat-1. With strong space heritage, this bus exceeded on-orbit lifetimes for ICESat-1 but also limits payload power significantly compared to the LEOStar-3 bus. The LEOStar-3 bus, which is slated for the ICESat-2 mission, is a larger and more capable bus but comes at an expense. The ability to provide more power to the payload and increased pointing accuracy makes this bus attractive for future missions, but its mass is a concern for future missions. The LEOStar-3 bus has a strong space heritage with the Landsat 8 and GEOEye-1 missions having flown on-board this bus.

Contractor	Ball Aerospace	Ball Aerospace	Lockheed Martin	Lockheed Martin	Northrop Grumman	Orbital	Orbital
Parameter Units	BCP 300	BCP2000	LMx	LM400	Eagle 0	300S	LEOStar 3
Cost in \$M	-	40	-	-	-	-	135
Orbit Average Payload Power (EOL) in Watts	200	400	427	409	100	125	775
Maximum Payload Mass In kg	250	500	460	75	86	65	4,000
External Payload Volume In meters	0.7 x 0.8 x 1.4	1.5-m hex (tip-to-tip) x 2.2-m height (3.5 m ³)	1.9-m dia x 1.8m h (ATLAS V 4m LPF)	0.6 x 0.66 x 0.3 h 0.338 x 0.7 x 0.4 h	0.42 m x 0.76 m x 0.31 m (X x Y x Z)	0.762 dia x 1.143	1.828 x 1.828 x 1.4
Bus Dry mass (w/o Payload) In kg	139	450	426	186	471	272	1,169
Science Data Downlink In kbps	2,000	80,000	mission-specific	mission-specific	1,000	40,000	220,000
Science Data Storage In Mbit	8,000	56,000	mission-specific	mission-specific	384,000	160,000	704,000
Pointing Knowledge In arcsec	< 300	10.5	60 (3s)	413 (3s)	1,550 (3s)	5 (1s)	<5
Pointing Control In arcsec	< 300	10.5	130 (3s)	462 (3s)	1,550 (3s)	120 (1s)	13.3
Pointing Stability (Jitter) In arcsec/sec	0.5	0.5	20 (3s)	5 (3s)	12	1.5	1.2
Mission Design Life In years	1	5	3	3	1	2	3
Smallest Compatible LV	Pegasus	Taurus XL	Minotaur IV	Pegasus XL	Falcon 9	Minotaur I	Minotaur IV

Table 9. Standard Bus Providers for NASA

Contractor	Orbital	SST-US LLC	SST-US LLC	SST-US LLC	Thales Alenia France	Thales Alenia Italy
Parameter Units	LEOStar-2	SSTL-150	SSTL-300	SSTL-600	PROTEUS	PRIMA
Cost in \$M	53.6	16.5	23.5	36	-	-
Orbit Average Payload Power (EOL) in Watts	850	50	140	386	300	1,100
Maximum Payload Mass In kg	500	50	150	200	300	1,138
External Payload Volume In meters	1.54 x 1.24 x 1.66	0.730 x 0.455 x 0.774	0.730 x 0.455 x 1	1.9 x 1.4 x 0.476	Depending on launch fairing envelope	1.3 x 1.3 x 0.7 (on top floor) 1.344 x 0.7 x 3.3 (on two lateral panels)
Bus Dry mass (w/o Payload) In kg	938	103	217.7	429	300	1,032
Science Data Downlink In kbps	300,000	80,000	105,000	105,000	1,000	310,000
Science Data Storage In Mbit	500,000	16,000	16,000	128,000	2,000	1,200
Pointing Knowledge In arcsec	42	25	72	360	20	< 18
Pointing Control In arcsec	48	36	360	605	72	< 36
Pointing Stability (Jitter) In arcsec/sec	1	1.5	2	mission-specific	3	< 1
Mission Design Life In years	5	7	7	4	5	7
Smallest Compatible LV	Falcon 9	Minotaur I	Minotaur 1	Taurus XL	Taurus XL	Falcon 9

Table 10. Standard Bus Providers for NASA Continued

The combination of standard buses and payload designs also drive the target launch platform, which can account for more than 20% of the total mission cost. Table 11 lists standard U.S. provided launches and their estimated costs. The U.S. providers were chosen due to strict International Traffic in Arms Regulations that regulate export of advanced space components, to include export restrictions to foreign launch providers.

Launch Vehicle	Atlas V	Falcon-9	Minotaur IV	Taurus XL	Minotaur I	Pegasus XL
Fairing Size	3.75 m	3.75 m	2.06 m	2.06 m	1.55 m	1.1 m
Mass to Orbit (600km 94 deg inc)	6,800 kg	6,500 kg	1,100 kg	850 kg	375 kg	250 kg
Cost	\$264 M	\$141 M	\$63 M	\$52.3 M	\$20 M	\$40 M

Table 11. Launch Vehicle Costs

D. HOSTED PAYLOAD

Hosted payloads provide an avenue outside of the traditional payload/spacecraft model, which enables the government to utilize excess room onboard a satellite. Some of these concepts allow for an augmentation to the satellite's payload, in the case of a Landsat-hosted payload, or provide room for a payload to operate completely outside of the spacecraft's primary mission. Due to the lack of hosted payload programs there is limited cost and performance data available to determine potential cost saving of this approach. Since the payload does not require separate bus procurement, a conservative cost savings of 20–30% may be realized based upon a set of small missions modeled within NASA's Cost Analysis Data Requirement (CADRe) database (Andraschko et al., 2012). The data also take into account experience from a handful of payloads that have been flown on commercial spacecraft such as those listed in Table 12.

The Commercially Hosted Infrared Payload (CHIRP) was one of the first high visibility, successful demonstrations for a major Air Force system on-board a commercial spacecraft. CHIRP was hosted on SES-2, a commercial

geostationary (GEO) communications satellite, and was a technology demonstrator and risk reduction for the U.S. Air Force's Space-Based Infrared System (SBIRS) GEO platform. With an infrared detector that covered one-quarter of the Earth, CHIRP was able to answer a number of technical questions at a fraction of a dedicated free-flier cost and was hailed a success. At roughly \$215M, CHIRP does not satisfy all the requirements of a SBIRS GEO satellite and is beholden to the SES-2 spacecraft. Platform jitter, survivability, and other performance downfalls do not make CHIRP a viable replacement for the SBIRS GEO constellation, which costs roughly \$1.3 billion per satellite. CHIRP, however, did demonstrate the viability of hosted payloads to satisfy non-operational requirements and other missions without stringent U.S. Air Force requirements. The cost savings demonstrated provide a large incentive to look for hosted payload options for missions that have flexibility in operations and can accommodate commercial, cost-saving practices.

Payload	Mass (kg)	Power (W)	Volume (m ³)	Customer Data Rate (bps)	Payload Type
WAAS	60	300	1	10M	L-band comm
AIS	3	8	0.003	10k	VHF comm
IRIS	90	450	0.127	60M	IP Router
CHIRP	115	275	0.3	70M	IR Sensor
ADF UHF	450	2000	8	4k	UHF comm

Table 12. Previous Commercially Hosted Payloads (from Andraschko, Antol, Horan, and Neil, 2011)

Iridium NEXT provides one of the most promising hosted payload opportunities for a LIDAR system due to its circular low-earth orbit and number of regularly spaced satellites providing global coverage with the constellation. While the satellite payload deck is relatively small, regular access to this platform may

provide an opportunity for rapid integration of new technologies, redundancy of multiple payloads in orbit and the potential to realize cost savings from a payload production line and amortized non-recurring engineering costs.

Iridium NEXT Hosted Payload Parameters	
Orbit Altitude	780 km
Orbit Inclination	86.4 degrees
Number of Satellites	11 satellites in each of 6 planes
Pointing Accuracy	0.5 degrees
Pointing Stability	0.05 degrees over 30 sec
Orbital Knowledge Post-Processed	< 2 cm rms (2-3 day processing)
Reference Frequency	10-MHz
Payload Power	50 W (average) / 200 W (peak)
Payload Mass	< 50 kg
Payload Volume	30 cm x 40 cm x 70 cm
Payload Data Rate	<1 Mbps (average)

Table 13. Iridium NEXT Hosted Payload Parameters (after Richard, Le Roy, Thouvenot, and Escudier, 2008)

V. LIDAR PAYLOAD DESIGN OPTIONS

Space LIDAR payloads are relatively complex instruments that must survive the rigors of space while maintaining tight tolerances due to the nature of laser systems and sensitive receivers. Radiation tolerance, efficiencies due to high power requirements, power handling and system complexity are all key parameters that affect a space LIDAR design. LIDAR payloads generally consist of three main subsystems: a laser transmitter, receiver and a beam-steering/dispersion mechanism. The laser transmitter provides a short pulse of photons that may either be directed towards the target with its inherent beam properties or steered/reshaped to accommodate the ground footprint desired (far-field projection). The receiver then measures the time of flight of the photons to calculate range values while maintaining signal-to-noise ratios (or dark counts) that are commensurate with mission goals. The interplay of these devices, their efficiency and simplicity are necessary to realize a low-cost system for future space-based LIDARs.

A. TRANSMITTER DESIGN

A number of different materials have been developed as lasing mediums for a multitude of applications. Solid-state, dye, chemical, metal-vapor, semiconductor and free-electron lasers are some of the many categories of lasers available today. Of these, few have been rated for space-use or are qualified to survive the rigors of launch and on-orbit operations in a minimal-atmosphere, radiation-rich environment. Solid-state lasers have made up the bulk of lasers launched into space for remote sensing purposes due to their relatively small-size, moderate efficiency, limited outgassing and ability to operate over extended periods of time from electrically-fed, diode sources.

Solid-state lasers, like all laser amplifiers, contain “two elements: a laser medium in which a population inversion... can be achieved, and a pump process to supply energy to the system...” (Koechner & Bass, 2003, p. 13). The laser

medium for solid-state lasers commonly consist of doped crystalline structures (e.g., ruby, Nd:YAG, Nd:glass, etc.) that allow photons to build up within the structure and “lase” at a particular interval. The pump process can utilize any photon source, but current-day LIDAR systems traditionally use pump diodes to supply energy to the system. Solid-state lasers that have been flown in space include ruby and Nd:YAG laser systems that mainly consisted of a switched, pulse-pumped medium that lased at low-frequencies and efficiencies. MOLA and MLA both used a single-stage device, which provided 2–3% electrical to photon conversion efficiencies at 4 and 2 Watts, respectively. These single-stage devices were replaced by a MOPA configuration in the GLAS payload for ICESat-1. MOPA configurations achieve higher powers and efficiencies due to their multi-stage design, using a master oscillator to create a low-power pulse profile that seeds one or more amplifier stages which are more heavily pumped. GLAS maintained 3% efficiency at 4W while achieving this at a wavelength double that of MLA and MOLA. (Coyle, 2005).

1. MOPA Transmitter Overview

The MOPA architecture, despite having experienced difficulties on-board ICESat-1’s mission, remains the most efficient and highest power solid-state lasers available and are on-track for ICESat-2’s ATLAS payload. Numerous trades were made in the ATLAS payload design, which requires short pulse lengths and high beam quality. The MOPA architecture trades included two high reliability master oscillator candidates and the three main types of solid-state power amplifiers, all of which are continuous-wave pumped (Figure 22). These same trades are relevant for the missions being explored in this paper (Yu et al., 2010).

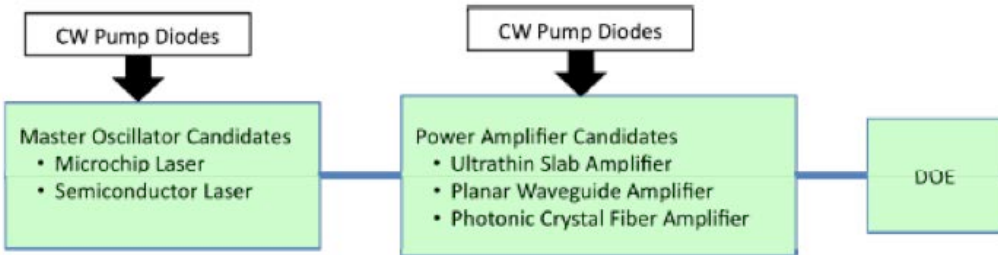


Figure 22. MOPA Laser Architecture in Development for ATLAS (from Yu et al., 2010)

2. Master-Oscillator Design Options

The front-end, or master oscillator, candidates for a space-based MOPA architecture include both microchip lasers and semiconductor lasers. Microchip lasers are compact passively Q-switched devices that are common throughout the commercial industry. Passive Q-switching involves a medium that, when pumped beyond a certain threshold, will lase. This threshold can be controlled within materials such as organic crystals, doped crystals or “bleach” diodes that enable a precise, constant-interval, and short-pulse seed laser. While commonly used throughout industry, the passive Q-switch is a complex device with fluctuations that may be induced by the environment. The inability to tune the pulse repetition frequency and pulse length requires precise design for these moderate power front-ends in order to maintain constant performance in a harsh thermal and radiation environment.

Semiconductor lasers rely on an alternative method of switching called direct modulation. The electrical signal applied to the semiconductor laser, or laser diode, provides the pulse length and pulse repetition frequency. These laser diodes operate in the multiple nanosecond range individually, but can be combined to produce very short pulse lengths at low front-end power levels (Starodoumov, 2008). These laser diode systems have the advantages of less-complexity coupled with increased flexibility and reliability due to reliance on technologies that have been space-qualified.

3. Power Amplifier Design Options

The amplifier is fed by the master-oscillator front-end and increases the power of the beam to levels commensurate with closing a LIDAR link. Three main amplification mediums are under consideration: bulk crystal, planar waveguides and fiber amplifiers. Bulk crystals, or slab lasers, “are mature technologies that have been used for most space-based laser systems (MOLA, GLAS, MLA, CALIPSO and LOLA). They are potentially very simple and robust systems. The biggest technical challenge for this type of amplifier is achieving high optical efficiency...” (Yu et al., 2010, p. 757809-5). The efficiency losses are due to poor spatial modes, since the laser beam has no three-dimensional confines, but slab lasers remain the highest power-handling laser available. Slab lasers have been demonstrated on-orbit over multiple missions with high reliability and long lifetimes, providing the confidence of space heritage in these designs.

Planar waveguides (PWGs) offer slightly higher performance and efficiencies due to one-dimensional confinement. PWGs confine the laser beam in one direction, allowing for an increase in optical efficiency over that of bulk by roughly 2 times (10-15% efficient), but maintain their ability to handle moderate power levels. “Planar waveguide lasers and amplifiers have the potential to achieve multi-kW output power with good beam quality and high efficiency” (Yu et al., 2010, p. 757809-6). Recent advancements in PWG development and space qualification prior to the ATLAS down-select have shown promising results for moderate-power, high PRF applications, but have yet to be flown on-board any satellite system. These lasers have demonstrated performance and reliable radiation performance through a number of government programs (Yu, Krainak, Harding, Abshire, and Sun, 2011).

Fiber amplifiers and photonic crystal rods provide further performance increases in terms of efficiency (15-20% efficient) and beam quality over that of PWGs and bulk crystals. By confining the beam in two directions, a fiber amplifier is able to utilize more photons in the amplification process, but also is limited in

power handling due to size constraints. Photonic crystal rods are inflexible fibers that are patterned to keep a single-mode performance while increasing their size to increase power handling. These rods have both launch survivability and packaging concerns, but do leverage the efficiencies gained by spatial confinement. Another advantage of fiber amplifiers is the ability to fiber-couple the components, thereby reducing the complexity of space-qualifying free space optics and the contamination that occurs from the initial outgassing of materials in space. Fiber lasers have yet to be demonstrated in space, but components have been tested to TRL 6, having proven their performance in space-like radiation environments. Radiation was a significant concern when fibers were first introduced and tested for the space environment, but additional work in Yb-doped fibers and additional rare-earth dopants have improved their radiation performance. These lasers have “exhibit[ed] reasonable radiation resistance to gamma exposures typical of a 5-year, low-earth-orbit environment. Maximum transmittance losses of less than 10% were observed for total gamma exposures of 2–5 krad (Si)” (Fox et al., 2007, p. 645328).

4. Beam Steering and Shaping Design Options

To increase efficient use of the photons from laser and receiver elements on a detector, the transmitter beam may need to be steered and shaped in order to provide the performance desired. For beam steering, body steering is an option, but for high PRF lasers this is difficult. Diffractive or holographic optical elements and field-steering mirrors are both options for controlling the footprint of a limited beam-width laser if body steering cannot be accomplished. DOEs are etched crystalline structures that redirect light to achieve the footprints and power levels needed in each beam. These dispersion elements may rotate to move the beams within the field of view or remain static so as to provide a consistent footprint. DOEs were first flown on the LOLA payload aboard the LRO and are planned for the ICESat-2 mission. LOLA provided 5 beams from a single laser (Figure 23) while ICESat-2 is designing a non-homogeneous 9-beam DOE, both of which are static (Ramos-Izquierdo et al., 2009).

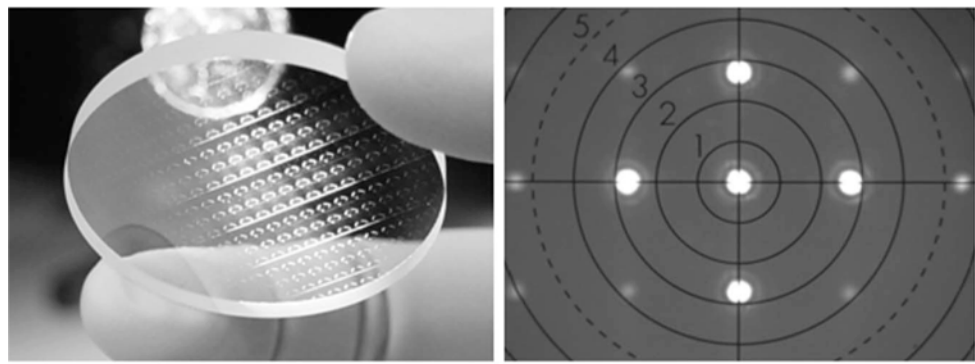


Figure 23. LOLA Diffractive Optical Element (from Ramos-Izquierdo et al., 2009)

Field steering mirrors (FSMs) are another option for controlling the beam footprint. FSMs are commonly used when greater beam control is needed, such as for sweeping or scanning, and are also aligned with the receive path. Steering mirrors are actuated structures and “capable of producing three-axis movements (tip, tilt, and piston)” to provide maximum pointing flexibility (Tapos et al., 2005, p. 587707-1). FSMs, however, add a level of complexity to system design due to the additional control software and thermal modeling needed. In a zero-gravity environment, the effects of FSM motion and jitter on the platform must also be considered, but are well understood with TRL-9, flight-proven products available.

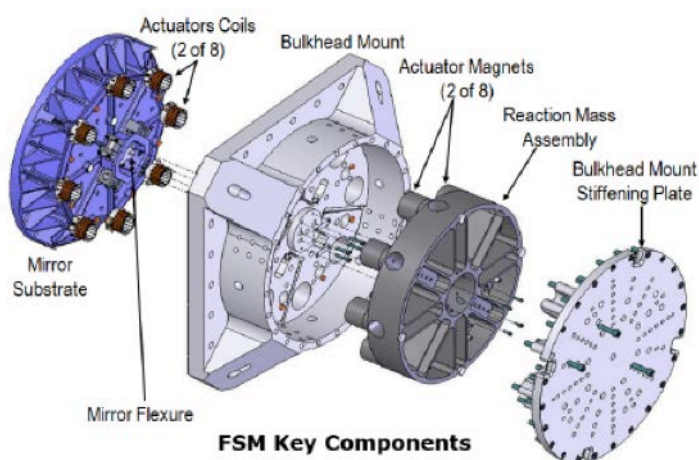


Figure 24. Fast Steering Mirror Exploded View (from Applied Technology Associates, 2011)

Other options exist for beam shaping depending on the transmitter selection, if any beam-shaping or steering is necessary. For multi-laser systems (e.g., fiber laser arrays), the pulse power can be apportioned across multiple transmitters versus a single pumped source. Since LIDAR does not rely on a coherent, phase-matched signal to make time-of-flight measurements, lasers can be tiled and incoherently combined in the far-field to produce the footprint desired. With laser light being highly collimated, divergence can also be controlled for each footprint with little added system complexity. In some cases, no beam-shaping or steering may be necessary and only beam divergence will need to be controlled to determine the optimal footprint.

B. RECEIVER DESIGN

Multiple sensitive, high-efficiency receivers exist to support space-based LIDAR missions that operate in photon-starved environments. The higher the efficiency of the detector, the lower the laser power required to obtain the same area collection rate, driving the need for high sensitivity receivers. NASA, as part of ICESat-2, recently examined the field of photon-multiplying receivers in both the visible (552-nm) and near-infrared (1064-nm) bands. Since the initial trades made by NASA for ICESat-2's LIDAR detectors by Krainak et al., significant research has been accomplished in the field of single-photon sensitive devices, with progress made in avalanche photodiode development.

NASA's examination of LIDAR detectors included a variety of photon-sensitive detectors such as: analog photo-multiplier tubes (PMTs), digital photodiodes and Geiger-mode avalanche photodiodes (GmAPDs). Analog PMTs have a long history aboard NASA space-based missions, providing robust space-qualified LIDAR receiver solutions. These detectors utilize dynodes, or photo-electron multiplication areas, to amplify a signal, but suffer from limited sensitivity and moderate noise. These detectors required tens to hundreds of photons to trigger a detection due to the gain and noise shortfalls. Recently, alternative low-noise single-photon-sensitive detectors have emerged, such as avalanche photodiodes.

Silicon APDs have been used in a number of space missions (ICESat-1's LIDAR Payload and PAMELA's astrophysics payload) with success. With high radiation tolerance and lifetimes in excess of 5 years, these detectors rely on high-bias voltages to enable single-photon sensitivity (Aull et al., 2002). There is, however, a balance between the photon detection efficiency and noise (or dark count) of the system. Dark counts in excess of 500 kHz existed on the GLAS SiAPD, limiting the performance of the 65% efficient detectors. On the other hand, PAMELA's detectors had low sensitivity (15%) and low dark count rates (100 Hz), but with large detector diameters. Si APDs have "two major limitations, namely, 1) each Si APD can detect only one photon at a time with a fifty-nanosecond dead time and 2) each Si APD has a nonlinear saturation effect at high photon count rates" (Krainak et al., 2010, p. 760827-1). The nonlinear saturation makes collection difficult with the detector easily overwhelmed by high background visible signal levels from sunlight and moonlight (Figure 25). In addition to the receiver limitations, silicon detectors mainly operate with laser transmitters at 532-nm wavelength, which requires a frequency-doubling of the native 1064-nm wavelength laser. By converting to the 532-nm wavelength, half the number of photons is transmitted (due to the higher energy of the 532-nm photons) and the laser efficiency is also lower, by roughly 20%. These two phenomena combined reduce the expected received signal from a 532-nm laser compared to the 1064-nm laser.

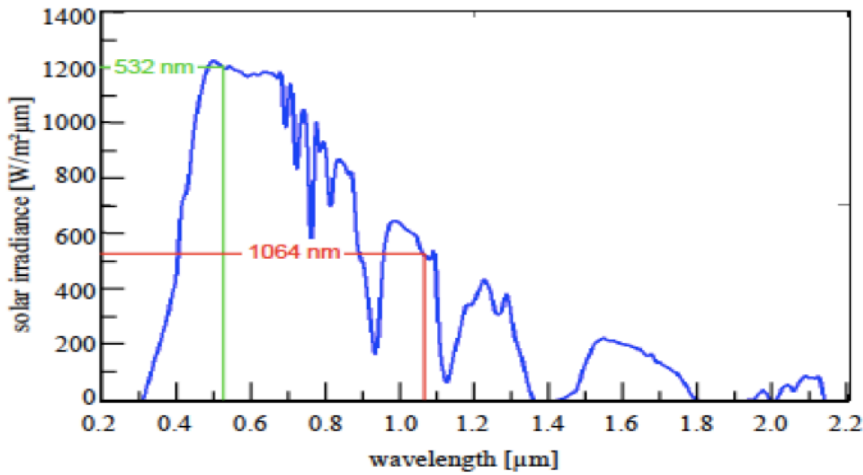


Figure 25. Solar Background Irradiance

One-micron avalanche photodiodes, most notably InP/InGaAsP Geiger-mode APDs, were also investigated in the NASA study. Operating at 1064 nm, these detectors use the same voltage biasing to achieve single-photon detection performance but do not experience such high levels of background solar illumination and take advantage of the increased number of photons as opposed to SiAPDs at 532 nm. GmAPDs suffer from the same dead time as SiAPDs, however, significant time between laser pulses alleviates this problem. NASA's study also pointed out a low photon detection efficiency and moderate dark count rate, nullifying many of the advantages of the 1064nm operating wavelength. Further analysis of GmAPD arrays from Spectrolab showed sensitivity to radiation damage leading to high dark count rates and only a 1–2 year expected lifetime (Figure 26) (Becker, Farr, and Zhu, 2007). These combined shortfalls led NASA to select SiAPDs for the ICESat-2 mission, but recent advancements in 1064-nm devices have improved the photon detection efficiency and have the potential to increase the radiation hardness of the detectors.

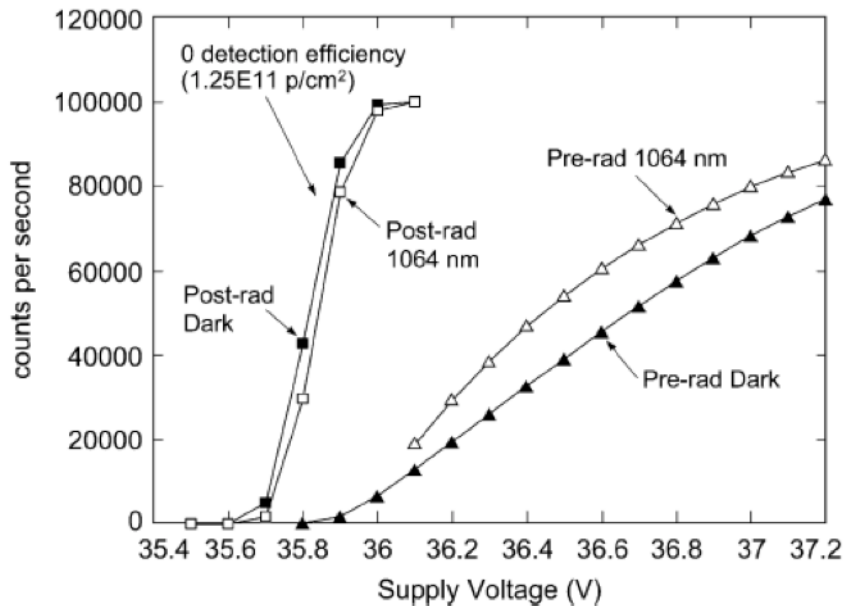


Figure 26. Pre and Post-Irradiation Curves for Spectrolab GmAPD (from Becker et al., 2007)

Continued research and development in InP GmAPDs have resulted in an increased detector array size (32x128) with reduced pixel pitch. As a result, the overall dark count rate and active area cross-section have been reduced, enabling higher overbias and a 40% photon detection efficiency (PDE) with 10 kHz dark count rate (Yuan et al., 2011). The 30-micron active area of the device, along with additional thermoelectric cooling, is estimated to increase radiation performance enough for a five-year lifetime. Spectrolab's GmAPDs currently show on-par performance with the SiAPDs but with greater system performance implications.

VI. LIDAR MISSION DESIGN

A. LINK BUDGET

There are a number of effects and physical processes that factor into the link budget for a space-based LIDAR system. Atmospheric absorption, Mie and Rayleigh scattering, atmospheric refraction and target surface reflectance characteristics are key environmental parameters in link budget calculations. Figure 27 illustrates a number of the variables that affect a space-based LIDAR system. In the transmission path, the atmosphere attenuates (or absorbs) part of the transmitted power due to water and aerosol absorption and scattering. This attenuation is wavelength dependent. The atmosphere also will refract the transmitted beam due to differences in atmospheric density. Atmospheric refraction is the bending of light through the atmosphere that causes both beam spreading and a transmitter/receiver spatial offset that also can be modeled and is assumed to be negligible in the design of this direct detect system. Also in the transmission path is additional beam-spreading caused by atmospheric turbulence and the transmit optics. This will ultimately determine the footprint of the laser on the ground. In addition to the atmospheric effects, jitter, drift and broadening of the laser pulse may occur and need to be compensated in the system. These effects may originate from thermal variations in the laser components as well as spacecraft structural warping from temperature differences.

In the receive path, the footprint must be aligned with the receiver footprint to maximize photons received. Footprint overlap may vary due to thermal variations in the transmitter and receiver as well as lead-lag considerations due to the high altitude and speed of the spacecraft. The lead-lag considerations require approximate terrain knowledge to understand the time of flight for a photon and the spacecraft pointing compensation required since it is moving at such a high rate of speed. Also in the receive path are the major effects of topographical scatter and multi-bounce. The laser will scatter off the surface of

an object based upon the object's surface roughness and the wavelength of the laser. After scattering off an object, the light may also reflect off another object and towards the receive aperture, creating a longer return pathway and a potential "false" return. In addition to the atmospheric effects in the transmit path, those same effects must be compensated for in the return path. Another effect in both the transmit and return paths is speckle. Speckle is the spatial interference of the laser beam due to atmospheric factors such as scintillation and the target's surface roughness (Andrews, L. C., & Phillips, R. L., 2005). This causes an interference pattern to form that can be addressed temporally, spectrally and spatially and is assumed to be negligible in the design of this direct detect system. Space and airborne demonstrations of direct detect, high PRF LIDAR systems have shown all of these effects can be compensated for in the system design with little impact on the basic link budget equation.

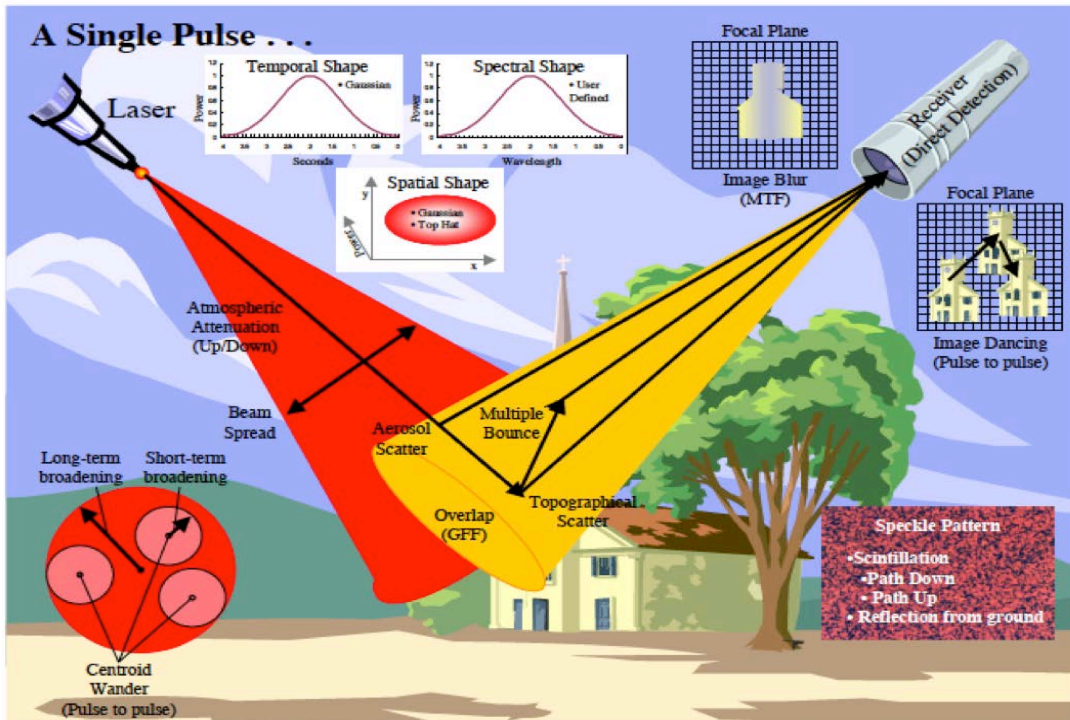


Figure 27. LIDAR Link Budget Variables (from Burton, 2002)

"The governing equation for the received signal captured by the sensor is derived from the general LIDAR equation for elastic scattering ... [T]he received number of photons from a range R due to elastic backscattered radiation can be written as" (Brown, Blevins, and Schott, 2005, p. 4)

$$N_{\text{detected}}(\lambda, R) = N_L(\lambda) \xi(\lambda, R) \frac{A_r}{R^2} \frac{\rho_s(\lambda)}{\pi} \exp \left[-2 \int_0^R \sigma_{\text{ext}}(\lambda, r) dr \right] \quad (1.3)$$

N_{detected} represents the number of photons received per detector based upon the wavelength and distance from the target. N_L represents the number of photons transmitted at the chosen wavelength, $\xi(\lambda, R)$ includes the efficiency of the detector and considerations for the overlap of the transmitter beam and receiver field of view, $\frac{A_r}{R^2}$ is the area of the receiving optics over the distance from the target squared, ρ_s is the scattering efficiency of the target at the chosen wavelength, σ_{ext} is the extinction coefficient which is mainly the atmospheric absorption that is integrated over a chosen distance (Brown et al., 2005).

There are a number of assumptions that simplify this equation both due to the space-based location, atmospheric considerations and target characteristics. Kim, Lee, and Kwon demonstrate that, considering, "...for an extended target, the footprint of the beam is smaller than the target surface, the returned power can be calculated using the transmitted power, the travel distance of the laser beam, the reflectance of the target surface, and the aperture diameter of the receiver..." (Kim, Lee and Kwon, 2013, p. 8472). Kim's equation is represented in Equation 1.4. P_r represents the overall power received per detector. P_t is the transmitted power, $\rho \frac{1}{\Omega_s}$ is the reflectance and scattering efficiency, $\frac{\pi D^2}{4}$ is the area of the optic, η_{atm} is the transmission efficiency of the atmosphere and η_{sys} is the transmission efficiency of the system. The transmission efficiency of the atmosphere must take into account both the transmission and return paths and is effectively a squared term. The efficiency of the system includes the efficiency of the transmit and receive optics, any filters and the fill factor of the receiver (Kim et al., 2013).

$$P_r = P_t \rho \frac{1}{\Omega} \frac{\pi D^2}{R^2} \frac{4}{s} \eta_{atm} \eta_{sys} \quad (1.4)$$

$$\eta_{atm} = T_{atmIX} T_{atmRX} = T_{atm}^2 \quad (1.5)$$

$$\eta_{sys} = T_{BPF} T_{ND} T_{FF} T_T T_R \quad (1.6)$$

$$P_r = \frac{P_t \rho D^2 T_{atm}^2 T_{BPF} T_{ND} T_{FF} T_T T_R}{4 R^2} \quad (1.7)$$

With single-photon sensitive GmAPDs, power at the receiver is not enough to determine the link margin due to the inability to resolve multiple photons. Instead of power at the receiver, the equation requires adjustments to determine the number of photoelectrons generated. In order to arrive at this conclusion, the power transmitted is multiplied by $\frac{\lambda}{\pi hc}$, adjusting the equations to calculate the number of photons received. For a detector array, to determine the number of photons per pixel per pulse, the area of the telescope must be divided by the number of pixels in the detector. Further, to arrive at the number of photoelectrons generated at the detector, the entire equation must be multiplied by the efficiency of the detector resulting in Equation 1.8.

$$N_{PE} = \frac{\rho}{\pi hc} \lambda T_{RO} T_{RO} \frac{A_{TEL}}{N_{Pixels}} f_{LL} \frac{T_{ATM}^2}{R^2} E_p \eta_{APD} \quad (1.8)$$

Multiple noise sources exist for a LIDAR system with the most prevalent being background radiation and dark count. Background radiation, or solar reflectance, varies throughout the day and is negligible during nighttime collects. At 1064 nm, the background radiation is significantly lower than previously built platforms operating at 532 nm. Based upon the Infrared Handbook, the solar irradiance at 1064 nm is 526 W/m²/μm (Zissis & Wolfe, 1978). Within the assumed bandpass filter of 5nm centered at 1064 nm, the power density is 2.63 μW/m² compared to 5.94 μW /m² at 532 nm. The power density is reported at sea level and can be inserted into the link budget (Equation 1.8) and substituted for the transmit power and multiplied by the detector array IFOV. A number of

other variables also need to be removed since the power density already accounts for a one-way atmospheric loss and does not pass through the transmit optics, arriving at Equation 1.9.

$$N_{SunPE} = \frac{\rho}{\pi hc} \lambda T_{RO} \frac{A_{TEL}}{N_{Pixels}} f_{LL} \frac{T_{ATM}^2}{R^2} E_{SunP} IFOV \eta_{APD} \quad (1.9)$$

The dark count rate also includes the LIDAR system noise and is detector dependent. The dark count rate is measured in Hz, kHz or dark counts per second and is inherent within the detector, thereby requiring no additional application of system losses. Digital detectors, like GmAPDs, rely on a single-photon counting strategy to determine where a surface lies in 3-D space. The read-out of a GmAPD is typically timed to a single pulse from the detector, requiring a range gate that assumes the approximate return time of the pulse. The range gate is divided into range bins to create a higher accuracy range measurement. To calculate the effect of noise on the system, both the dark count rate and background noise need to take into account the length of the range gate. Equation 1.10 shows a calculation of the number of “noise” photoelectrons per pixel per pulse where $T_{RangeGate}$ is the total amount of time the range gate is open per pulse. The range gate is assumed to be variable due to the need to characterize large variations in height in urban and high relief terrains. The range gate will vary from 3.3 μ s (\sim 1km) to 0.33 μ s (\sim 100m) with the noise calculated at the worst-case scenario of 3.3 μ s. Equation 1.11 then calculates the Poisson statistical probability of false alarm from the noise within the range gate.

$$N_{NoisePE} = (N_{SunPE} + DCR)T_{RangeGate} \quad (1.10)$$

$$P_{fa} = 1 - e^{(-N_{NoisePE})} \quad (1.11)$$

B. ASSUMPTIONS

The push towards lower cost missions and payloads has driven the need for simplicity and efficiency for space-borne LIDAR designs. Advanced technologies may also reduce cost by reducing bus requirements such as power, mass and thermal dissipation. Progress made since ICESat-2’s System

Requirements Review has increased the robustness of fiber lasers and radiation performance of 1064-nm GmAPD detectors, two key enablers for low-cost, high-performance space LIDAR missions. As the full system has yet to be developed, multiple assumptions will need to be made.

1. Transmitter Assumptions

Fiber-based MOPA architectures represent a significant improvement on slab lasers in terms of power density and efficiency. With efficiencies more than double that of the LOLA and GLAS transmitters, a conservative estimate of the two new proposed architectures', tiled and tapered fiber lasers, characteristics can be found in Table 14. These estimates are based upon coiled Yb-doped fibers, nLight Element diodes and the need for minimal additional equipment such as couplers, thermal sinks, power converters and minor optical elements (nLight, 2013; Farrow et al., 2006).

	Yb-Doped Tiled Fiber Laser	Yb-Doped Tapered Fiber Laser
Operational Wavelength	1064 nm	1064 nm
Average/Peak Power	2.5 W / 260 kW	4 W / 420 kW
Power per Pulse	250 μ J	400 μ J
Pulse Repetition Frequency	10 kHz	10 kHz
Electrical to Optical Efficiency	15%	20 %
Dimensions	30 cm x 30 cm x 4 cm	40 cm x 40 cm x 6 cm
Mass	4 kg per fiber	6 kg per fiber
Heat Dissipation Required	14.16 W per fiber	21.34 W per fiber

Table 14. Yb-Doped Tiled and Tapered Fiber Lasers Predicted Performance

Beam-steering and shaping may also be necessary due to limited optics size, limited platform agility or the need for a higher collection swath. Utah State Space Dynamics Laboratory has designed a compact, lightweight and low-cost FSM for space with characteristics detailed in Table 15 (Wasson et al., 2006).

For beam-shaping, collimating and refractive optics are negligible and assumed to be contained within the transmitter calculations.

Utah State University's Fast-Steering Mirror	
Aperture Size	75mm
Mass	1 kg
Power	0.4 W
Along Track Pointing	+/- 30 degrees
Across Track Pointing	+/- 60 degrees
Slew Rate	>75 degrees/second

Table 15. Utah State University's FSM Performance Characteristics (after Wassam et al., 2006)

2. Receiver Assumptions

The receiver selection is based upon Spectrolab's Spectrocam line, both the commercially available 32 x 32 pixel camera and conservative estimates of a 32 x 128 and 2 x 32 x 128 pixel camera in development. The SpectroCam LG3D is a commercially available terrestrial product from Boeing Spectrolab that is based on the 32 x 32 pixel GmAPD array. The camera and detector specifications can be seen in Table 16; however, some variables have been updated to reflect the expected DCR and PDE for the new series of smaller pixel pitch detectors. In addition to these terrestrial camera specifications and extrapolation out to larger sizes, a doubling of the camera mass is assumed to accommodate the extra thermal and radiation environment hardening needs (copper cores, thermal straps, spot shielding, etc.).

Array Size	32 x 32	32 x 128	32 x 256
Pixel Pitch	25 μm	25 μm	25 μm
Dark Count Rate	4 kHz	4 kHz	4 kHz
Photon Detection Efficiency	40%	40%	40%
Frame Rate	10 kHz	10 kHz	10 kHz
Power	30 W	40 W	50 W
Mass (including environment hardening)	2.27 kg	3.18 kg	4.08 kg
Thermal Load	15 W	20 W	25 W
Dimensions	12x12x12 cm	13x13x13 cm	15x15x15 cm

Table 16. Estimated GmAPD Receiver Performance Characteristics

A payload processor is also necessary to coordinate the timing of the laser firing and the receiver opening its range gate along with a host of other functions. A radiation hardened Virtex-5 SIRF chip is planned as the processing solution with an assumed mass of 4 kg, a size of 10 x 20 x 5 cm and power consumption of 20 W. Along with controlling the payload, the processor will also provide data thinning and compression functions to reduce the data rate by 60% (e.g., discarding beginning and end of range gate returns). The data rate is governed by the array size, a system timestamp associated with a laser pulse and the receiver range gate boundaries, a vehicle pointing solution, a vehicle ephemeris solution and a payload pointing solution if there is a steering mechanism. The system data rate takes these all into account and assumes the vehicle pointing and ephemeris data are handled by the host telemetry system while the timestamps, triggered pixel mapping and payload pointing are handled by the payload data downlink. The data rate assumes a worst-case scenario, where all pixels are triggered on every pulse, the timestamps are 64-bits and payload pointing is 64-bits, resulting in Equation 1.12.

$$DataRate = N_{pixels} + 2N_{Timestamp} + N_{pointing} F_R \lceil 0.6 \quad (1.12)$$

3. Thermal Assumptions

With the potential for high heat loads due to the inefficiency of the laser transmitters, thermal dissipation must be taken into account. Both silvered Teflon and aluminized kapton, at an emissivity of 0.9, can reject a substantial amount of heat and are standard materials for spacecraft thermal radiators. The main radiator is assumed to operate at room temperature (298K) and deep space facing. Equation 1.13 calculates the heat dissipation power of a radiator with surface area A, emittance of ϵ , operating at an absolute temperature in Kelvin of T and all multiplied by the Stephan-Boltzmann constant of σ . According to the equation, the total thermal dissipation of the radiators per meter is calculated to be 402 W/m². In addition to the transmitter radiators, the detectors are run at 240 K with a single-stage thermoelectric cooler. At 240 K, a secondary radiator is needed with a heat dissipation of 169 W/m².

$$Q = A\epsilon\sigma T^4 \quad (1.13)$$

4. Telescope Mass Assumptions

The telescope aperture, playing a key role in the link budget equation, is the main driver for the payload mass and volume. Combining both the Stahl parametric cost equation based on diameter and equation based on mass, an estimated OTA mass can be calculated based upon diameter (Equation 1.15).

$$Cost_{OTA} \approx Mass_{OTA}^{0.72} \quad (1.14)$$

$$Mass_{OTA} \approx (D_{OTA}\lambda^{-0.2})^{1.389} \quad (1.15)$$

5. Mission Assumptions

A number of assumptions are also made within the link budget equation and mission space that will aid in the determination of transmitter power required and area collection rates. The LIDAR target is assumed to be lambertian or isotropically scattering due to the anticipated surface roughness of most non-man-made objects at 1064 nm, the transmitter frequency. Highly polished and glossy materials may have different scattering properties (non-isotropic) and will

not be evaluated as part of this model. The hemispherical reflectivity of the target is assumed to be a conservative 20% based upon previous experiences with airborne LIDAR testing. Foliage, man-made targets, ice sheets, etc., all maintain individual reflectivities at the wavelength chosen and span a wide range of values, requiring a simplification for the purposes of this thesis. The efficiency of the transmit optics is assumed to be 95%, due to additional refractive optics and collimators that may be necessary. The efficiency of the receive optics is assumed to be 75% due to inefficiencies in the reflective optics, telescope obscuration and any filters and folding optics. The fill factor of the detectors is assumed to be 80%, due to the inefficiency of the GmAPD lenslets. At nadir, the one-way atmospheric transmission of the 1064nm wavelength is 94%. Accounting for these assumptions, the link budget equation then becomes:

$$N_{PE} = \frac{0.20}{\pi hc} (1.064 \times 10^{-6}) (0.95) (0.75) \frac{A_{tel}}{N_{pixels}} (0.80) \frac{0.942}{R^2} E_p (0.40) \quad (1.16)$$

Additional assumptions are required to determine area collection rates and optimize the space-based LIDAR solutions. With GmAPDs, only one photoelectron can be detected per pixel per range gate, therefore if more than one photoelectron were to be generated, transmitter power would be wasted. To optimize the system's efficiency, the number of expected photoelectrons per pixel per pulse should be tuned to between 0.2 and 0.3, reducing the likelihood that two transmitted photons would arrive at the detector and trigger photoelectrons. For link budget purposes and to increase the probability of detection in the presence of noise, the number of photoelectrons per pixel per pulse is set at 0.3. To determine area coverage rates, the number of detections per surface must be set and account for noise factors and returns from atmospheric particulates. Historical airborne LIDAR data have demonstrated that the minimum number of detections per surface to perform coincident processing is between 3 and 6. In order to remain conservative, the number of detections per surface or GSD will be set at 6. With 6 detections necessary for a surface detection and 0.3 photoelectrons per pixel per pulse anticipated, 20 pulses would be required to

close the link in a noiseless environment. While noise and false returns represent a very small potential number of photoelectrons, to combat this, a margin of 10X is levied on the system, requiring 50 pulses to resolve a surface. With the number of samples required per GSD, the area collection rate can now be determined assuming a uniform beam distribution on the detector (Equation 1.17).

$$ACR = \frac{prf}{\frac{N_{samples}}{GSD \cdot N_{pixels}}} \quad (1.17)$$

$$ACR = \frac{\frac{10000}{50}}{GSD \cdot N_{pixels}} \quad (1.18)$$

THIS PAGE INTENTIONALLY LEFT BLANK

VII. LIDAR SYSTEM DESIGN AND COSTS

A. IRIDIUM HOSTED PAYLOAD DESIGN

The Iridium Hosted Payload may be the lowest cost solution by leveraging the already procured host bus and ground infrastructure, however hosting considerations limit the size, mass and power of the payload substantially. The volume constraint is one of the most stringent, requiring an optic of less than 1 meter with little room for the transmitter and receiver. The payload mass and power parameters further restrict this active system, beyond a usable point.

1. 32x32 Array Detector-Based Payload Design

At 780 km in altitude, a number of trades were made to determine, for a fixed detector (32x32) and a varying number of transmit fibers, the aperture diameter needed to close the link budget. The assumptions from previous chapters were used and the corresponding mass and power requirements were calculated. Figures 28 and 29 portray the mass and power of the payload as the number of fiber lasers is decreased. The increase in mass is due to the need to maintain 0.3 photons per pixel per pulse at each of the 1024 detector elements, requiring the aperture size to compensate for the reduced transmit power and thereby increasing the mass substantially. None of the trades for a 32x32 array satisfy the Iridium NEXT hosted payload parameters. With the transmitter driving power requirements, there are very few options that could be sustained at 100% duty cycle. Reducing the duty cycle to 10%, all of the transmitter options studied meet the Iridium power requirements with at least 2X power margin. Looking at Figure 29 again, however, it becomes apparent that all potential payload options exceed the 50 kg mass requirement by 2X. Figure 30 shows the major mass driver, the receive optics, and its relationship with payload mass.

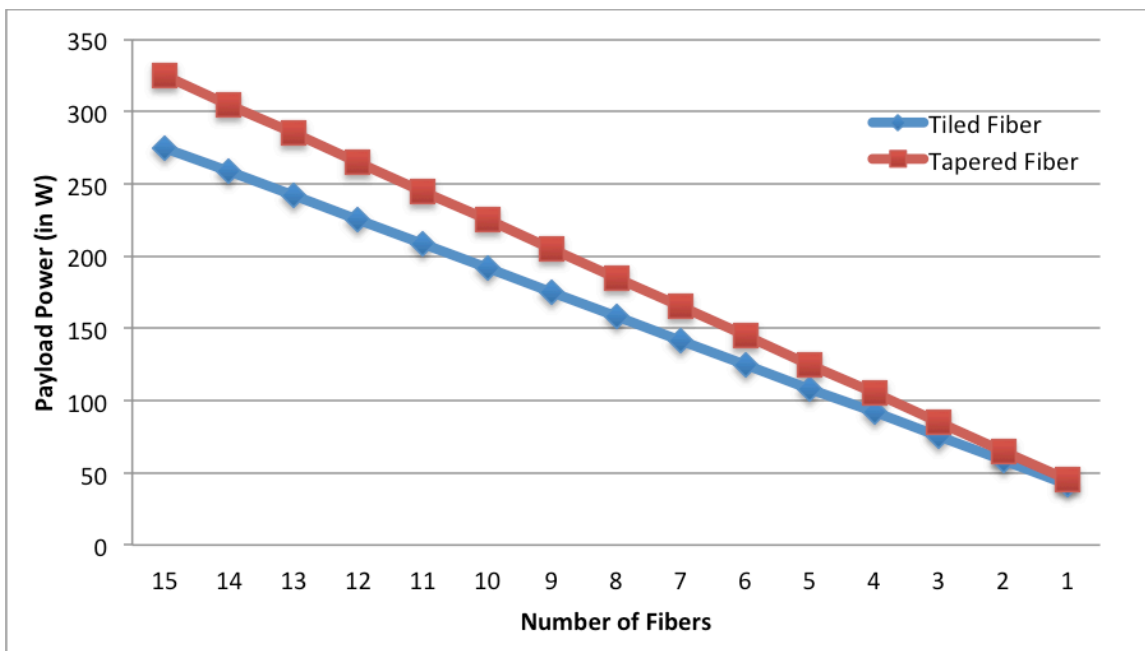


Figure 28. Iridium NEXT 32x32 Array Payload Power Design Trades

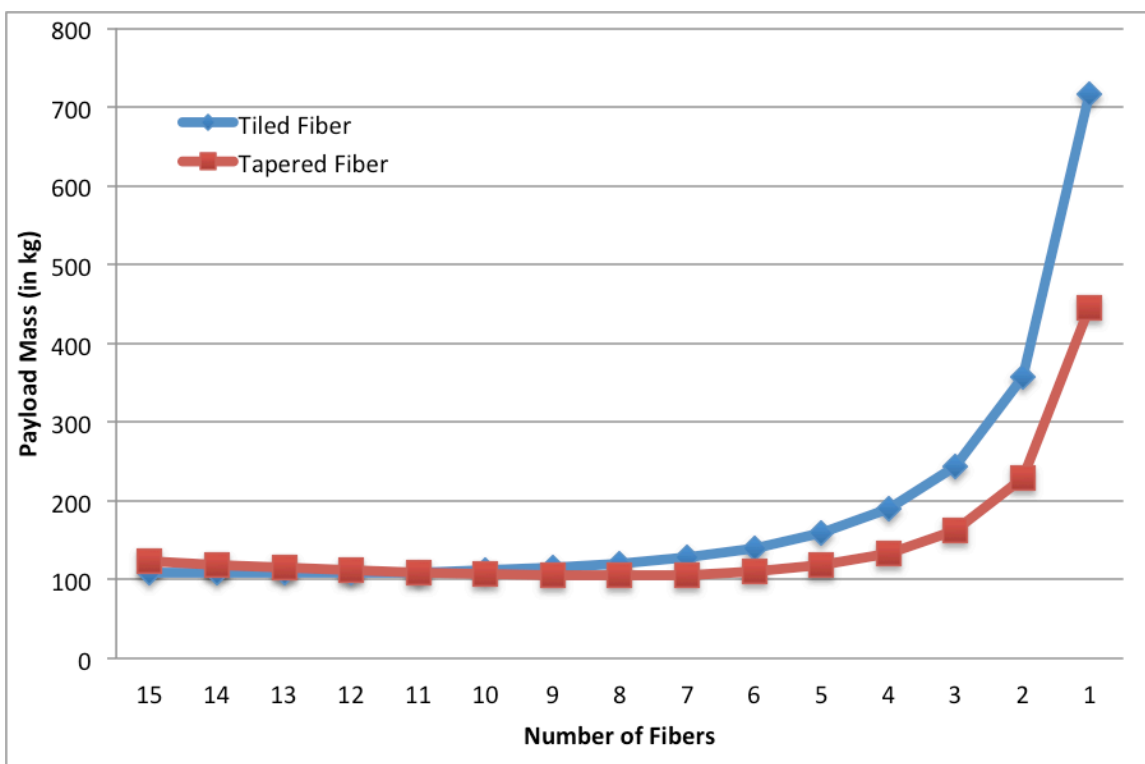


Figure 29. Iridium NEXT 32x32 Array Payload Mass Design Trades

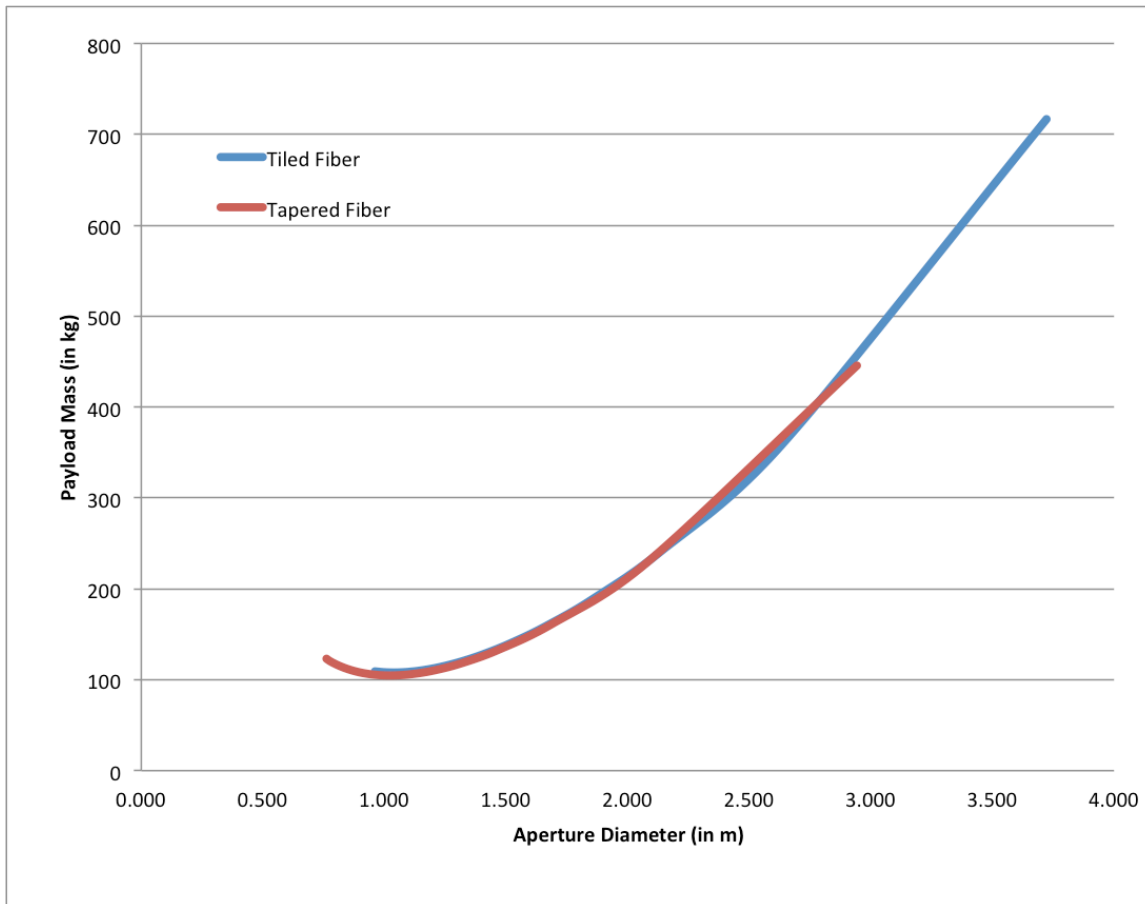


Figure 30. Iridium NEXT 32x32 Array Payload Mass Versus Aperture Diameters

2. 10X10 Array Detector-Based Payload Design

The smallest aperture identified by the link budget equation is 0.76 meters, which exceeds the required dimensions, and has a mass over 123 kg. To reduce the mass and aperture size, the number of “illuminated” pixels must be reduced. Maintaining a 32x32 pixel detector will allow for the leveraging of a commercial product, however, given the mass constraints, the transmitter beam must be shaped to only illuminate a 10x10 pixel area within the detector array. Figures 31 through 33 show the impact of a reduced illumination area while only having to close the link on 100 pixels and maintaining a 10% duty cycle. These calculations allow for a 2X margin in power and significantly reduced aperture sizes, allowing a LIDAR payload to meet the Iridium mass and power constraints.

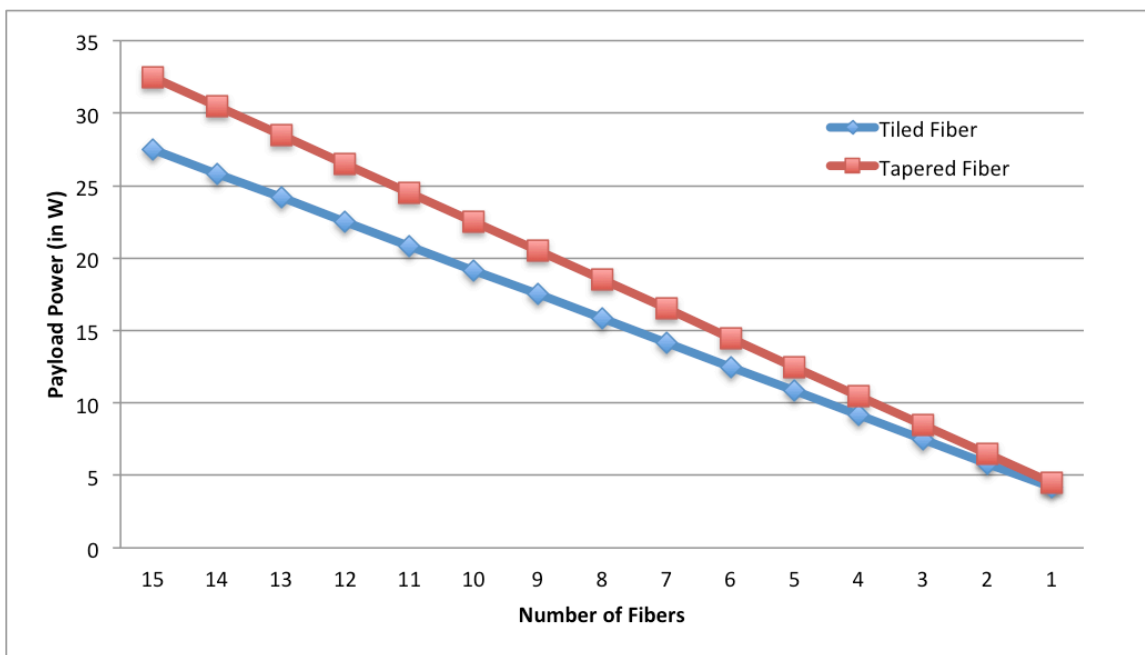


Figure 31. 10% Duty Cycle Iridium NEXT 10x10 Array Payload Power Design Trades

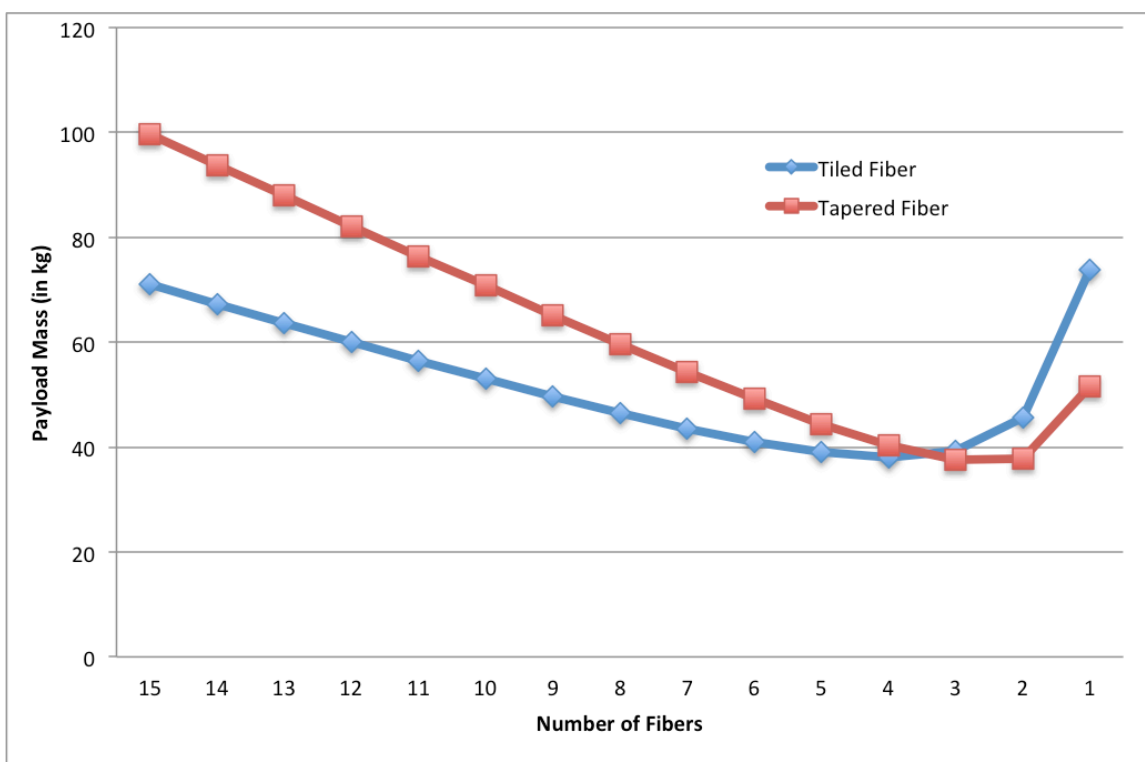


Figure 32. 10% Duty Cycle Iridium NEXT 10x10 Array Payload Mass Design Trades

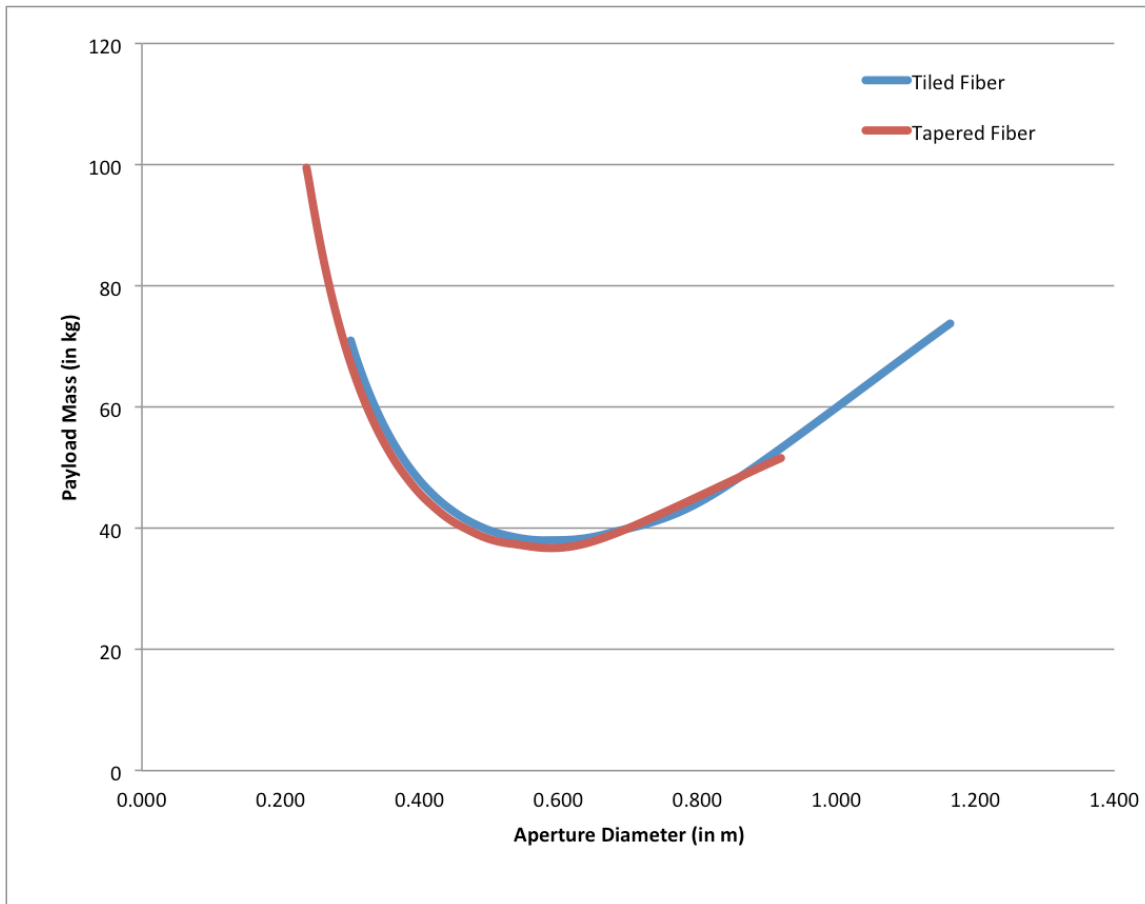


Figure 33. 10% Duty Cycle Iridium NEXT 10x10 Array Payload Mass Versus Aperture Diameters

Beyond the mass and power constraints, volume is the next major consideration, with the aperture being of greatest concern. Deployable and compact optical systems are possible and being developed for small spacecraft such as cubesats and other nano-class satellites. These systems may reduce the launch volume of optical systems by roughly 40%, using either deployable optics or compact optics that create a larger focal length by innovative light path folding techniques. The total payload volume vs. mass is seen in Figure 34, and demonstrates that most of the payload options exceed the system volume constraints. None of the tapered fiber options provide a viable payload from a volumetric perspective, but eight of the tiled fiber options narrowly meet the volumetric requirements of the system.

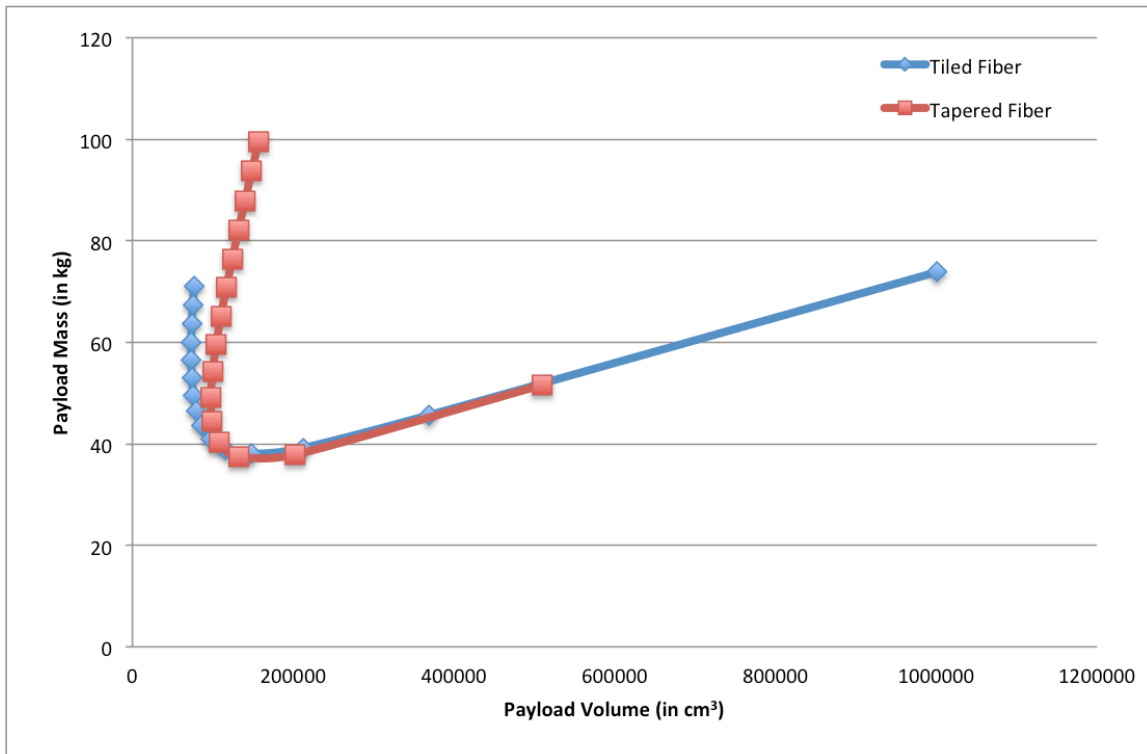


Figure 34. 10% Duty Cycle Iridium NEXT 10x10 Array Payload Mass Versus Volume Designs

Comparing the eight options that meet the volumetric constraints, only two satisfy the mass, power and volume constraints (Table 17). At 10% duty cycle, these systems easily meet the power requirements with greater than 65% margin. The mass margin is nearly negligible for the 9-fiber system, having only a 0.8% margin, while the 8-fiber system has little volumetric margin at 5%. Considering cost and the need to reduce complexity while maximizing overall margin in the payload, the 8-fiber, 0.411-m aperture design is the payload of choice. Additional considerations are the thermal constraints of 0.282 meters of radiator at 298 K for the transmitter and payload electronics and 0.089 meters of radiator at 240 K for the receiver, as well as a data rate of 1.752 Mbits/sec. The data rate is of little concern since the payload would be run at a 10% duty cycle, effectively reducing the average data rate to 0.1752 Mbits/sec.

Number of Fibers	Mass/Margin	Power/Margin	Volume/Margin
15	71/-42%	28/45%	76563/8.9%
14	67/-34.5%	26/48.3%	74973/10.7%
13	64/-27.2%	24/51.7%	73767/12.2%
12	60/-19.9%	23/55%	73057/13%
11	56/-12.8%	21/58.3%	73001/13.1%
10	53/-5.9%	19/61.6%	73832/12.1%
9	50/0.8%	18/65%	75898/9.6%
8	46/7.1%	16/68.3%	79746/5%

Table 17. Iridium NEXT Payload Options Performance and Margin

3. Estimated Mission Cost and Collection Rate

Looking at the cost considerations for this platform, only the payload and integration costs are included. The integration cost for the Iridium host payload is assumed to be a conservative \$5M due to commercial practices and other platform testing considerations. Using NASA's mass-based model and accounting for only payload mass, the total mission cost, including the payload, would cost an estimated \$45M with a 1.3X factor for complexity. With the optical telescope assembly parametric model, assuming a payload cost breakout of 39%, the LIDAR payload would cost \$30M. Accounting for integration at \$5M and ground operations at \$3M per year, the total mission cost for a five-year mission is estimated to be \$55M.

This payload would be capable of imaging 0.5 km²/s or 1,576,800 km²/year at a 5-meter post-spacing. With the Antarctic and Greenland ice sheets totaling 15.7 million km², these portions of the cryosphere could be mapped in entirety (assuming ideal conditions and no data voids) in just under ten years (National Snow and Ice Data Center, 2013). With the payload costing between \$45M and \$55M per copy and 60 satellites available for hosting in the Iridium constellation, additional payloads could be launched for redundancy and additional collection. Ten satellites would be needed to map the cryosphere at 5-meter post-spacing within a year at a cost of nearly \$500M (assuming shared ground cost). For forested areas, at 39.52 million km², a constellation of ten

hosted payloads would be able to provide 5-meter post-spacing for forest carbon monitoring projects within 2.5 additional years (Nabuurs & Masera, 2007). The USGS mission of 1-meter post-spacing for the United States, at 9,147,420 km², would reduce the area collection rate to 0.02 km²/s or 630,720 km²/year per payload, requiring 15 payloads to map the United States within a year (The World Bank, 2013). While this may be costly at over \$885M, a smaller constellation could help map more expensive mapping areas and could be included in the cost-benefit analysis for future elevation data studies.

NASA Objectives		**Iridium does not meet Pointing Requirements			
Area of Study	Post-Spacing	Range Resolution	Refresh Rate / Area per year	# Hosted Payloads Required / Total Cost	
Ice Sheets	25 km	2 cm	.5 Years / 31.4M km ²	20 Payloads / \$1100M	
Vegetation	25 m	1 m	3 Years / 13.17M km ²	9 Payloads / \$495M	
Topography	5 m	<10 cm	Unknown	N/A	
Hydrology	N/A	10 cm	Weekly / Negligible	N/A	
USGS Objectives (Assuming 9,147,420 km² Area for US)					
Quality Level / Update Frequency	Post-Spacing	Range Resolution	Airborne Annual Cost	Estimated Annual Benefit	# Hosted Payloads Required / Total Cost
1 (Yearly)	0.7 m	46.3 cm	\$1,646 M	\$1,111 M	30 / \$1650M
1 (3 Years)	0.7 m	46.3 cm	\$659 M	\$1,110 M	10 / \$550M
1 (5 Years)	0.7 m	46.3 cm	\$366 M	\$1,066 M	6 / \$330M
1 (8 Years)	0.7 m	46.3 cm	\$206 M	\$800 M	4 / \$220M
1 (10 Years)	0.7 m	46.3 cm	\$110 M	\$403 M	3 / \$165M
2 (Yearly)	1 m	18.5 cm	\$1,006 M	\$923 M	15 / \$825M
2 (3 Years)	1 m	18.5 cm	\$402 M	\$922 M	5 / \$275M
2 (5 Years)	1 m	18.5 cm	\$224 M	\$888 M	3 / \$165M
2 (8 Years)	1 m	18.5 cm	\$126 M	\$674 M	2 / \$110M
2 (10 Years)	1 m	18.5 cm	\$67 M	\$339 M	2 / \$110M
3 (Yearly)	5 m	9.25 cm	\$760 M	\$697 M	6 / \$330M
3 (3 Years)	5 m	9.25 cm	\$304 M	\$696 M	2 / \$110M
3 (5 Years)	5 m	9.25 cm	\$169 M	\$673 M	2 / \$110M
3 (8 Years)	5 m	9.25 cm	\$95 M	\$501 M	1 / \$55M
3 (10 Years)	5 m	9.25 cm	\$51 M	\$252 M	1 / \$55M

Table 18. Iridium Fulfillment of NASA and USGS LIDAR Objectives

The Iridium hosted payload option has a number of advantages and disadvantages. Its low initial cost and redundant spacecraft make it attractive from a risk reduction and revisit rate perspective. It would also allow for a gradual scaling up or down of the number of systems based on insights gathered from the data and could be more resilient from a budgetary planning perspective than one large program. Technology advancements and payload fixes could also be

included as new payloads are built. There are, however, some disadvantages of Iridium hosted payloads. The bus does not meet the pointing knowledge and accuracy requirements, making the geolocation of LIDAR returns in 3-D space more difficult. This may be alleviated through additional attitude determination hardware such as gyros, which would increase pointing knowledge but possibly not accuracy. While the number of hosted payloads required is high to meet the NASA objectives, the system is collecting at 5-meter post spacing. The number of satellites could be reduced if the data was down-sampled to the objective post spacing and a smaller number of returns were expected per detector IFOV.

For the USGS objectives, the Iridium hosted payload has a number of attractive options at different quality levels. Depending on the lifetime of each satellite and its LIDAR payload, the monetary benefits of a space-based approach could outweigh that of the airborne approach. In Table 18, the airborne costs are per year, however the hosted payload costs may include multiple years of operation. With an estimated five-year lifetime for the payload, the Iridium hosted option could provide a five times greater return on investment than the airborne options. Taking into account NASA and USGS's objectives and assuming down-sampling is possible, ice sheets sampled at a 1-km post spacing would only need one satellite to fulfill the requirement and would be limited by spacecraft speed and orbital constraints. For vegetation, at a down-sampled 25-m post spacing, only two hosted payloads would be required and could also subsume the ice sheet measurements as well. For USGS requirements, the highest returns on investment are for the 0.7-m post spacing with updates every three years and 0.7-m post spacing with updates every five years. Updating the USGS elevation data set every three years would require ten payloads at a cost of \$550M, while over the course of five years providing a return of \$5,550M. Updating the data set every five years would require six payloads at a cost of \$330M, while providing a return of \$5,330M.

Taking into account total mission costs of less than \$250M and \$500M, a constellation of four and nine payloads could be chosen, respectively. With a

four-payload constellation, two would be reserved for NASA objectives and the capacity of the other two could fulfill USGS objectives providing a return on investment of \$3,480M over five years with a 5-m post spacing and updates every three years. With a nine payload constellation, two would again be reserved for NASA objectives and the capacity of the other seven could provide a return on investment of \$5,330M over five years with a 0.7-m post spacing and updates every five years.

B. FREE-FLIER SATELLITE DESIGNS

Free flyer payloads offer additional flexibility over hosted payloads that can increase mission performance, but introduce a number of other costs that require consideration (e.g., launch, bus, full test and integration, program management). Two options will be explored for both a low-cost small satellite (less than \$250M) and a mid-cost larger satellite (less than \$500M) for the LIDAR mission. Exploring the NASA cost model and associated standard buses, there are a number of options that satisfy both cost points.

1. Low Cost: Less than \$250M Satellite Design

The low-cost small satellite must balance both the mission life of the bus and the associated cost. Two methods are used to determine the overall cost of the system. First, an aperture-based approach is used which uses standard detector sizes (32x32, 32x128 and 32x256) and a varying number of lasers with associated powers. From here, the aperture size is determined by closing the link for each pixel of the array. Larger apertures are needed for large arrays with a small number of lasers, while smaller detector arrays with a large number of lasers need smaller apertures to close the link. After determining the aperture sizes commensurate with a less than \$250M mission, these constraints are applied to the mass-based model. Only if the two models agree that the cost is below \$250M, will the satellite design be accepted.

A number of iterations were completed to determine the potential options for a less than \$250M mission based on the aperture cost model. The number of

lasers was limited from one to fifteen due to the need to limit the system complexity. All three detector sizes were modeled, but even at a maximum of 15 lasers, both the 32x128 and 32x256 detectors had aperture sizes that, when run through the cost model, exceeded the \$250M mark. The 32x128 detector was only able to close the link with a minimum aperture size of 1.169 meters and a spacecraft cost of \$370.568M. The 32x256 detector was only able to close the link with a minimum aperture size of 1.653 meters and a spacecraft cost of \$623.218M. The 32x32 detector is the only detector that was able to be fully illuminated and had a number of aperture sizes that satisfied the less than \$250M cost ceiling. In Figure 35, the aperture-based cost model curves are shown for the 32x32 detector. Both the tapered and tiled lasers look to satisfy the constraints with a number of options. Due to the benefits of increased power with the tapered lasers, only these lasers were considered in the mass-based estimates. For the tapered lasers, the seven to fifteen laser range was able to satisfy the cost constraints with aperture sizes ranging from 0.856 to 0.584 meters and costs ranging from \$232.042M to \$131.015M, respectively. These choices were then used to limit the iterations needed on the mass-based model.

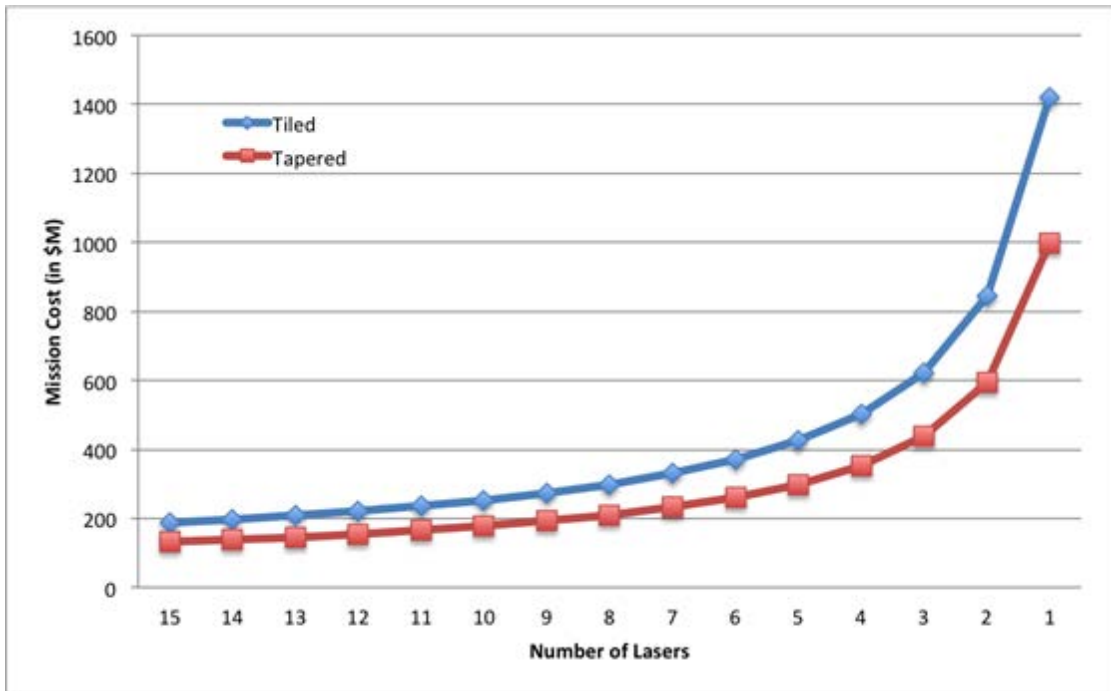


Figure 35. Low-Cost Payload 32x32 Array Mission Cost Versus Number of Transmitters (Aperture-Based Cost Estimate)

The mass-based cost estimates for the low-cost small satellite are inconsistent with the aperture-based models, however the cost insights from both models can be used to develop a ceiling for aperture sizes, bus options, array size and number of lasers. The aperture-based model constrains the design to a 32x32-sized detector with seven to fifteen tapered lasers. The mass-based models show a flat relationship with respect to different payload options (number of lasers and aperture size) due to the large proportion of mass in the bus itself and the addition of a 10% fuel load based upon total spacecraft dry mass (for station keeping and minimal maneuvers). The mass-based estimates have also filtered out buses with volume and mass constraints that cannot accommodate the payload selected, displaying those values as zeroes. Of the buses available, the BCP300, BCP2000, LMx, LM400, SSTL600 and Proteus all fall under \$250M for spacecraft and launch. Of note, ICESat-2's LEOStar-3 bus has a mass, when combined with the payload, that exceeds the mass-based cost. At over \$500M, the LEOStar-3 option is not a viable candidate for this low-cost mission. ICESat-

1's BCP-2000 bus, however, is a candidate for this low-cost mission, providing ample power while remaining under the mass-based cost constraints.

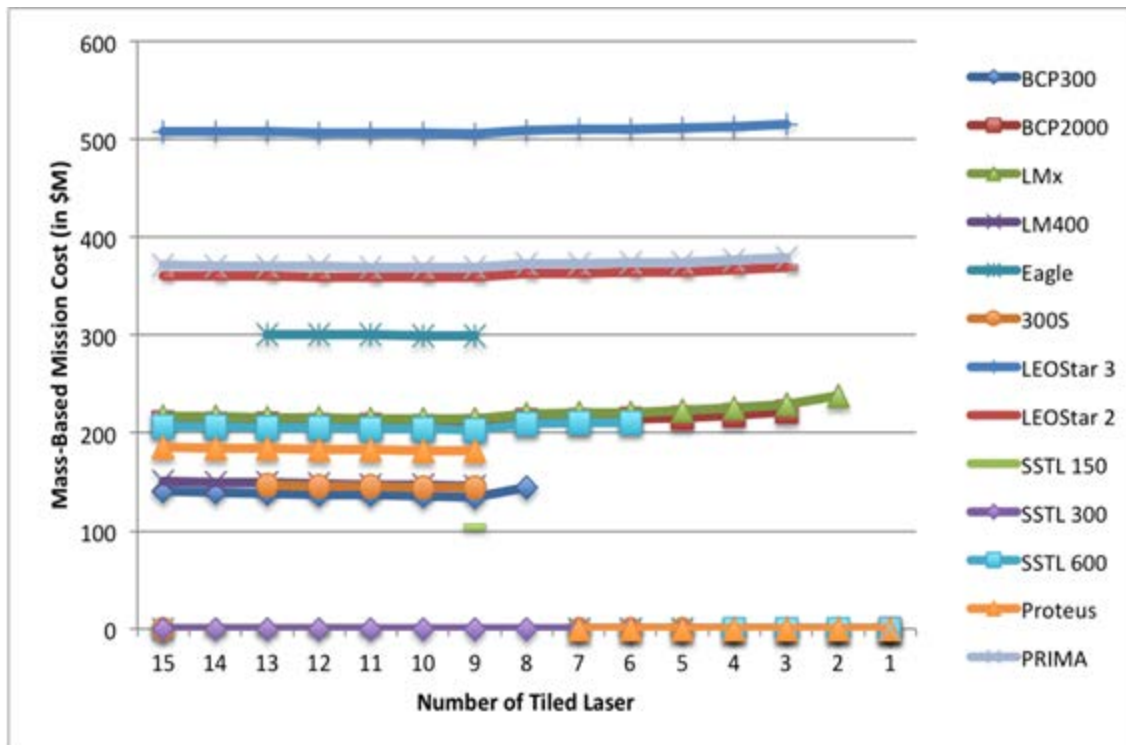


Figure 36. Low-Cost Payload 32x32 Array Mission Cost Versus Number of Transmitters and Standard Buses

In order to meet a five-year mission design life, the list is narrowed down further to the BCP2000 and Proteus. Table 19 displays these two options and their associated margin in a number of critical areas as benchmarked against a 15-element tapered laser system with a 0.584-meter aperture. The Proteus bus, while the lowest cost of the two options, does not meet the power and data rate requirements, which would require a lower duty cycle and limit system performance. The BCP-2000 is the highest cost bus, though it meets all the requirements with substantial margin. This bus also has the best pointing capabilities with pointing knowledge and control within 30.54 meters. The BCP-2000, in addition to the requirements in Table 19, would need 0.089 meters of radiator space at 240K for the receiver and 0.8 meters of radiator at 298K for the

transmitters and payload electronics to accomplish the mission. Even with varying the number of lasers and aperture size, the BCP-2000 has a number of capabilities that would significantly enhance the mission while keeping it under \$250M (\$216.6M for the mass-based model and \$131.015M for the aperture-based model).

	Requirement	BCP-2000	Margin	Proteus	Margin
Mass	112	500	346.4%	300	167.9%
Volume	279315	4950000	1672.2%	-	-
Power	325	400	23.1%	300	-7.7%
Cost	250	216.6	13.4%	193	29.5%
Data Rate	7296000	80000000	996.5%	1000000	-86.3%
Data Storage	N/A	56,000	-	2000	-
Pointing	N/A	10.5	-	72	-
Design Life	5 Years	5	-	5	-

Table 19. Low-Cost Satellite Payload and Bus Performance and Margin

The payload aboard a BCP-2000 would be capable of imaging $5.12 \text{ km}^2/\text{s}$ or $161,464,320 \text{ km}^2/\text{year}$ at a 5-meter post-spacing. With the Antarctic and Greenland ice sheets totaling 15.7 million km^2 , these portions of the cryosphere could be mapped in entirety (assuming ideal conditions, no data voids and no orbital constraints) in 36 days. For forested areas, at 39.52 million km^2 , this payload would be able to provide 5-meter post-spacing for forest carbon monitoring projects within 90 additional days or 30 days for a three-year refresh rate. The USGS mission of 1-meter post-spacing for the United States would reduce the area collection rate to $0.2048 \text{ km}^2/\text{s}$ or $6,458,572 \text{ km}^2/\text{year}$, requiring just under a year and a half to map the United States.

NASA Objectives		**BCP-2000 does not meet pointing requirements			
Area of Study	Post-Spacing	Range Resolution	Refresh Rate / Area per year	Payload Capable of Meeting Objectives	
Ice Sheets	25 km	2 cm	.5 Years / 31.4M km ²	Yes / 72 Days at 5-m Post Spacing	
Vegetation	25 m	1 m	3 Years / 13.17M km ²	Yes / 30 Days at 5-m Post Spacing	
Topography	5 m	<10 cm	Unknown	N/A	
Hydrology	N/A	10 cm	Weekly / Negligible	N/A	
USGS Objectives (Assuming 9,147,420 km² Area for US)					
Quality Level / Update Frequency	Post-Spacing	Range Resolution	Airborne Annual Cost	Estimated Annual Benefit	Capable of Meeting Objectives (Post-NASA)
1 (Yearly)	0.7 m	46.3 cm	\$1,646 M	\$1,111 M	No
1 (3 Years)	0.7 m	46.3 cm	\$659 M	\$1,110 M	No
1 (5 Years)	0.7 m	46.3 cm	\$366 M	\$1,066 M	Yes
1 (8 Years)	0.7 m	46.3 cm	\$206 M	\$800 M	Yes
1 (10 Years)	0.7 m	46.3 cm	\$110 M	\$403 M	Yes
2 (Yearly)	1 m	18.5 cm	\$1,006 M	\$923 M	No
2 (3 Years)	1 m	18.5 cm	\$402 M	\$922 M	Yes
2 (5 Years)	1 m	18.5 cm	\$224 M	\$888 M	Yes
2 (8 Years)	1 m	18.5 cm	\$126 M	\$674 M	Yes
2 (10 Years)	1 m	18.5 cm	\$67 M	\$339 M	Yes
3 (Yearly)	5 m	9.25 cm	\$760 M	\$697 M	Yes
3 (3 Years)	5 m	9.25 cm	\$304 M	\$696 M	Yes
3 (5 Years)	5 m	9.25 cm	\$169 M	\$673 M	Yes
3 (8 Years)	5 m	9.25 cm	\$95 M	\$501 M	Yes
3 (10 Years)	5 m	9.25 cm	\$51 M	\$252 M	Yes

Table 20. Low-Cost Free-Flyer Fulfillment of NASA and USGS LIDAR Objectives

The low-cost free-flyer option has a number of advantages and disadvantages. Its total cost requires stable funding from a budgetary process, and does not have any built in redundancy in the design configuration. Integrating this new technology on one satellite also increases the risk of anomalies with no opportunity to reduce risk on the next platform like the Iridium option. Of all the bus options, none of them satisfy the pointing control or

knowledge requirements, but the BCP-2000 bus may need minor modifications to meet NASA's pointing requirements. At 10.5 arcsec of pointing control and 10.5 arcsec of pointing knowledge, the BCP-2000 falls short of the 10 arcsec pointing control and 1.5 arcsec of pointing knowledge requirements. NASA may waive the pointing control requirements due to only a 0.5 arcsec difference, or advanced control algorithms could be employed to reduce the pointing control error without modifying the hardware. The pointing knowledge may be increased through the use of advanced gyros or other hardware with minimal bus rework.

Aside from the disadvantages of the BCP-2000 low-cost free-flyer, the area collection rate from this platform enables a number of missions to be completed. Without the need for down-sampling, NASA's ice sheet and vegetation missions could be completed at 5-meter post spacing within 102 days assuming no weather or orbital constraints. The extra capacity on this satellite could be used to complete the USGS objectives, with 263 days of collection remaining. Of these objectives, the greatest benefit is achieved by collecting at a 0.7-meter post spacing with a five year update frequency. This would provide roughly \$1,066M in estimated annual benefit and provides a lower cost option than airborne collection, which costs roughly \$366M per year. Over the course of a five-year period, the airborne option would continue to incur annual costs while the upfront cost of the space-based option would yield \$5,330M worth of annual benefit while incurring minimal annual operating costs.

2. Mid Cost: Less than \$500M Satellite Design

The mid-cost (less than \$500M) satellite must also balance lifetime requirements with performance and cost. In Figure 37, there are clear aperture-based cost curves that show a 32x256 detector cannot meet the mission requirements in terms of cost. Even with 15 tapered lasers, a 1.65-meter aperture is needed, driving the aperture-based cost estimate up to \$628M, too expensive for this mid-cost satellite design. The 32x32 detector trades, while under the \$500M mark, do not maximize the performance of the payload, making the 32x128 detector the prime candidate. Again, only the tapered laser is being

modeled and a maximum of 15 lasers are being considered, resulting in Figure 38 for the 32x128 detector.

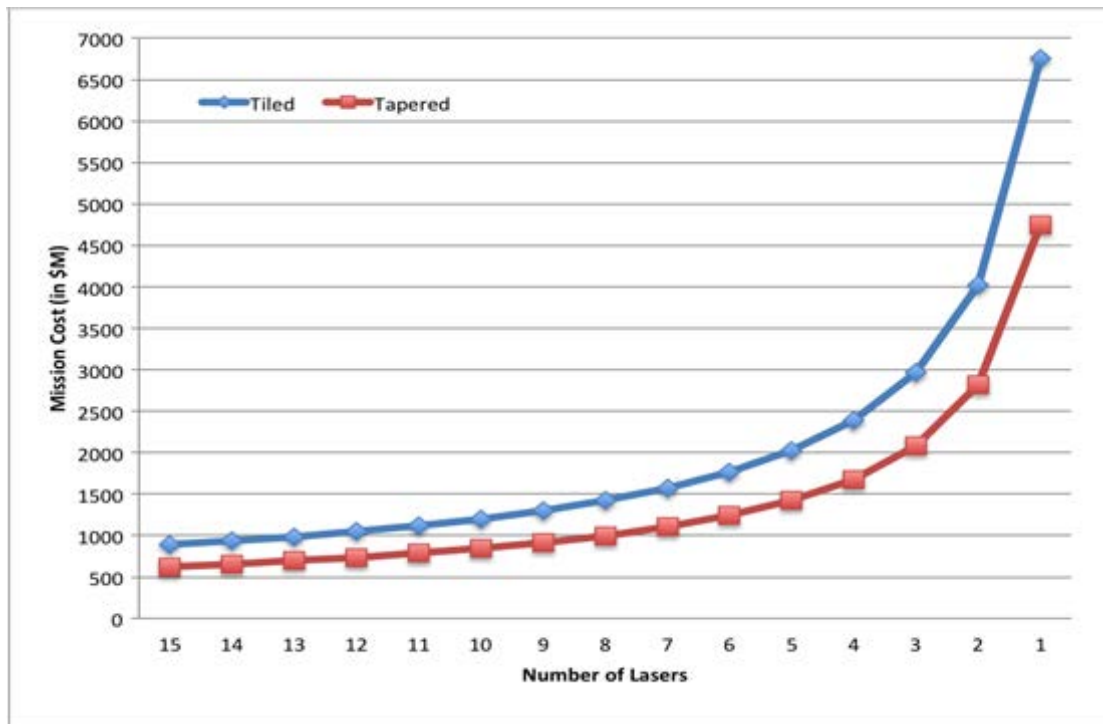


Figure 37. Mid-Cost Payload 32x256 Array Mission Cost Versus Number of Transmitters (Aperture-based Cost Estimate)

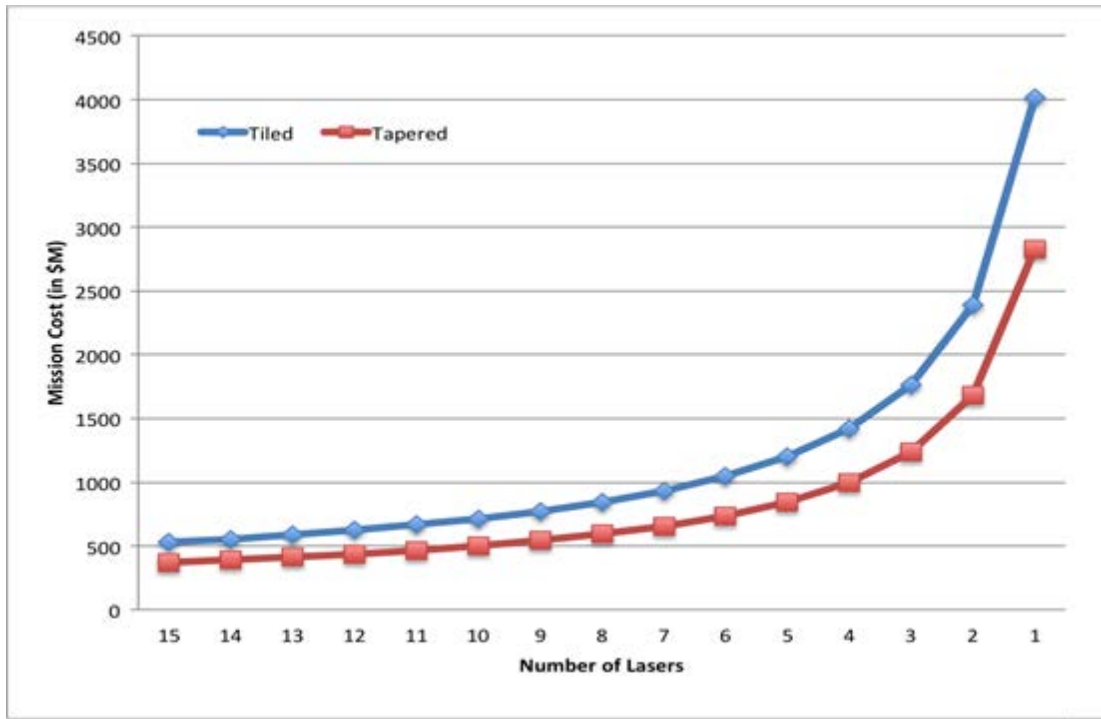


Figure 38. Mid-Cost Payload 32x128 Array Mission Cost Versus Number of Transmitters (Aperture-based Cost Estimate)

The mass-based cost estimates for the mid-cost small satellite are inconsistent with the aperture-based models, however the cost insights from both models can be used to develop a ceiling for aperture sizes, bus options, array size and number of lasers. The aperture-based model constrains the design to a 32x128-sized detector with eleven to fifteen tapered lasers. The mass-based models show a flat relationship with respect to different payload options (number of lasers and aperture size) due to the large proportion of mass in the bus itself and the addition of a 10% fuel load based upon total spacecraft dry mass (for station keeping and minimal maneuvers). The mass-based estimates have also filtered out the buses whose volume and mass constraints cannot accommodate the payload selected, displaying those values as zeroes. Of the buses available, the BCP2000, LMx, LEOStar-2, SSTL600 and PRIMA all fall under \$500M for spacecraft and launch. Of note, ICESat-2's LEOStar-3 bus has a mass, when combined with the payload, which exceeds the mass-based cost. At over \$500M, the LEOStar-3 option is not a viable candidate for this mid-cost mission. ICESat-

1's BCP-2000 bus, however, is a candidate for this low-cost mission, providing ample power while remaining under the mass-based cost constraints.

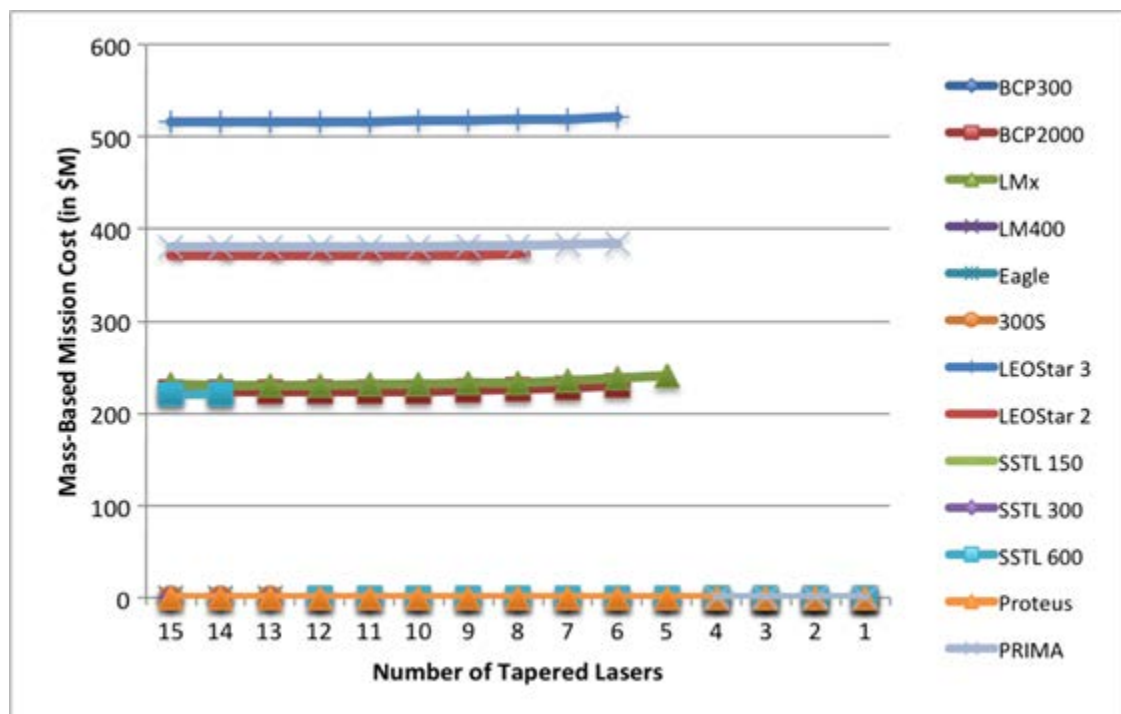


Figure 39. Mid-Cost Payload 32x128 Array Mission Cost Versus Number of Transmitters and Standard Buses

In order to meet a five-year mission design life, the list is narrowed down further to the BCP2000, LEOStar-2 and PRIMA. Table 21 displays these three options and their associated margin in a number of critical areas as benchmarked against a 15-element tapered laser system with a 1.17-meter aperture. All of the options meet the bus requirements to support the chosen payload with the BCP2000 being the lowest cost option, LEOStar-2 the mid-point and the PRIMA bus being the most expensive. The LEOStar-2 bus provides significant power and data margin over the BCP2000 bus but at a cost of \$47.1M. The PRIMA bus also provides significant margin in all areas except for cost, with nearly 100% margin in all areas and 600% mass margin at a cost of \$56.7M above that of BCP2000.

The BCP2000 bus provides the lowest cost solution with adequate margin in all areas and the best pointing capabilities with pointing knowledge and control within 30.54 meters. The BCP-2000, in addition to the requirements in Table 21, would need 0.12 meters of radiator space at 240K for the receiver and 0.8 meters of radiator at 298K for the transmitters and payload electronics to accomplish the mission. Even with varying the number of lasers and aperture size, the BCP-2000 has a number of capabilities that would significantly enhance the mission while keeping it under \$500M (\$223.7M for the mass-based model and \$370.568M for the aperture-based model).

	Requirement	BCP-2000	Margin	LEOStar-2	Margin	PRIMA	Margin
Mass	161	500	210.6%	500	210.6%	1138	606.8%
Volume	1155623	4950000	328.3%	3169936	174.3%	4287640	271.0%
Power	330	400	21.2%	850	157.6%	1100	233.3%
Cost	500	223.7	123.5%	370.8	34.8%	380.4	31.4%
Data Rate	25728000	80000000	67.8%	300000000	91.4%	310000000	91.7%
Data Storage	N/A	56,000	-	500,000	-	1200	-
Pointing	N/A	10.5	-	48	-	36	-
Design Life	5 Years	5	-	5	-	7	-

Table 21. Mid-Cost Satellite Payload and Bus Performance and Margin

The payload aboard a BCP-2000 would be capable of imaging 20.48 km²/s or 645,857,280 km²/year at a 5-meter post-spacing. With the Antarctic and Greenland ice sheets totaling 15.7 million km², these portions of the cryosphere could be mapped in entirety (assuming ideal conditions, no data voids and no orbital constraints) in 9 days or 18 days for a bi-annual update. For forested areas, at 39.52 million km², this payload would be able to provide 5-meter post-spacing for forest carbon monitoring projects within 23 additional days or 8 days for a three-year refresh rate. The USGS mission of 1-meter post-spacing for the United States would reduce the area collection rate to 0.8192 km²/s or 25,834,291.2 km²/year, requiring 130 days to map the United States.

NASA Objectives		**BCP-2000 does not meet pointing requirements			
Area of Study	Post-Spacing	Range Resolution	Refresh Rate / Area per year	Payload Capable of Meeting Objectives	
Ice Sheets	25 km	2 cm	.5 Years / 31.4M km ²	Yes / 18 Days at 5-m Post Spacing	
Vegetation	25 m	1 m	3 Years / 13.17M km ²	Yes / 8 Days at 5-m Post Spacing	
Topography	5 m	<10 cm	Unknown	N/A	
Hydrology	N/A	10 cm	Weekly / Negligible	N/A	
USGS Objectives (Assuming 9,147,420 km² Area for US)					
Quality Level / Update Frequency	Post-Spacing	Range Resolution	Airborne Annual Cost	Estimated Annual Benefit	Capable of Meeting Objectives (Post-NASA)
1 (Yearly)	0.7 m	46.3 cm	\$1,646 M	\$1,111 M	Yes
1 (3 Years)	0.7 m	46.3 cm	\$659 M	\$1,110 M	Yes
1 (5 Years)	0.7 m	46.3 cm	\$366 M	\$1,066 M	Yes
1 (8 Years)	0.7 m	46.3 cm	\$206 M	\$800 M	Yes
1 (10 Years)	0.7 m	46.3 cm	\$110 M	\$403 M	Yes
2 (Yearly)	1 m	18.5 cm	\$1,006 M	\$923 M	Yes
2 (3 Years)	1 m	18.5 cm	\$402 M	\$922 M	Yes
2 (5 Years)	1 m	18.5 cm	\$224 M	\$888 M	Yes
2 (8 Years)	1 m	18.5 cm	\$126 M	\$674 M	Yes
2 (10 Years)	1 m	18.5 cm	\$67 M	\$339 M	Yes
3 (Yearly)	5 m	9.25 cm	\$760 M	\$697 M	Yes
3 (3 Years)	5 m	9.25 cm	\$304 M	\$696 M	Yes
3 (5 Years)	5 m	9.25 cm	\$169 M	\$673 M	Yes
3 (8 Years)	5 m	9.25 cm	\$95 M	\$501 M	Yes
3 (10 Years)	5 m	9.25 cm	\$51 M	\$252 M	Yes

Table 22. Mid-Cost Free-Flyer Fulfillment of NASA and USGS LIDAR Objectives

The mid-cost free-flyer option has a number of advantages and disadvantages. Its total cost requires stable funding from a budgetary process, and does not have any built in redundancy in the design configuration. Integrating this new technology on one satellite also increases the risk of anomalies with no opportunity to reduce risk on the next platform like the Iridium option. Of all the bus options, none of them satisfy the pointing control or

knowledge requirements, but the BCP-2000 bus may need minor modifications to meet NASA's pointing requirements. At 10.5 arcsec of pointing control and 10.5 arcsec of pointing knowledge, the BCP-2000 falls short of the 10 arcsec pointing control and 1.5 arcsec of pointing knowledge requirements. NASA may waive the pointing control requirements due to only a 0.5 arcsec difference, or advanced control algorithms could be employed to reduce the pointing control error without modifying the hardware. The pointing knowledge may be increased through the use of advanced gyros or other hardware with minimal bus rework.

Aside from the disadvantages of the BCP-2000 low-cost free-flyer, the area collection rate from this platform enables a number of missions to be completed. Without the need for down-sampling, NASA's ice sheet and vegetation missions could be completed at 5-meter post spacing within 26 days assuming no weather or orbital constraints. The extra capacity on this satellite could be used to complete the USGS objectives, with 339 days of collection remaining. Of these objectives, the greatest benefit is achieved by collecting at 0.7-meter post spacing with a one-year update frequency. This would provide roughly \$1,111M in estimated annual benefit and provides a lower cost option than airborne collection, which costs roughly \$1,646M per year. Over the course of a five-year period, the airborne option would continue to incur annual costs while the upfront cost of the space-based option would yield \$5,555M worth of annual benefit while incurring minimal annual operating costs.

THIS PAGE INTENTIONALLY LEFT BLANK

VIII. CONCLUSIONS

The monitoring of the cryosphere and forest carbon stocks with high-quality digital elevation data remains a national imperative as we look toward a future with a changing climate. Technological advancements over the past decade continue to push the bounds of what is possible in efficient laser transmitters and single-photon sensitive receivers. Both fiber lasers and GmAPDs enable very high area collection rates for these mission-sets and other national priorities like the National Elevation Dataset. These new technologies have the potential to reduce the cost of space-based LIDAR satellites beyond that of the ICESat-1 and ICESat-2 missions, enabling a continuous monitoring capability.

Three different satellite designs were explored: a low-cost hosted payload, a low-cost free flyer under \$250M and a mid-cost free flyer under \$500M. Two parametric cost models were used to determine, at this stage of conceptual mission design, what the estimated mission costs would be associate with these satellite designs. The mass-based and aperture-based cost models did not line-up with one another in these three design cases, but provide a conservative cost ceiling for the designs.

All three designs have the ability to fulfill most NASA mission requirements, but have tradeoffs based upon cost and pointing knowledge. A comparison of these designs with ICESat-1, ICESat-2 and CALIPSO and each system's estimated performance can be found in Table 23.

Parameters	Hosted Payload	Low-Cost Payload	Mid-Cost Payload	ICESat-1	ICESat-2	CALIPSO
Bus Platform	Iridium NEXT	BCP-2000	BCP-2000	BCP-2000	LEOSTAR-3	PROTEUS
Aperture Size	0.411 m	0.584 m	1.17 m	1.00 m	1.00 m	1.00 m
Number of Lasers	8 Tiled Fibers	15 Tapered Fibers	15 Tapered Fibers	1 Slab with 3 Redundant Diode Pumps	1 Slab Frequency Doubled	2 Redundant Slabs
Power per pulse / PRF	2 mJ / 10 kHz	6 mJ / 10 kHz	6 mJ / 10 kHz	110 mJ / 40 Hz	900 µj / 10 kHz	220 mJ / 20.16 Hz
Receiver Array Size	32x32 InGaAs APD with 10x10 active	32x32 InGaAs APD	32x128 InGaAs APD	8 Silicon APDs	UNK See Table 1	One Silicon APD / Two PMTs
Total Mass	-	618.2 kg	672.1 kg	900 kg	~1324 kg	587 kg
Mass-Based Cost	\$45M	\$216.6M	\$223.7M	~\$462M Actual Cost	~\$860.3M GAO Estimated Cost	\$298M Actual Cost
Aperture-Based Cost	\$55M	\$131.015M	\$370.568M			
Time to Map Cryosphere (at 5- Meters)	9.96 Years	36 Days	9 Days	~183 Days Planned	~91 Days	N/A
Time to Map Forest Carbon (at 5-Meters)	25.1 Years	90 Days	23 Days	N/A	2 Years at 2km Spacing	N/A
Estimated Annual USGS Benefit	\$501M for one Dedicated Payload	\$1,066M	\$1,111M	N/A	N/A	N/A
Payload Power	16W (@10% Duty Cycle)	325W	330W	330W	UNK	197W
Payload Mass	46 kg	112 kg	161 kg	~300 kg	UNK	172 kg
Payload Volume	79,746 cm ³	279,315 cm ³	1,155,623 cm ³	~1,750,000 cm ³	UNK	UNK
Pointing Knowledge	680 m	10.5 arcsec	10.5 arcsec	~2 arcsec	<5 arcsec	20 arcsec

Table 23. Hosted, Low-Cost and Mid-Cost LIDAR Payload Parameters

Based upon the cost modeling and estimated performance of these designs, low-cost space-based LIDAR satellites have the ability to accomplish the NASA and USGS mission while increasing performance over previous LIDAR satellite designs. Technology advancements have allowed for increased area collection rates in a smaller package and could benefit the pursuit of advanced knowledge of the cryosphere, forest carbon stocks and the nation's third dimension. With multiple hosted payloads aboard Iridium or free flier payloads paired with the BCP-2000 commercial bus, all three options have the ability to exceed the performance characteristics of previous space-based LIDAR systems. The area collection rates enabled by high efficiency, high pulse-power and high PRF fiber lasers coupled with advanced InGaAs GmAPDs far exceed that of the ICESat and CALIPSO missions. Recent advancements since the design of ICESat-2 have the potential to reduce the cost of the mission. The replacement of 532-nm planar waveguide lasers and detectors with more modern 1064-nm fiber lasers and GmAPD detector arrays could yield a lower cost system with higher performance.

Preliminary analysis shows the potential for these new technologies to outperform any previous space-based LIDAR mission. At \$55M, the Iridium-hosted solution is 1/16th the cost of ICESat-2 at roughly one-third its capability. With three hosted payloads, the ICESat-2 mission could be accomplished at just over 1/5th the cost. Two additional solutions are estimated at \$216M and \$370M, providing over 3X and 10X the estimated capability of ICESat-2 at roughly one-quarter and one-half the cost, respectively. These cost estimates and performance numbers, however, are less mature than ICESat-2's estimates and should currently be viewed as options to be explored further for the future. Nevertheless, these advancements and potential satellite designs enable a potential future mission to satisfy both NASA and USGS objectives while reducing the cost of such systems.

THIS PAGE INTENTIONALLY LEFT BLANK

LIST OF REFERENCES

- Abdalati, W., Zwally, H. J., Bindschadler, R., Csatho, B., Farrell, S. L., Fricker, H. A., et al. (2010). The ICESat-2 laser altimetry mission. *Proceedings of the IEEE*, 98(5), 735–751.
- Abshire, J. B. (2010). NASA's space lidar measurements of earth and planetary surfaces. *Frontiers in Optics 2010/Laser Science XXVI*, pp. SMB1.
- Andraschko, M., Antol, J., Baize, R., Horan, S., Neil, D., Rinsland, P., Zaiceva, R. (2012). The potential for hosted payloads at NASA. *Aerospace Conference, 2012 IEEE*, 1–12.
- Andraschko, M., Antol, J., Horan, S., & Neil, D. (2011). Commercially hosted government payloads: Lessons from recent programs. *Aerospace Conference, 2011 IEEE*, 1–15.
- Andrews, L. C., & Phillips, R. L. (2005). *Laser beam propagation through random media*. Bellingham, Wash: SPIE Press.
- Applied Technology Associates. (2011). *Fast steering mirror*. Retrieved August 18, 2013, from http://www.aptec.com/fast_steering_mirror.html
- Aull, B. F., Loomis, A. H., Young, D. J., Heinrichs, R. M., Felton, B. J., Daniels, P. J., et al. (2002). Geiger-mode avalanche photodiodes for three-dimensional imaging. *Lincoln Laboratory Journal*, 13(2), 335–349.
- Becker, H. N., Farr, W. H., & Zhu, D. Q. (2007). Radiation response of emerging high gain, low noise detectors. *Nuclear Science, IEEE Transactions on*, 54(4), 1129–1135.
- Brown, S. D., Blevins, D. D., & Schott, J. R. (2005). Time-gated topographic LIDAR scene simulation. *Defense and Security*, 342–353.
- Burton, R. R. (2002). Elastic LADAR modeling for synthetic imaging applications (Doctoral dissertation). Rochester Institute of Technology, Rochester, NY.
- Cavanaugh, J. F., et al. (2007). The Mercury Laser Altimeter Instrument for the MESSENGER Mission. *Space Science Reviews*, Vol. 131, 1–4, 451–479.
- Cole, T. D. (1998). NEAR laser rangefinder: A tool for the mapping and topologic study of asteroid 433 eros. *Johns Hopkins APL Technical Digest*, 19(2), 143.
- Coyle, D. B. (2005). *Applications of fiber amplifier for space: Laser altimetry and mapping*. Unpublished manuscript.

- Dewberry. (2012). *National enhanced elevation assessment*. Fairfax, Virginia: United States Geological Survey.
- Farrow, R. L., Kliner, D. A., Schrader, P. E., Hoops, A. A., Moore, S. W., Hadley, G. R., et al. (2006). High-peak-power (> 1.2 MW) pulsed fiber amplifier. *Lasers and Applications in Science and Engineering*, pp. 61020L–61020L-11.
- Fox, B., Schneider, Z., Simmons-Potter, K., Thomas Jr, W., Meister, D., Bambha, R., et al. (2007). Gamma radiation effects in yb-doped optical fiber. *Fiber Lasers IV: Technology, Systems, and Applications, Proc. SPIE*, 6453, 645328.
- Government Accountability Office. (2012). *NASA Assessment of Selected Large-Scale Projects*, GAO-13-276SP. Washington, D.C.: Government Accountability Office.
- Guerra, L. (2008). *Cost estimating module space systems engineering*. Unpublished manuscript.
- Harwood, W. (2009). *Atlas 5 rocket launches NASA moon mission*. Retrieved August 14, 2013, from http://news.cnet.com/8301-19514_3-10268241-239.html
- Henson, R. (2008). *Satellite observations to benefit science and society: Recommended missions for the next decade*. Washington, DC: National Academies Press.
- Huffington Post. (2011). *A first: NASA MESSENGER spacecraft orbiting mercury*. Retrieved August 14, 2013, from http://www.huffingtonpost.com/2011/03/18/nasa-MESSENGER-mercury_n_837503.html
- Kichak, R. (2003). Independent GLAS anomaly review board executive summary. Greenbelt, Maryland: Goddard Space Flight Center.
- Kim, S., Lee, I., & Kwon, Y. J. (2013). Simulation of a geiger-mode imaging LADAR system for performance assessment. *Sensors*, 13(7), 8461–8489.
- Koechner, W., & Bass, M. (2003). *Solid-state lasers: A graduate text*. New York, New York: Springer.
- Krainak, M. A., Anthony, W. Y., Yang, G., Li, S. X., & Sun, X. (2010). Photon-counting detectors for space-based laser receivers. *Opto*, pp. 760827-760827-9.

- Leone, D. (2012). *U.S. Air Force deferral of last DMSP upends plan for launching ICESat 2*. Retrieved August 14, 2013, from
<http://www.spacenews.com/article/us-air-force-deferral-last-dmsp-upends-plan-launching-ICESat-2>
- Maiman, T. (1960). Stimulated optical radiation in ruby. *Nature*, 187(4736), 493–494.
- Masursky, H., Colton, G. W., El-Baz, F., & Doyle, F. J. (1978). Apollo over the moon: A view from orbit. *NASA Special Publication*, 362.
- McGill, M. (2011). *Multiple altimeter beam experimental lidar (MABEL) first flights and initial results*. Retrieved August 14, 2013, from
<http://atmospheres.gsfc.nasa.gov/science/slides.php?sclid=6>
- McGill, M., Markus, T., Scott, V. S., & Neumann, T. (2013). The multiple altimeter beam experimental lidar (MABEL): An airborne simulator for the ICESat-2 mission. *Journal of Atmospheric and Oceanic Technology*, 30(2), 345–352.
- Nabuurs, G., & Masera, O. (2007). *IPCC fourth assessment report: Climate change 2007, working group 3, forestry*. Switzerland: Intergovernmental Panel on Climate Change.
- NASA. (2007). *Report from the ICESat-II workshop*. Linthicum, Maryland: National Aeronautics and Space Administration.
- NASA assessments of selected large-scale projects (2013). No. GAO-13-276SP. Washington, DC: Government Accountability Office.
- NASA *ICESat cryospheric sciences lab code 615*. (2013). Retrieved September 30, 2013, from <http://ICESat.gsfc.nasa.gov/ICESat/>
- NASA: *ICESat-2*. (2013). Retrieved September 30, 2013, from
<http://ICESat.gsfc.nasa.gov/ICESat2/>
- National Research Council (U.S.) Committee on Earth Science. (2007). *Earth science and applications from space: National imperatives for the next decade and beyond*. Washington, DC: National Academies Press.
- National Snow and Ice Data Center. (2013). *Quick facts on ice sheets*. Retrieved September 30, 2013, from
<http://nsidc.org/cryosphere/quickfacts/icesheets.html>
- Neumann, G. (2001). Some aspects of processing extraterrestrial LIDAR data: Clementine, NEAR, MOLA. *International Archives of Photogrammetry and Remote Sensing, Volume XXXIV-3/W4*, pp. 73–80.

- nLight. (2013). *nLight high power lasers fiber-coupled*. Retrieved September 30, 2013, from <http://www.nlight.net/products/fiber-coupled/>
- Ramos-Izquierdo, L., Scott III, V. S., Connelly, J., Schmidt, S., Mamakos, W., Guzek, J., et al. (2009). Optical system design and integration of the lunar orbiter laser altimeter. *Applied Optics*, 48(16), 3035–3049.
- Richard, J., Le Roy, Y., Thouvenot, E., & Escudier, P. (2008). *Altimetry payload specification for Iridium NEXT*. Bethesda, MD: Iridium Satellite LLC.
- Riris, H., & Cavanaugh, J. F. (2010). *Calibration document for the lunar orbiter laser altimeter (LOLA) instrument*. Unpublished manuscript.
- Riris, H., Sun, X., Cavanaugh, J. F., Jackson, G. B., Ramos-Izquierdo, L., Smith, D. E., et al. (2007). The lunar orbiter laser altimeter (LOLA) on NASA's lunar reconnaissance orbiter (LRO) mission. *Defense and Security Symposium*, pp. 65550I-65550I-8.
- Rosette, J., Field, C., Nelson, R., DeCola, P., & Cook, B. (2011). A new photon-counting lidar system for vegetation analysis. *Proceedings of SilviLaser 2011, 11th International Conference on LiDAR Applications for Assessing Forest Ecosystems*, University of Tasmania, Australia, 16–20 October 2011.
- Sawruk, N. W., Stephen, M. A., Litvinovitch, S., Edelman, J. E., Albert, M. M., Edwards, R. E., et al. (2013). Space qualified laser transmitter for NASA's ICESat-2 mission. *Spie Lase*, pp. 85990O-85990O-7.
- Smith, D. E., & Zuber, M. T. *LOLA fact sheet*. Unpublished manuscript.
- Smith, D. E., Zuber, M. T., Frey, H. V., Garvin, J. B., Head, J. W., Muhleman, D. O., et al. (2001). Mars orbiter laser altimeter: Experiment summary after the first year of global mapping of mars. *Journal of Geophysical Research: Planets (1991–2012)*, 106(E10), 23689–23722.
- Snyder, G. I. (2013). The benefits of improved national elevation data. *Photogrammetric Engineering & Remote Sensing*, 79(2), 105.
- Sorensen T.C. and P.D. Spudis (2005), The Clementine Mission: A 10-year perspective. *J. Earth System Sci*, 114(6), 645–668.
- Spudis, P. D. (1994). *The Clementine mission: initial results from lunar mapping*. Washington, DC: National Aeronautics and Space Administration.
- Stahl, H. P., Henrichs, T., Luedtke, A., & West, M. (2012). Update on multivariable parametric cost models for ground and space telescopes. *SPIE Astronomical Telescopes Instrumentation*, pp. 844224-844224-6.

- Starodoumov, A. (2008). *Sequentially-Modulated Diode-Laser Seed-Pulse Generator*. U.S. Patent No. US20090296759 A1. Washington, DC.
- Tapos, F. M., Edinger, D. J., Hilby, T. R., Ni, M. S., Holmes, B. C., & Stubbs, D. M. (2005). High bandwidth fast steering mirror. *Optics & Photonics 2005*, pp. 587707-587707-14.
- USA Today*. (2003). *Rocket carrying NASA satellites launched*. Retrieved August 14, 2013, from http://usatoday30.usatoday.com/weather/news/2003-01-13-nasa-ICESat_x.htm
- Wassom, S., Davidson, M., Newswander, T., Cook, J., Casper, Z., & Shelley, A. (2006). Fine steering mirror for smallsat pointing and stabilization. *AIAA/USU Small Satellite Conference 2006*. Logan, Utah.
- Winker, D., Couch, R., & McCormick, P. (1996). An overview of LITE: NASA's lidar in-space technology experiment. *Proceedings of the IEEE*, 84(2), 164–180.
- Winker, D., Hunt, W., Hostetler, C. (2004). Status and performance of the CALIOP lidar. *Laser Radar Techniques for Atmospheric Sensing, Proceedings of the SPIE*, 5575, 8–15.
- Winker, D. M., Hunt, W., & McGill M. (2007). Initial performance assessment of CALIOP. *Geophys. Res. Lett.*, 34, L19803
- The World Bank. (2013). Data: Land area. Retrieved September 2013, 2013, from <http://data.worldbank.org/indicator/AG.LND.TOTL.K2>
- Yu, A. W., Harding, D. J., Abshire, J. B., Krainak, M. A., & Sun, X. (2011). Technologies development for the lidar surface topography (LIST) mission. *16th Coherent Laser Radar Conference*. Long Beach, California.
- Yu, A. W., Stephen, M. A., Li, S. X., Shaw, G. B., Seas, A., Dowdye, E., et al. (2010). Space laser transmitter development for ICESat-2 mission. *Proceedings of the SPIE*, pp. 757809-757809-11.
- Yuan, P., Sudharsanan, R., Bai, X., Boisvert, J., McDonald, P., Labios, E., et al. (2011). Geiger-mode LADAR cameras. *SPIE Defense, Security, and Sensing*, pp. 803712-803712-10.
- Zissis, G. J., & Wolfe, W. L. (1978). *The infrared handbook*. Ann Arbor, Michigan: Environmental Research Institute of Michigan.
- Zuber, M. T., Smith, D. E., Solomon, S. C., Phillips R. J., Peale S. J., Head, J. W. III, ... Harmon, J. K. (2008). Laser altimeter observations from MESSENGER's first Mercury flyby. *Science*, 321, 77.

Zuber, M. T., Smith, D. E., Phillips, R. J., Solomon, S. C., Neumann, G. A., Hauck, S. A. II, ... Yang, D. (2012). Topography of the northern hemisphere of Mercury from MESSENGER laser altimetry. *Science*, 336, 217.

INITIAL DISTRIBUTION LIST

1. Defense Technical Information Center
Ft. Belvoir, Virginia
2. Dudley Knox Library
Naval Postgraduate School
Monterey, California